Wind-Tunnel Test of an Articulated Helicopter Rotor Model With Several Tip Shapes

John D. Berry and Raymond E. Mineck

Structures Laboratory, AVRADCOM Research and Technology Laboratories
Langley Research Center
Hampton, Virginia

SUMMARY

A wind-tunnel investigation has been conducted using an articulated heli-
copter model rotor system to determine the effects of several blade tip designs
on both the performance and acoustic characteristics of the rotor. Only the
performance characteristics are presented in this paper. Six tip shapes were
tested: a square (baseline) tip, an ogee tip, a subwing tip, a swept tip, a
winglet tip, and a short ogee tip. Tests were conducted at two rotor rota-
tional speeds and five advance ratios including hover.

In hover at the lower rotational speed and a given lift coefficient, the
swept, ogee, and short ogee tips had about the same torque coefficient, and the
subwing and winglet tips had a larger torque coefficient than the baseline
square tip blades. In simulated forward flight, the ogee tip had values of
torque coefficient very close to or less than the baseline square tip blades.
In simulated forward flight at 1200 rpm, the ogee tips showed a decrease in
torque coefficient relative to the baseline blades as drag coefficient
decreased. The swept tip blades required less torque coefficient at lower rota-
tional speeds than the baseline square tip blades and roughly equivalent torque
coefficient at higher rotational speeds in forward flight. The short ogee tip
was tested in limited forward flight conditions and it required higher torque
coefficient at higher lift coefficient than the baseline square tip blade.

INTRODUCTION

Excessive noise has limited the acceptability of the helicopter near popu-
lated areas to such an extent that noise reduction has become an important fac-
tor in helicopter design. The effect on rotor performance of the changes in the
design to reduce noise must be evaluated. Many past tests of these designs have
included thorough investigations of either the performance or acoustic charac-
teristics but not both. It is difficult to determine the effect of design
changes on the rotor acoustics and performance because the past tests ze been
performed on different rotor systems with different scale factors. Several
rotor blade tip shape designs have demonstrated improved acoustic character-
istics. To evaluate the effect of tip shape on the performance characteristics
of a rotor, a wind-tunnel test has been conducted using a single articulated
model rotor system with five interchangeable sets of blade tips. Subsequent
to the first test, a sixth tip shape was evaluated for performance in a limited
range of flight conditions. The first five tip shapes were evaluated for acous-
tic performance. The acoustic results from the tests may be found in refer-
ence 1; the performance results are presented herein.

The six removable tips tested were a square tip (baseline), an ogee tip,
a swept tip, a subwing tip, a winglet tip, and a short ogee tip. Each set of
tips was tested in hover at a rotational speed of 1200 rpm. Because the radii
for all tip shapes were not identical, this speed corresponded to tip speeds
ranging from 198 m/sec (649 ft/sec) to 207 m/sec (680 ft/sec) depending on the

radius. The square tip, the ogee tip, and the swept tip were subsequently tested in hover at 1340 rpm and in simulated forward flight at 1200 rpm and 1340 rpm and four advance ratios of 0.2, 0.3, 0.35, and 0.40. The short ogee tip was tested in simulated forward flight at 1200 rpm at an advance ratio of 0.3.

SYMBOLS

The units used for the physical quantities defined in this paper are given in the International System of Units (SI) and parenthetically in the U.S. Customary Units. Measurements and calculations were made in the U.S. Customary Units. Conversion factors relating the two systems are presented in reference 2. The rotor performance data have been resolved in the stability axis system with the moment reference center located at the center of the rotor hub.

B_1 longitudinal cyclic pitch, deg

b number of blades, 4

C_D/σ conventional rotor drag coefficient, $\dfrac{D}{\rho \pi \Omega^2 R^4 \sigma}$

C_L/σ conventional rotor lift coefficient, $\dfrac{L}{\rho \pi \Omega^2 R^4 \sigma}$

C_L/σ_T thrust weighted solidity lift coefficient, $\dfrac{L}{\rho \pi \Omega^2 R^4 \sigma_T}$

C_Q/σ conventional rotor torque coefficient, $\dfrac{Q}{\rho \pi \Omega^2 R^5 \sigma}$

C_Q/σ_Q torque-weighted solidity torque coefficient, $\dfrac{Q}{\rho \pi \Omega^2 R^5 \sigma_Q}$

C_T/σ conventional rotor thrust coefficient, $\dfrac{T}{\rho \pi \Omega^2 R^4 \sigma}$

c rotor blade local chord, m (ft)

$\bar{c}$ rotor blade reference chord, 0.08 m (0.353 ft)

2

c_Q torque-weighted effective blade chord, $\dfrac{4\displaystyle\int_0^R cr^3\,dr}{R^4}$, m (ft)

c_T thrust-weighted effective blade chord, $\dfrac{3\displaystyle\int_0^R cr^2\,dr}{R^3}$, m (ft)

D rotor drag, N (lbf)

L rotor lift, N (lbf)

N rotor rotational speed, rpm

Q rotor torque, N-m (lbf-ft)

R rotor radius, m (ft)

r distance along rotor blade span measured from center of rotation, m (ft)

T rotor thrust, N (lbf)

V_T rotor tip speed, ΩR, m/sec (ft/sec)

V_∞ free-stream velocity, m/sec (ft/sec)

α_c control axis angle of attack, $\alpha_s - B_1$, deg

α_s rotor shaft angle of attack, deg

μ rotor advance ratio, $\dfrac{V_\infty}{V_T}$

ρ free-stream density, kg/m^3 (slugs/ft^3)

σ rectangular rotor solidity, $\dfrac{b\bar{c}}{\pi R}$

σ_Q torque-weighted solidity, $\dfrac{bc_Q}{\pi R}$

σ_T thrust-weighted solidity, $\dfrac{bc_T}{\pi R}$

Ω rotor rotational speed, rad/sec

ω rotor blade natural frequency, rad/sec

MODEL AND APPARATUS

The general rotor model system (GRMS) was used in the Langley V/STOL Tunnel for this investigation. A sketch of the model appears in figure 1, which also presents the axis system. Details of the model may be found in references 3 and 4. The rotor hub used in the investigation was fully articulated. The flapping and lagging hinges were coincident at 7.6 cm (3.0 in.) from the center of rotation. The pitch-flap coupling angle was set at -2°. (Negative pitch-flap coupling angles correspond to a decrease in blade pitch with an increase in blade flapping.) Position potentiometers were mounted on the flapping and lagging hinges of the reference blades to provide a readout of the flapping and lagging motions. The rotor control system was instrumented to provide a readout of the rotor control positions. The pitch link of the reference blade had a strain gage to measure control loads.

The rotor was driven by two 67-kW (90-hp) electric motors driving a common transmission. The rotor, transmission, and motor assembly was mounted on a six-component strain-gage balance. The balance was supported by a gimbal system of springs and dampers to insure that the rotor would be free from ground resonance.

The rotor blades used in the investigation had an NACA 0012 airfoil section. Each blade had provision for a removable tip. Six tip shapes were tested in this investigation: a square tip (baseline), an ogee tip, a swept tip, a subwing tip, a winglet tip, and a short ogee tip. (See fig. 2 and table I.) The square tip, the swept tip, and the winglet tip were all the same length so that the radii of these blade sets were equal. The ogee tip was longer than the baseline square tip so that its blade radius was larger but the blade area was the same as that of the square tip. The subwing tip consisted of a basic square tip with a subwing added so that both the radius and area were larger for the subwing tip than for the square tip. The short ogee tip had the same planform as the ogee tip except that the radius was reduced by beginning the ogee curvature at the point of tip attachment and shortening the extreme tip slightly which resulted in a radius only 1.12 cm (0.44 in.) longer than the baseline square tip. Details of the rotor blades are given in table I.

The blades and tips were designed to keep the change in mass between the different types of tips small. The change is reflected in the blade flapping inertias shown in table I. The natural frequencies of the rotor blade with each tip were determined by the method described in reference 5 and the frequencies for all six tips were very similar. (See table II.) The effect of blade dynamics on the performance of the rotor should be the same for each tip.

The short ogee tip shape was tested subsequent to the main test. The rotor system is identical to that used in the main test, but the helicopter model body mounted on the GRMS during testing of the sixth tip shape was that of the YAH-64 attack helicopter. The helicopter model used during the main

4

test was a research helicopter body designed to be configuration-independent and easily modeled analytically.

Photographs of the models in the Langley V/STOL Tunnel are shown in figure 3. The model was mounted on a second strain-gage balance attached to a special model sting. This sting model support system permits the angle of attack and angle of sideslip to be varied over wide ranges while the model is maintained at a fixed position in the tunnel.

TEST PROCEDURES AND CONDITIONS

This investigation was conducted in the Langley V/STOL Tunnel, which is a closed return, atmospheric tunnel. The tunnel may be configured with a closed test section or an open test section with the walls and ceiling removed. The closed test section measures 4.42 m (14.50 ft) by 6.63 m (21.75 ft). Testing at forward speed was conducted in the closed test section with the rotor hub 2.9 m (9.5 ft) above the tunnel floor. Hover testing was conducted in the open test section at several heights above the tunnel floor: 4.5 m (14.7 ft), 2.9 m (9.5 ft), and 1.6 m (5.4 ft). Five sets of rotor blade tips were tested in hover, and after analysis of the hover results, it was decided that only three of those tips - the square tip, the swept tip, and the ogee tip - would be tested at simulated forward speeds. The short ogee tip was subsequently tested in hover and at one forward flight condition.

The three tips initially tested at simulated forward flight conditions were tested at rotational speeds of 1200 rpm and 1340 rpm and at advance ratios of 0.0 (hover), 0.20, 0.30, 0.35, and 0.40. These values were chosen to cover the practical range used in helicopters. At each combination of rotational speed and advance ratio, tests were made at six nominal shaft angles: 0°, -3°, -6°, -9°, -12°, and -15°. At each shaft angle the rotor collective pitch was varied in 1° or 2° increments until one or more of the following limits was reached: maximum temperatures in the electric drive motors, available collective and cyclic pitch, lead-lag motion of the blades, and/or stress limits on the blades, pitch links, and strain-gage balances. Combinations of rotor rotational speed, advance ratio, and shaft angle are shown in table III. At each collective pitch setting, the first harmonic longitudinal and lateral flapping with respect to the shaft were reduced to zero by varying the cyclic pitch settings.

The model hub configuration used is representative of a true scale hub. For comparison with the baseline blade shape, data presented have not been adjusted for force and moment contributions due to aerodynamic forces acting on the model rotor hub. The data for simulated forward flight have been corrected for wall effects by using the methods described in reference 6. The corrected tunnel free-stream dynamic pressure and flow direction are used to compute the simulated flight speed and rotor shaft angle of attack.

The rotor balance forces and moments, rotor control positions, and tunnel test conditions were recorded on the tunnel digital data acquisition system. The instrumented rotor blade flapping angle, pitch link load, and azimuth were recorded on an analog tape.

PRESENTATION OF RESULTS

The results of this wind-tunnel investigation have been presented in dimensional and nondimensional form in figures 4 to 14. The data are resolved in the stability axis system with the moment reference center at the center of the rotor hub. Complete results are presented as follows:

Result	α_s, deg	N, rpm	Figure for data at μ of -				
			0.0	0.20	0.30	0.35	0.40
Effect of solidity in nondimensionalizing		1200	4(a)		4(b)		
Rotor performance comparison (thrust as a function of torque): Square, ogee, swept, subwing, and winglet tips on research body	0	1200	5(a)				
Square, ogee, and swept tips on research body	-3	1200		6(a)	6(b)		
	-6	1200		6(c)	6(d)	6(e)	6(f)
	-9	1200		6(g)	6(h)	6(i)	
	-12	1200			6(j)	6(k)	
	-15	1200				6(l)	
	0	1340	5(b)				
	-9	1340		6(m)			
	-12	1340			6(h)	o(o)	
Square and short ogee tips[a] on YAH-64 body	0	1200	7(a)				
	-6	1200			7(b)		
Rotor performance (aerodynamic coefficients): Square tip		1200	8(a)	8(b)	8(c)	8(d)	8(e)
		1340	8(f)	8(g)	8(h)	8(i)	
Ogee tip		1200	9(a)	9(b)	9(c)	9(d)	9(e)
		1340	9(f)	9(g)	9(h)	9(i)	
Swept tip		1200	10(a)	10(b)	10(c)	10(d)	10(e)
		1340	10(f)	10(g)	10(h)	10(i)	
Subwing tip		1200	11				
Winglet tip		1200	12				
Short ogee tip		1200	13(a)		13(b)		
Comparison of tip shape performance (aerodynamic coefficients)		1200	4(a)	14(a)	14(b)	14(c)	14(d)
		1340		14 ;	14(f)	14(g)	

[a]The data in figures 7 and 13 compare the performance of the short ogee tip with the baseline square tip when both are tested with the YAH-64 helicopter model shell mounted. A comparison of performance of the baseline square tip blades at the two short ogee blade test conditions with both the research and the YAH-64 model shells mounted produced no significant deviation in the results.

DISCUSSION OF RESULTS

Effect of Nondimensionalizing

Rotor force and moment data are traditionally presented in coefficient form nondimensionalized by the test medium density, rotor tip speed squared, and either the rotor blade area or disk area. The different planforms tested in the investigation complicate the choice of the proper values of radius and area. A proper nondimensionalization will result in a comparison of values corresponding to forces and moments resulting from tip shape changes only. Since changes in tip planform also affect the rotor swept disk area, the tip speed, and the rotor solidity, the effects of these quantities on the nondimensionalization are examined.

The blade element analysis method of reference 7 represents the forces and moments in the rotor system as the sums of incremental forces and moments acting at different blade radial stations. These incremental forces and moments are assumed to be only a function of their radial location. Reference 7 gives a technique for determining weighted solidities for blades of arbitrary planform based on blade element theory.

The basis for the weighted solidities found in reference 7 is an equivalent effective chord for an imaginary rectangular blade of the same radial length as the nonrectangular blade. Forces at a given radial station are proportional to the square of the radial distance from the center of rotation to that station, and moments generated at a given radial station about the center of rotation are proportional to the cube of the radial distance from the center of rotation to that station. Effective chords for use in thrust (force) and torque (moment) calculations are given by

$$
c_T \equiv \frac{\int_0^R cr^2 \, dr}{\int_0^R r^2 \, dr} = \frac{3 \int_0^R cr^2 \, dr}{R^3}
$$

$$
c_Q \equiv \frac{\int_0^R cr^3 \, dr}{\int_0^R r^3 \, dr} = \frac{4 \int_0^R cr^3 \, dr}{R^4}
$$

Weighted solidities, based on the effective chords computed, are given by

$$\sigma_T = \frac{bc_T}{\pi R} \qquad\qquad \sigma_Q = \frac{bc_Q}{\pi R}$$

For comparison with this method of nondimensionalization a rotor solidity for each tip was computed assuming a rectangular planform to the full blade radius, as given by

$$\sigma = \frac{b\bar{c}}{\pi R}$$

Values for these solidities for all tip shapes studied are given in table IV. Comparison of the results of these methods of nondimensionalizing for hover and a forward flight condition can be found in figure 4. The same data presented in a dimensional form can be found in figures 5(a) and (c).

It is apparent that one's perception of the effect of tip shape on rotor performance is influenced by the normalizing procedure chosen to analyze the data. Nondimensionalization by the weighted-solidity technique, which, in effect, distributes planform variations uniformly along the blade span, obscures the influence of shape changes occurring in a highly localized area of distinctly three-dimensional flow effects because the normalizing technique is based on the two-dimensional blade element theory. On the other hand, nondimensionalization of the data by a rectangular-solidity method, where the basic blade chord is retained out to the full tip radius, yields a closer approximation to the actual physical processes involved, since the planform variations are confined to a comparatively small portion of the blade. Although some variation due to unequal blade planform areas is present when the rectangular-solidity technique is used, it is believed that this procedure is more effective in representing tip shape change effects than the weighted-solidity method. Accordingly, data presented in this report, unless otherwise specified, have been normalized by the rectangular-solidity technique.

Effect of Tip Shape in Hover

The nondimensional rotor hover performance at 1200 rpm is presented in part (a) of figures 4, 5, 7 to 10, and 13 and figures 11 and 12. When the results at practical nondimensional lift coefficients ($C_L/\sigma > 0.04$) are compared, both the ogee and the swept tip blades require the same torque coefficient at a given lift coefficient as the baseline square tip blades. The subwing and the winglet tip blades required a larger torque coefficient at a given lift coefficient than the baseline square tip blades. Because the subwing and the winglet tips experienced significantly higher torque coefficients than the other tips during the 1200 rpm hover testing, they were

8

eliminated from further testing. The short ogee tip shows less torque coef-
ficient required below a moderate lift coefficient ($C_L/\sigma < 0.05$) than t... ...i
line square tip blades.

The hover performance at 1340 rpm is presented in figures 8(f), 9(f), and
10(f) for the square, ogee, and swept tip blades. As was noted at 1200 rpm,
the ogee tip requires the same torque coefficient at a given lift coefficien'
as the square tip blades. The swept tip requires an increase in torque coef-
ficient for practical lift coefficients when compared with the baseline square
tip blades.

Effect of Tip Shape at Simulated Forward Speed

The rotor performance data from the wind-tunnel investigation are presented
in figure 8 for the baseline square tip blades, in figure 9 for the ogee tip
blades, and in figure 10 for the swept tip blades. The rotor lift coefficient,
drag coefficient, torque coefficient, and control-axis angle of attack are pre-
sented for each combination of advance ratio and rotor rotational speed. For
hover comparison the baseline square tip data are also presented in figures 9(a),
9(f), 10(a), and 10(f).

A direct comparison of the results for the three tip shapes is complicated
by the small differences in rotor shaft angle of attack. Therefore, the results
for the three sets of tip shapes have been interpolated to several values of
rotor lift coefficient. These results are presented in figures 14(a) to 14(d)
for 1200 rpm and in figures 14(e) to 14(g) for 1340 rpm.

Data at 1200 rpm indicate that the ogee tip blades required a torque coef-
ficient less than or very close to that required by the baseline square tio
blades except in the following two conditions: (1) low advance ratio ($\mu = 0.20$)
and low lift coefficient ($C_L/\sigma = 0.04$) above a drag coefficient of -0.003 and
(2) advance ratio of 0.30 and lift coefficients of 0.06 and higher at drag coef-
ficients above -0.001. When compared to the baseline square tip blades, the
ogee tip blades demonstrated a significant reduction in torque required at an
advance ratio of 0.35 with lift coefficients of 0.06 and 0.07 below a drag coef-
ficient of -0.006. The data presented indicate a general performance improve-
ment (reduction in torque required) for the ogee tip blades as the drag coef-
ficient decreases when compared with the data for the baseline square tip
blades. At 1340 rpm, the data presented indicate that relative to the baseline
square tip blades, there is a smaller torque coefficient required for the ogee
tip blades at the higher lift coefficient at all but the lowest advance ratio
where the torque requirements are very close.

Data at 1200 rpm for the swept tip blades indicate a torque coefficient
requirement of less than that for the baseline square tip blades for all cases
except those where torque coefficients were very close, as follows: (1) at an
advance ratio of 0.20 and low lift coefficient ($C_L/\sigma = 0.04$) below a drag coef-
ficient of -0.003; (2) at the advance ratio of 0.35 and (a) lift coefficient
of 0.04 and drag coefficien less than -0.002, (b) lift coefficient of 0.06
and drag coefficient less th -0.006, (c) lift coefficient of 0.07 and drag
coefficient less than -0.007; and (3) at an advance ratio of 0.40 and lift

9

coefficients of 0.04 and 0.06. At 1340 rpm, the data presented for the swept tip blades indicates torque coefficients very close to those required by the baseline square tip blades except at an advance ratio of 0.35 and lift coefficient of 0.07 where the torque required by the swept tip blade was less.

The limited data presented for the short ogee tip show a smaller torque coefficient at low lift coefficient ($C_L/\sigma \approx 0.04$) and higher torque coefficient at high lift coefficient ($C_L/\sigma = 0.07$) than the baseline square tip blade.

CONCLUDING REMARKS

An investigation was conducted to determine the performance characteristics of tip shapes designed to produce acoustic advantages on a four-bladed, articulated helicopter rotor. It is clear from the results that performance improvements over certain portions of the flight envelope of a helicopter are possible by changing the tip of a square tip rotor blade. However, no tip tested showed a clear performance advantage over the entire range of test conditions. Because the level of performance differences between various tips was generally quite small, any conclusion as to a "best" tip would be arbitrary at best. For these reasons, the data are presented without analysis or conclusions.

SUMMARY OF RESULTS

The results of a wind-tunnel investigation to determine th   ts of several blade tip designs on the performance characteristics of   r-bladed, articulated rotor are presented. The effects of the tip shapes   be summarized as follows:

1. For practical values of hover lift coefficient ($C_L/\sigma > 0.04$) at the lower rotational speed, for a given lift coefficient, the swept and ogee tips had about the same torque coefficient and the subwing and winglet tips had greater torque coefficients than the baseline square tips.

2. At 1200 rpm the ogee tip blades required a torque coefficient of less than or equal to that of the baseline square tip blades for most of the test conditions. The ogee tip blades generally required less torque coefficient as the drag coefficient decreased than the baseline square tip blades. At 1340 rpm the data presented indicate that the ogee tip blades required a torque coefficient less than or equal to that of the baseline square tip blades at most test conditions.

3. For most test conditions at 1200 rpm the swept tip blades required less torque coefficient than the baseline square tip blades. At 1340 rpm the swept tip blades required the same torque coefficient as the baseline square tip blades at most test conditions.

4. In the limited test conditions, the short ogee tip requires more torque coefficient at higher lift coefficients than the baseline square tip blades.

Langley Research Center
National Aeronautics and Space Administration
Hampton, VA 23665
November 12, 1980

REFERENCES

1. Hoad, Danny R.: An Experimental Investigation of the Effect of Rotor Tip Shape on Helicopter Blade-Slap Noise. NASA TM-80066, 1979.

2. Standard for Metric Practice. E 380-79, American Soc. Testing & Mater., c.1980.

3. Murrill, Robert J.: Operation and Maintenance Manual for the General Rotor Model System. NASA CR-145230, 1977.

4. Wilson, John C.: A General Rotor Model System for Wind-Tunnel Investigations. J. Aircr., vol. 14, no. 7, July 1977, pp. 639-643.

5. Weller, William H.; and Mineck, Raymond E.: An Improved Computational Procedure for Determining Helicopter Rotor Blade Natural Modes. NASA TM-78670, 1978.

6. Heyson, Harry H.: Use of Superposition in Digital Computers To Obtain Wind-Tunnel Interference Factors for Arbitrary Configurations, With Particular Reference to V/STOL Models. NASA TR R-302, 1969.

7. Gesson, Alfred; and Meyers, Garry C., Jr : Aerodynamics of the Helicopter. Macmillan Co., c.1952. (Republished 1967 by Frederick Ungar Pub. Co.)

TABLE I.- DETAILS OF ROTOR BLADES

Hub type . . . . Fully articulated

Number of blades 4

Airfoil section . . . . NACA 0012 (except where noted in fig. 2)

Hinge offset, cm (in.) 7.5 (3.0)

R . cutout, cm (in.) 31.8 (12.5)

Pitch-flap coupling angle, deg . . . . -2

Twist rate, deg/cm (deg/in.) . . . . -0.051 (-0.129)

Calculated flapping inertia:
  Square tip, kg-m^2 (slug-ft^2) 0.654 (0.482)
  Ogee tip, kg-m^2 (slug-ft^2) 0.640 (0.472)
  Swept tip, kg-m^2 (slug-ft^2) 0.632 (0.466)
  Subwing tip, kg-m^2 (slug-ft^2) 0.667 (0.492)
  Winglet tip, kg-m^2 (slug-ft^2) 0.694 (0.512)
  Short ogee tip, kg-m^2 (slug-ft^2) 0.635 (0.468)

Radius:
  Square tip, cm (in.) 157.4 (61.98)
  Ogee tip, cm (in.) 164.9 (64.92)
  Swept tip, cm (in.) 157.4 (61.98)
  Subwing tip, cm (in.) 160.6 (63.23)
  Winglet tip, cm (in.) 157.4 (61.98)
  Short ogee tip, cm (in.) 158.5 (62.40)

TABLE II.- ROTOR BLADE ROTATING NATURAL FREQUENCIES

Mode type	ω/Ω for -					
	Square	Ogec	Swept	Subwing	Winglet	Short ogee
N = 1200 rpm						
Horizontal	0.28	0.28	0.28	0.28	0.28	0.28
Vertical	1.04	1.04	1.04	1.04	1.04	1.04
Vertical	2.74	2.74	2.75	2.73	2.74	2.75
Torsion	4.24	4.27	4.31	4.20	4.21	4.21
Horizontal	4.59	4.63	4.67	4.54	4.48	4.65
Vertical	5.12	5.14	5.17	5.10	5.09	5.16
Vertical	8.31	8.37	8.46	8.25	8.21	8.44
N = 1340 rpm						
Horizontal	0.28	0.28	0.28	0.28	0.28	0.28
Vertical	1.04	1.04	1.04	1.04	1.04	1.04
Vertical	2.70	2.70	2.70	2.69	2.70	2.70
Torsion	3.82	3.84	3.87	3.78	3.78	3.79
Horizontal	4.22	4.26	4.29	4.19	4.13	4.28
Vertical	4.89	4.90	4.93	4.87	4.87	4.92
V tical	7.78	7.82	7.91	7.79	7.69	7.89

TABLE III.- MATRIX OF ROTOR TEST CONDITIONS

(a) N = 1200 rpm

(b) N = 1340 rm

Key:

Sub		
O g e e	Square	S w e p t
		Winglet

● Denotes general test condition

◉ Denotes additional short ogee tip test condition
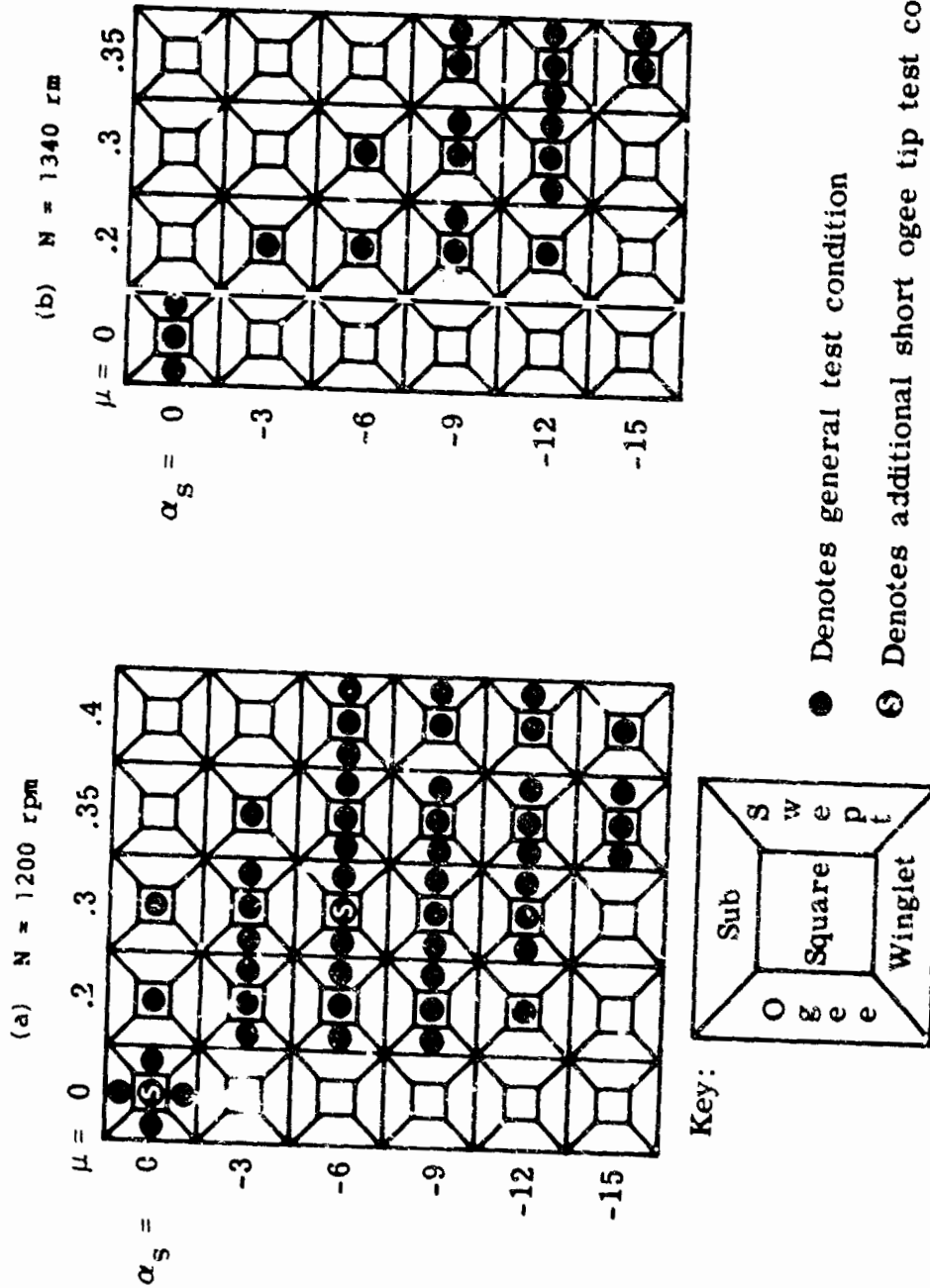
TABLE IV.- SOLIDITY VALUES USED IN

NONDIMENSIONALIZATION

Tip	σ	σ_T	σ_Q
Square	0.0871	0.0858	0.0854
Swept	.0871	.0809	.0790
Ogee	.0832	.0711	.0676
Subwing	.0854	.0801	.0784
Winglet	.0871	.0858	.0854
Short ogee	.0865	.0744	.0708

15
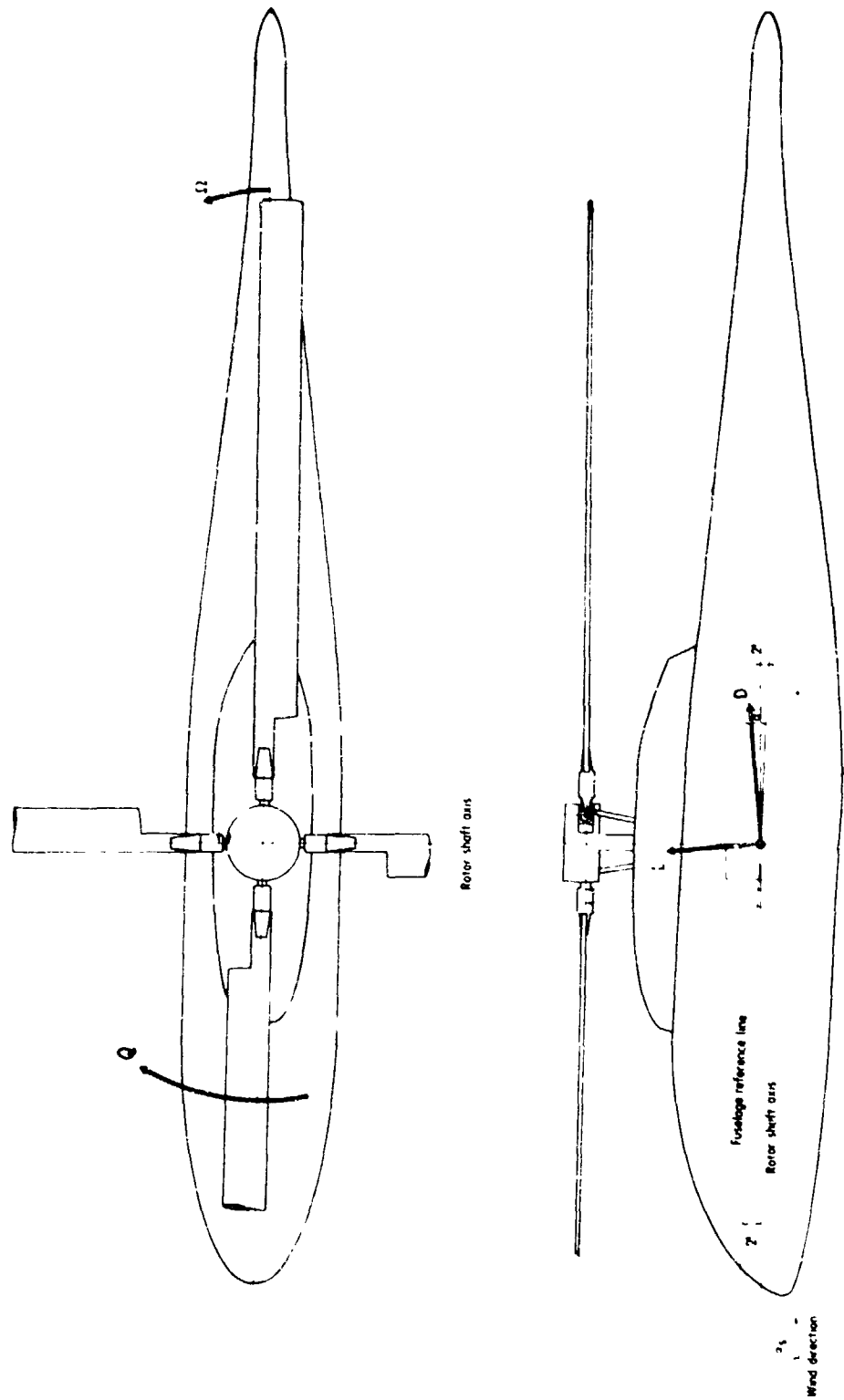
Figure 1.- System of axes.

Tip path plane

a_s

T

D

L

Shaft axis

Q

B_1

a_c

No feathering plane

V_∞
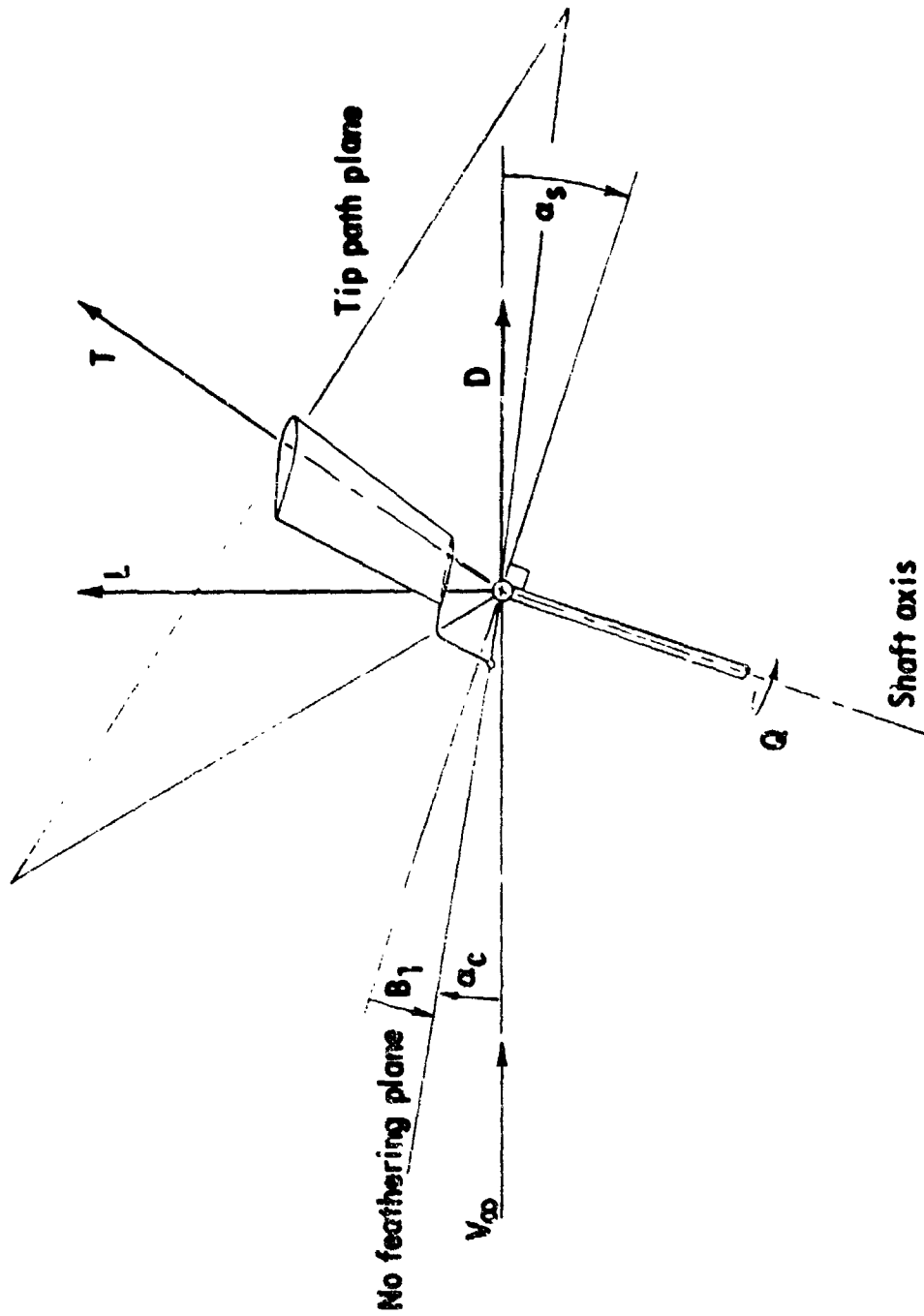
Figure 1.- Concluded.

17
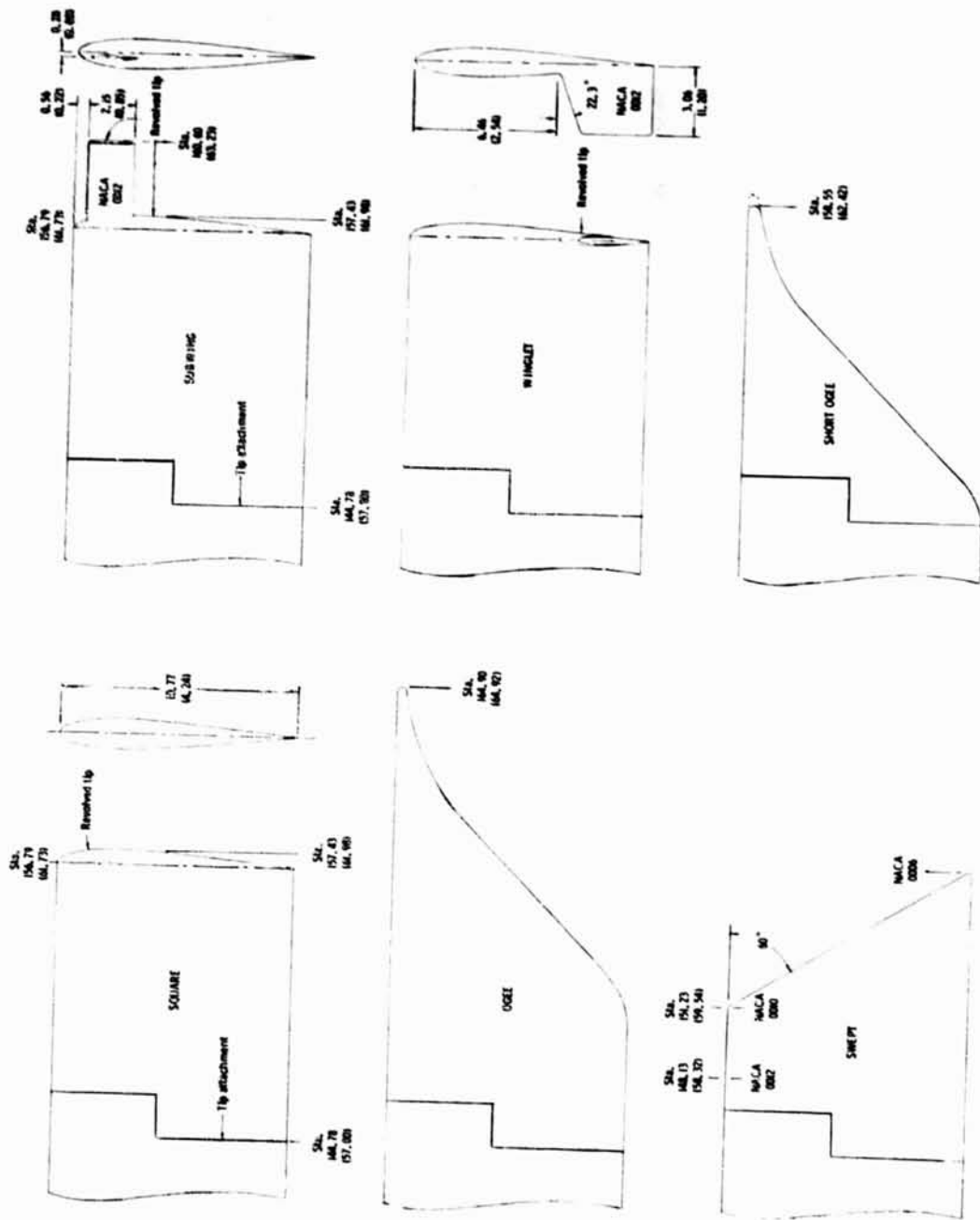
Figure 2.- Tip shapes. All dimensions are in centimeters (inches).

L-78-4383

(a) GRMS with research helicopter model shell.

Figure 3.- Models in V/STOL Tunnel.

19
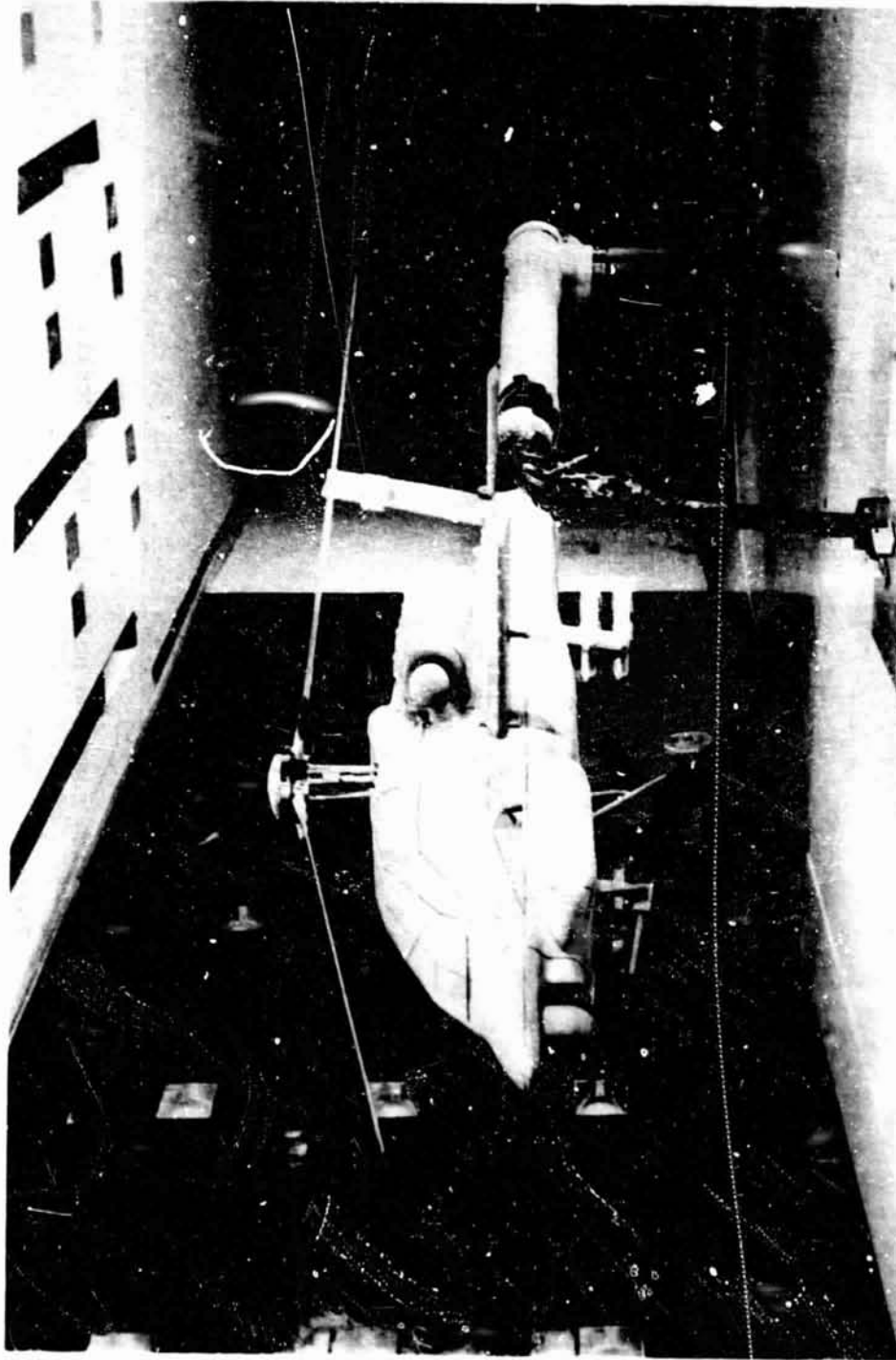
L-79-7039

(b) With YAH-64 model shell.

Figure 3.- Concluded.
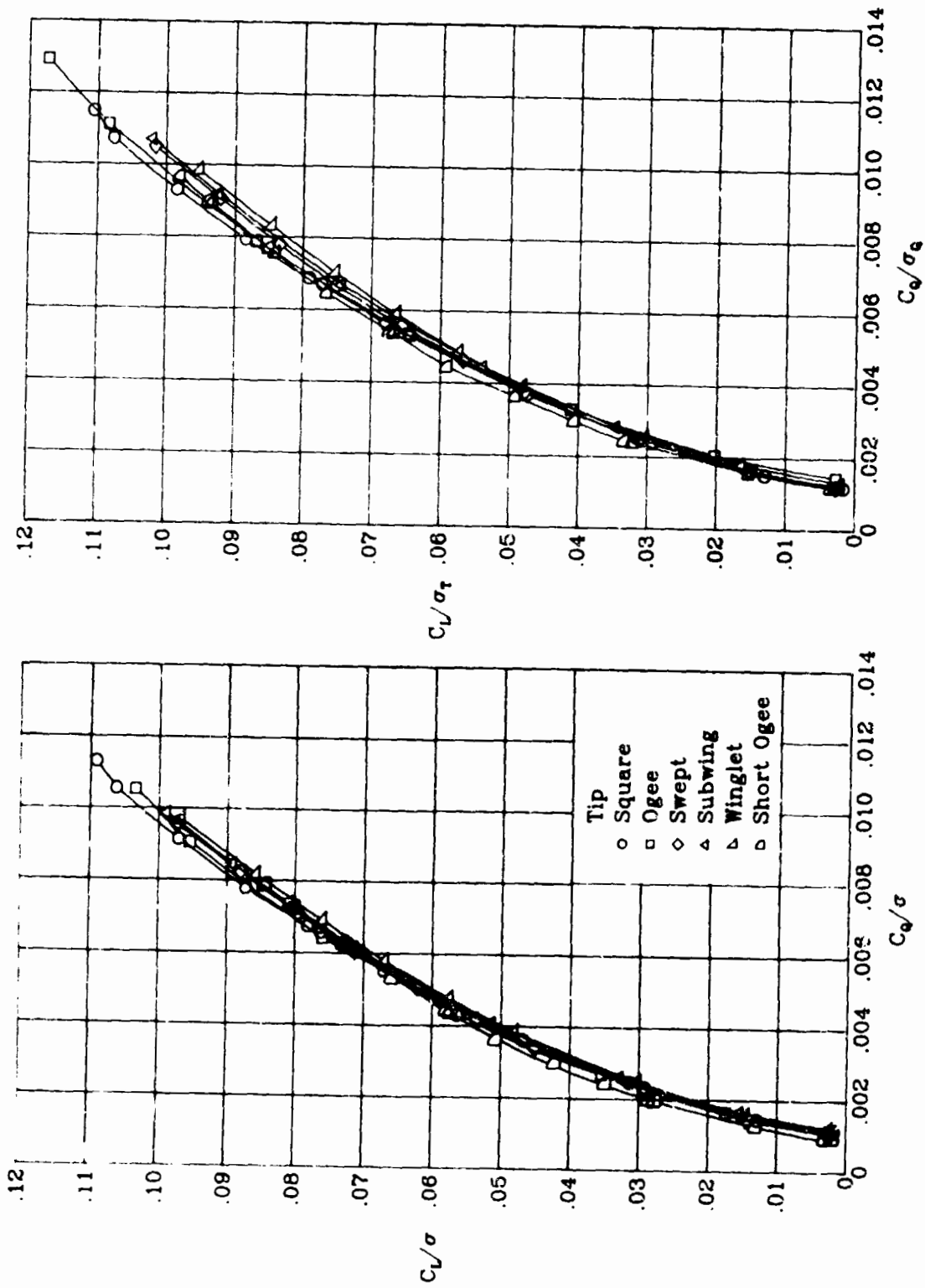
Figure 4.- Comparison of effect of solidity in nondimensionalization on rotor lift and torque coefficient.

(a) μ = 0.0; N = 1200 rpm.

21
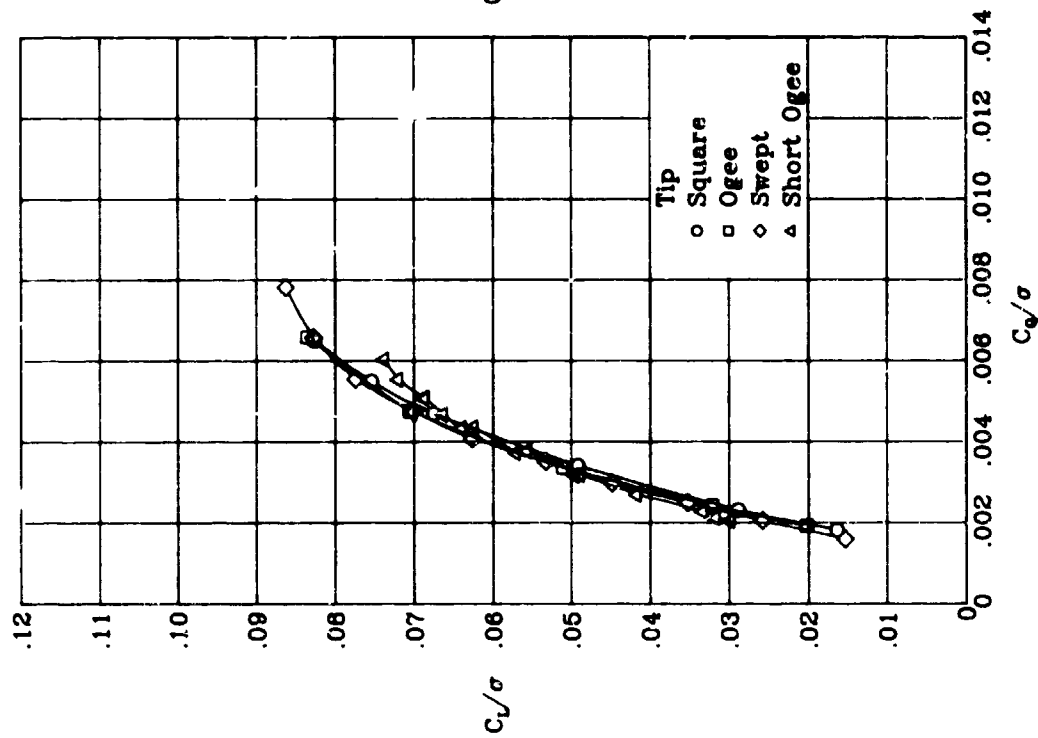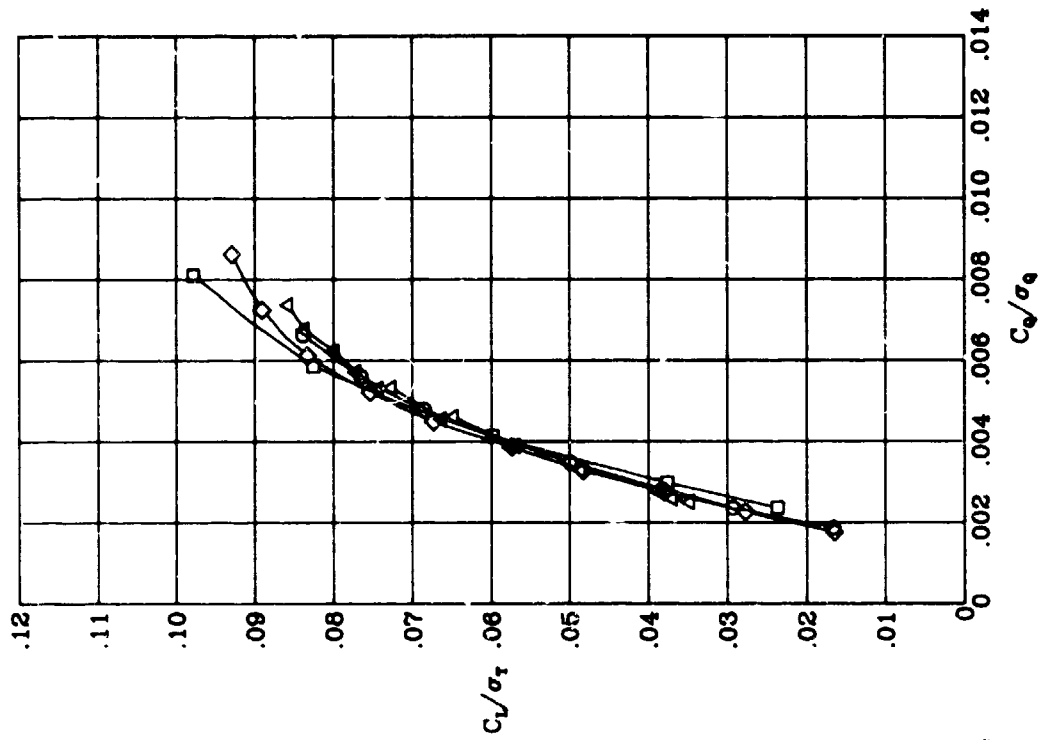
(b) $\mu = 0.30$; $N = 1200$ rpm; $\alpha_s = -6°$.

Figure 4.- Concluded.
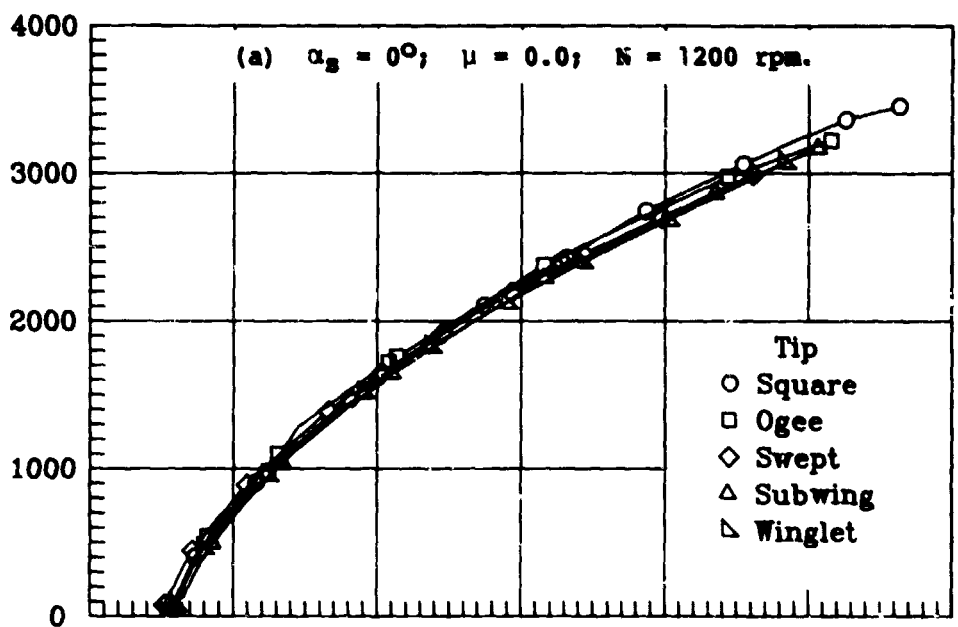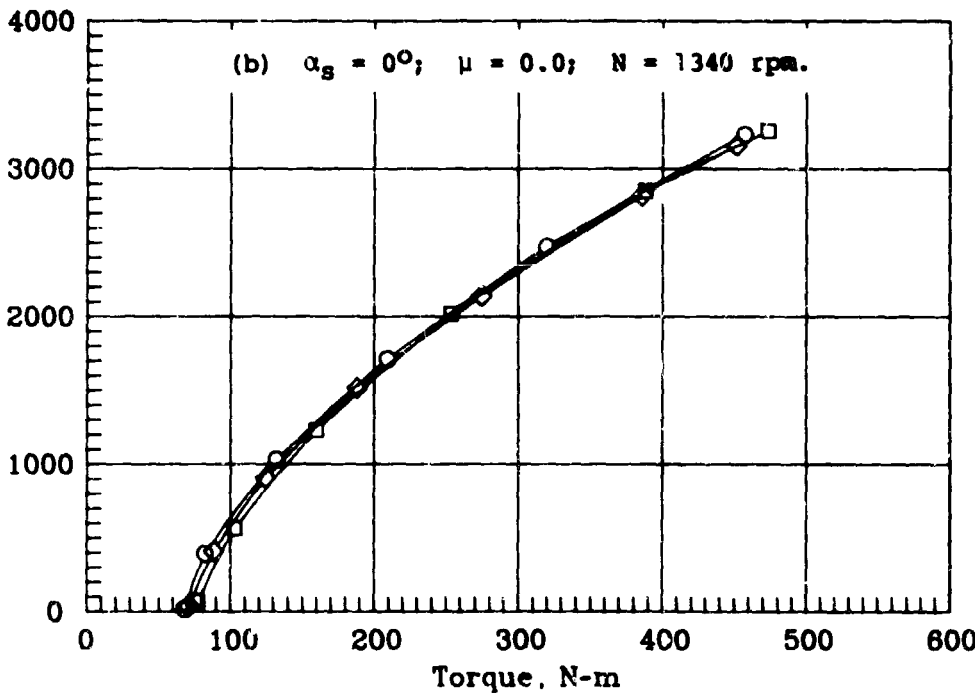
Figure 5.- Hover performance.
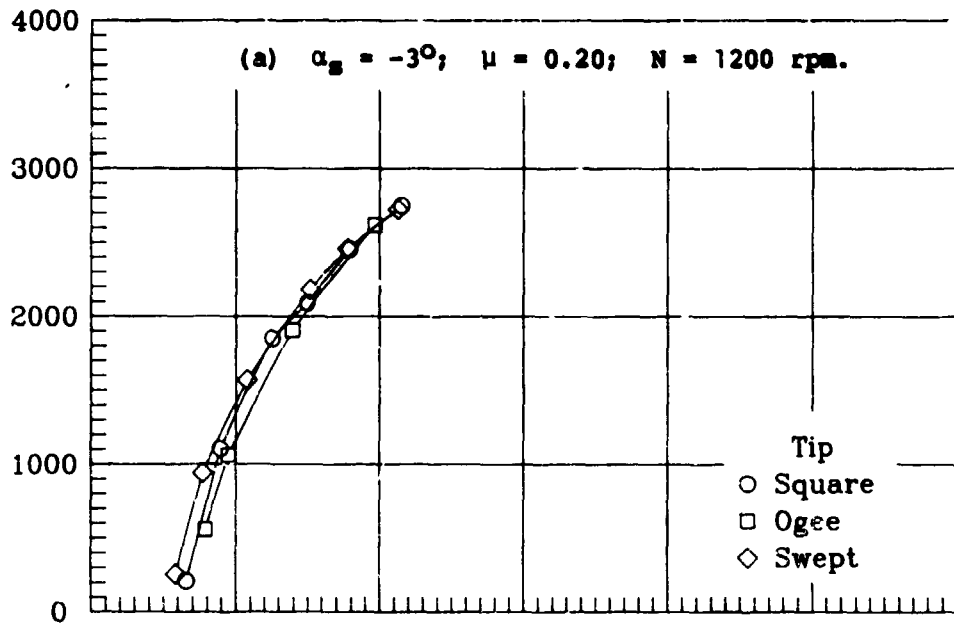
Thrust, N
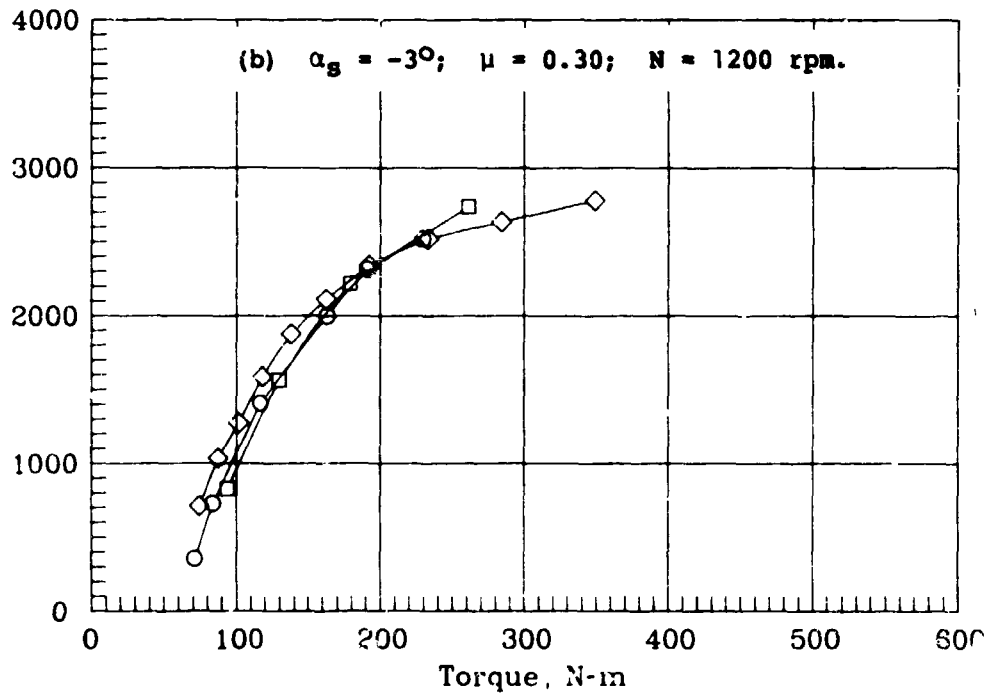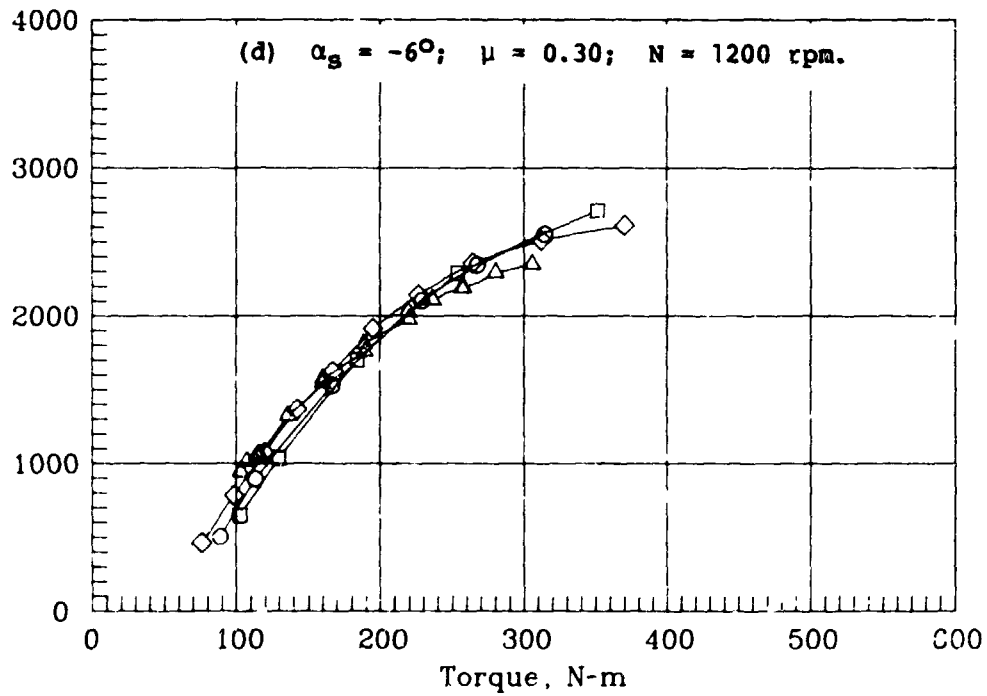
Figure 6.- Forward flight performance.
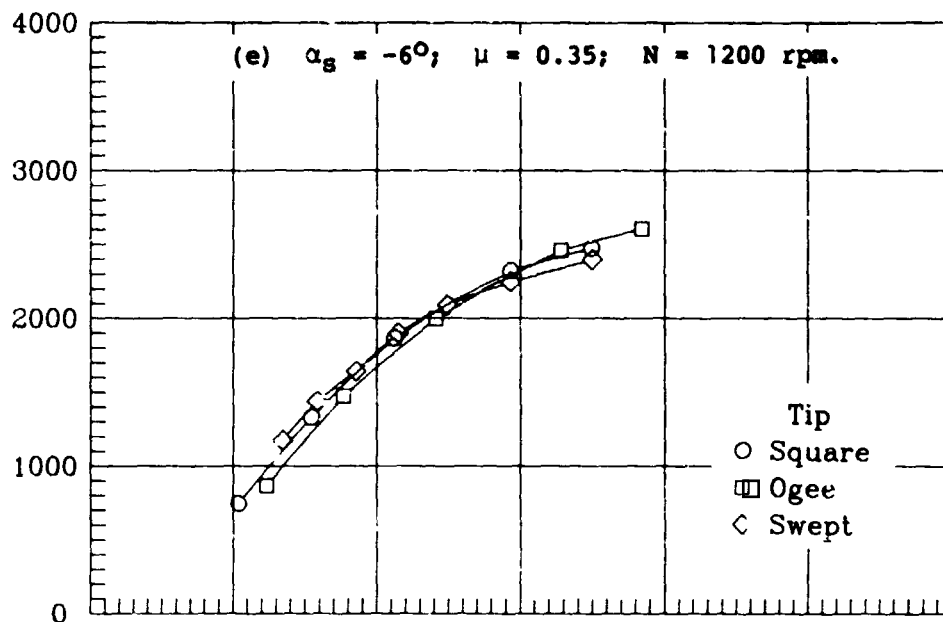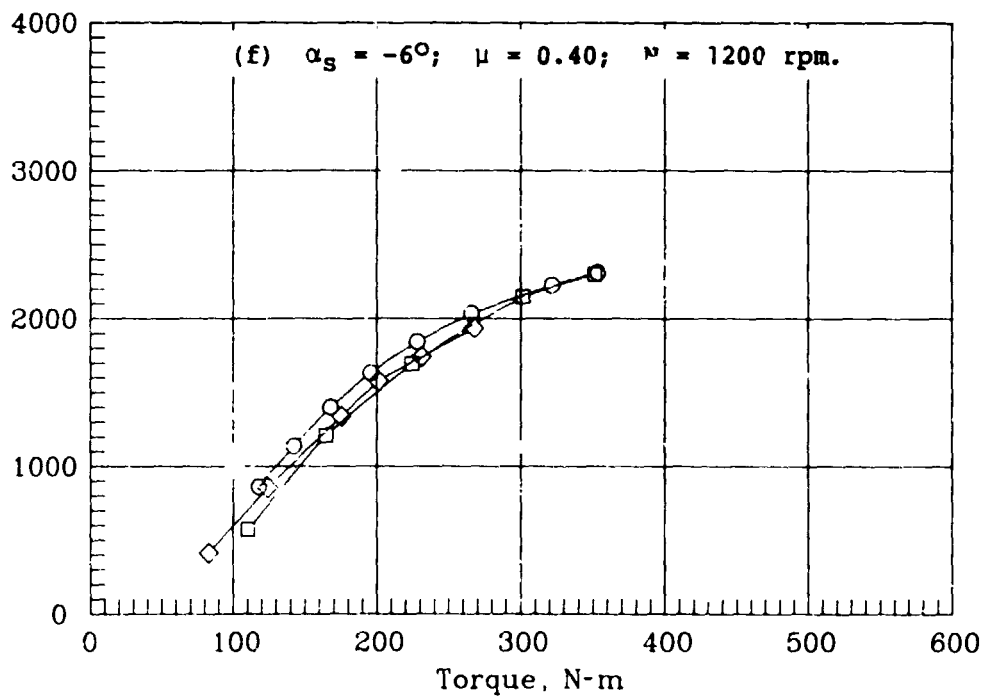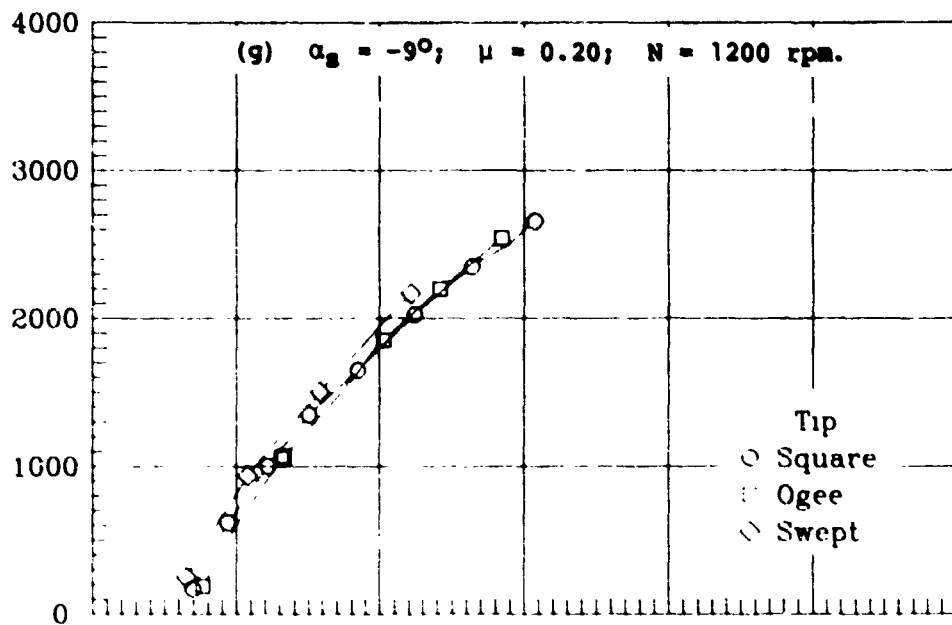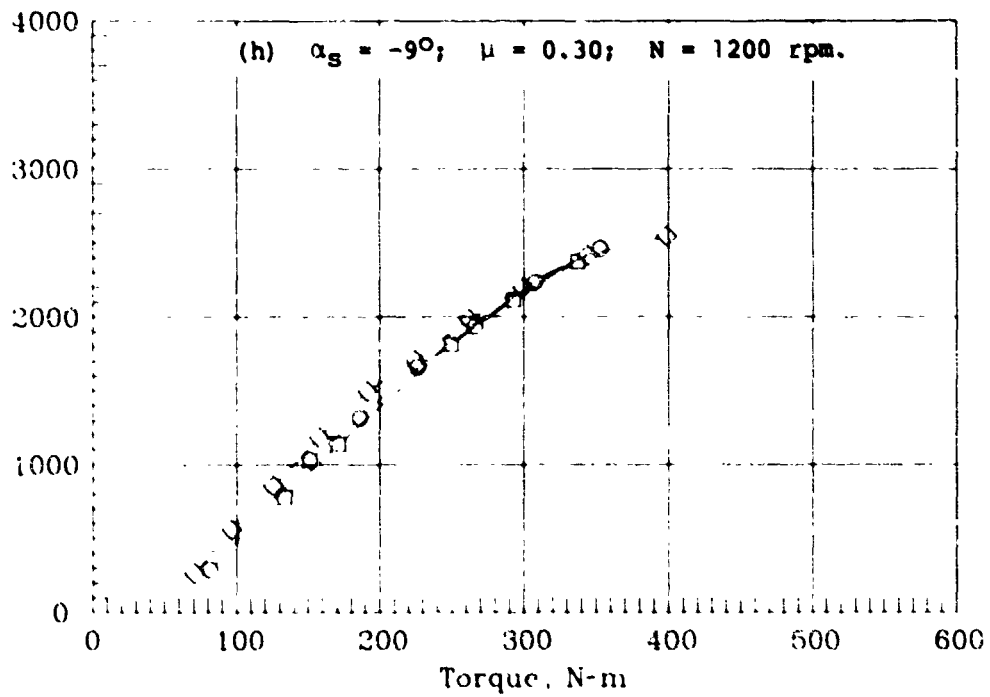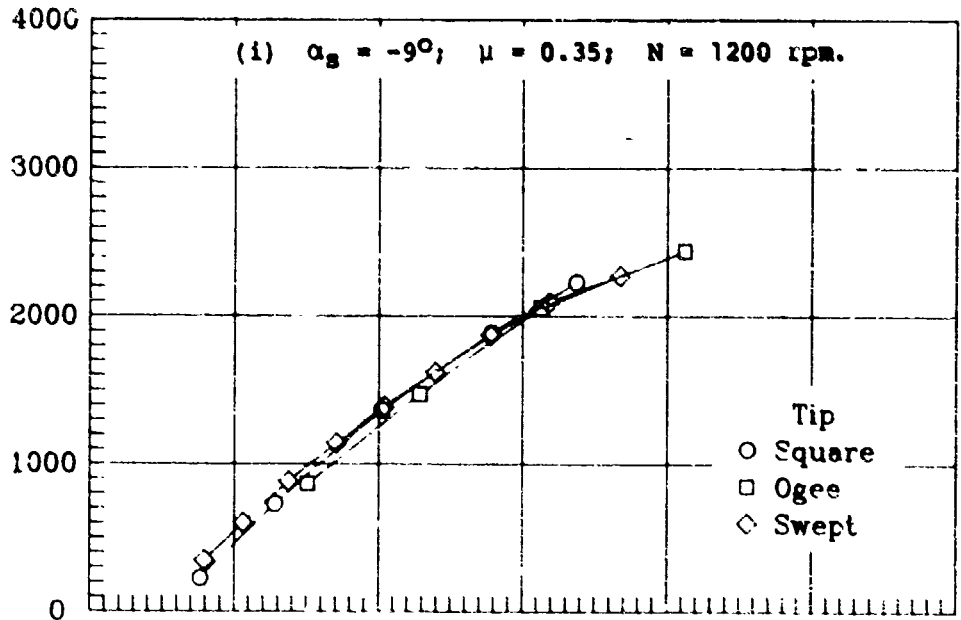
(c) $\alpha_s = -6^o$; $\mu = 0.20$; N = 1200 rpm.

Tip
○ Square
□ Ogee
◇ Swept
△ Short Ogee

Thrust,
N

(d) $\alpha_s = -6^o$; $\mu = 0.30$; N = 1200 rpm.

Torque, N-m

Figure 6.- Continued.

(e) $\alpha_s = -6°$; $\mu = 0.35$; $N = 1200$ rpm.

Tip
○ Square
⊞ Ogee
◇ Swept

Thrust,
N

(f) $\alpha_s = -6°$; $\mu = 0.40$; $N = 1200$ rpm.

Torque, N-m

Figure 6.- Continued.

26

(g) $\alpha_s = -9°$; $\mu = 0.20$; N = 1200 rpm.

Tip
○ Square
▫ Ogee
◇ Swept

Thrust.
N

(h) $\alpha_s = -9°$; $\mu = 0.30$; N = 1200 rpm.

Torque, N-m

Figure 6.- Continued.

(i) $\alpha_s = -9°$; $\mu = 0.35$; N = 1200 rpm.

Tip
○ Square
□ Ogee
◇ Swept

Thrust,
N

(j) $\alpha_s = -12°$; $\mu = 0.30$; N = 1200 rpm.

Torque, N-m

Figure 6.- Continued.

(k) $\alpha_s = -12°$; $\mu = 0.35$; $N = 1200$ rpm.

Tip
○ Square
▢ Ogee
◇ Swept

Thrust,
N

(l) $\alpha_s = -15°$; $\mu = 0.35$; $N = 1200$ rpm.

Torque, N-m

Figure 6.- Continued.

(m) $\alpha_s = -9°$; $\mu = 0.20$; N = 1340 rpm.

Tip
O Square
□ Ogee
◇ Swept

Thrust,
N

(n) $\alpha_s = -12°$; $\mu = 0.30$; N = 1340 rpm.

Torque, N·m

Figure 6.- Continued.

(o) $\alpha_s = -12°$; $\mu = 0.35$; N = 1340 rpm.
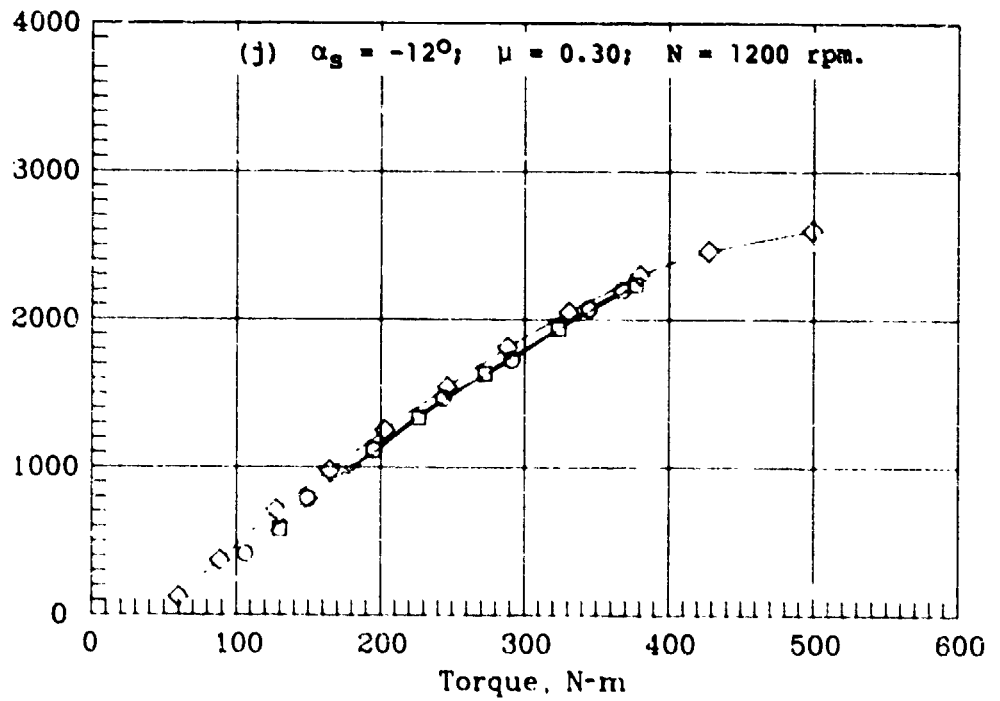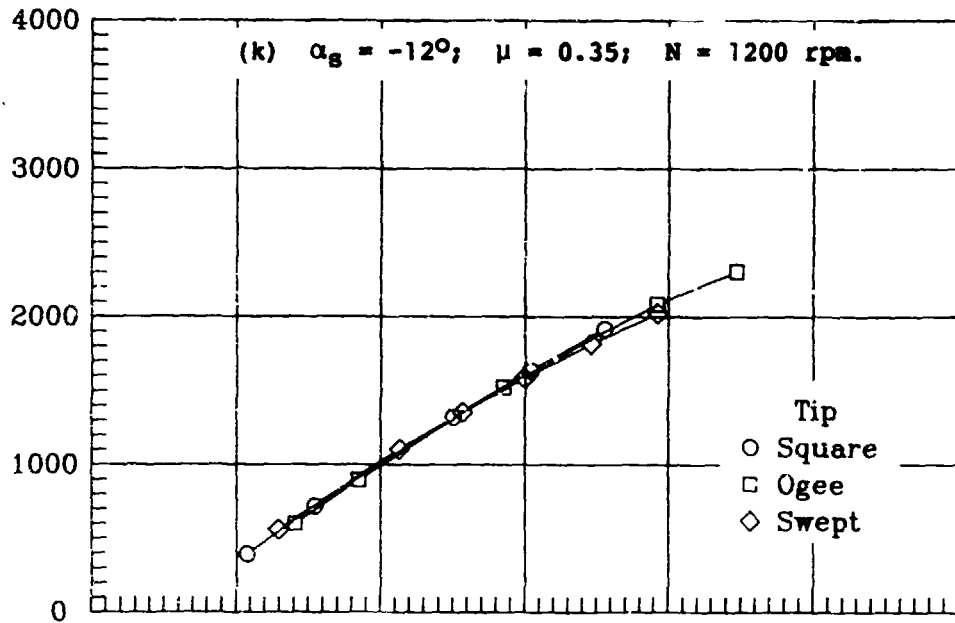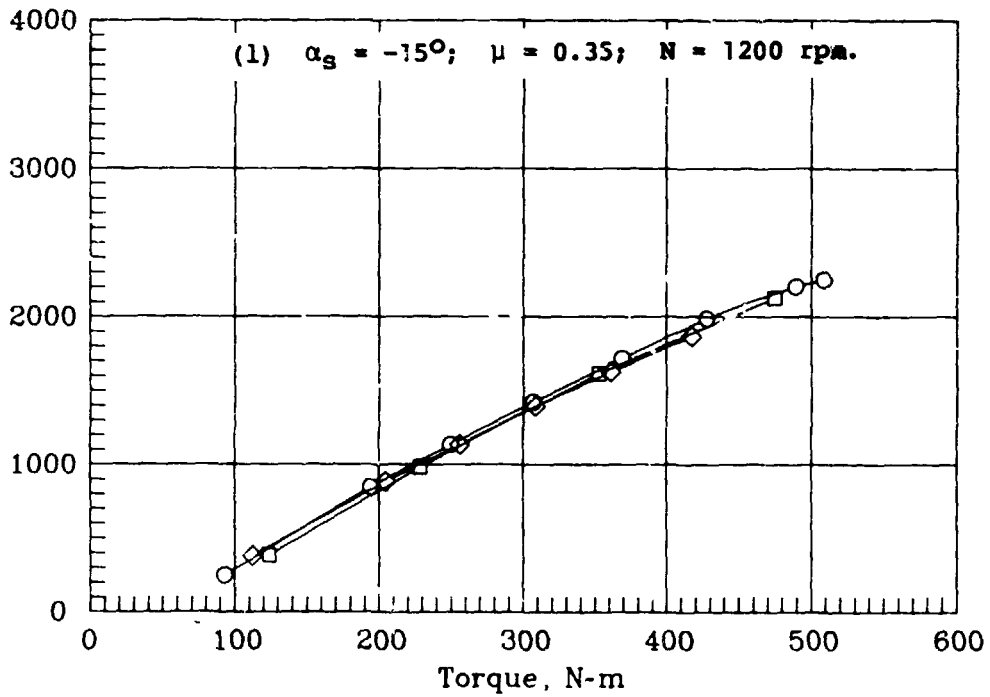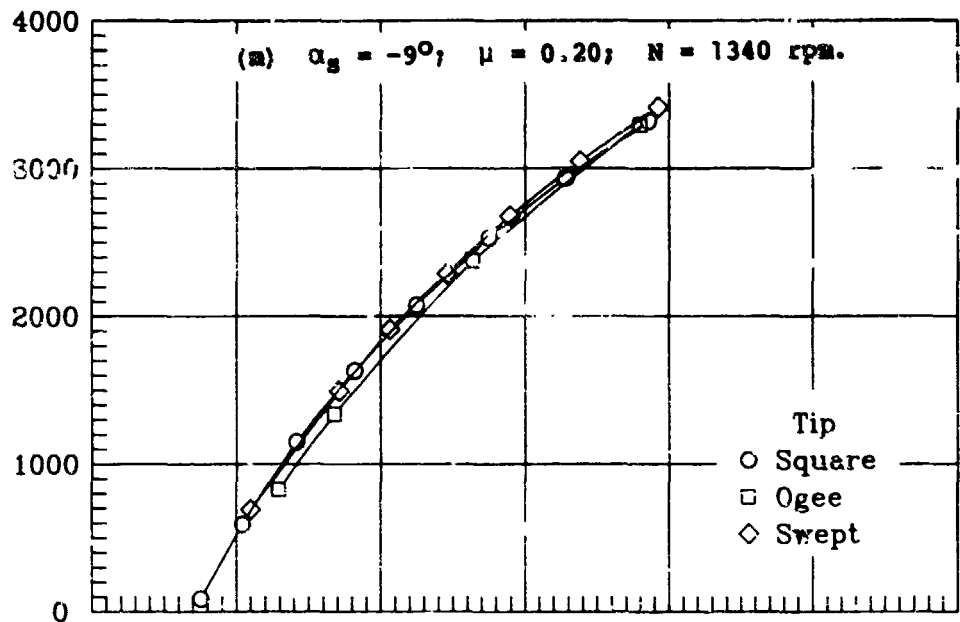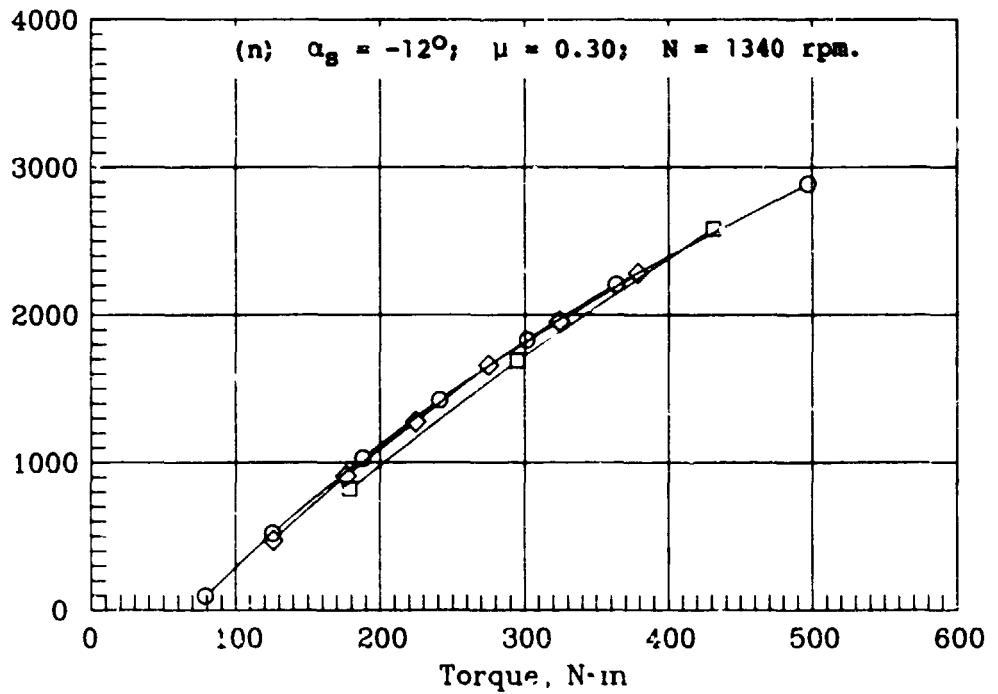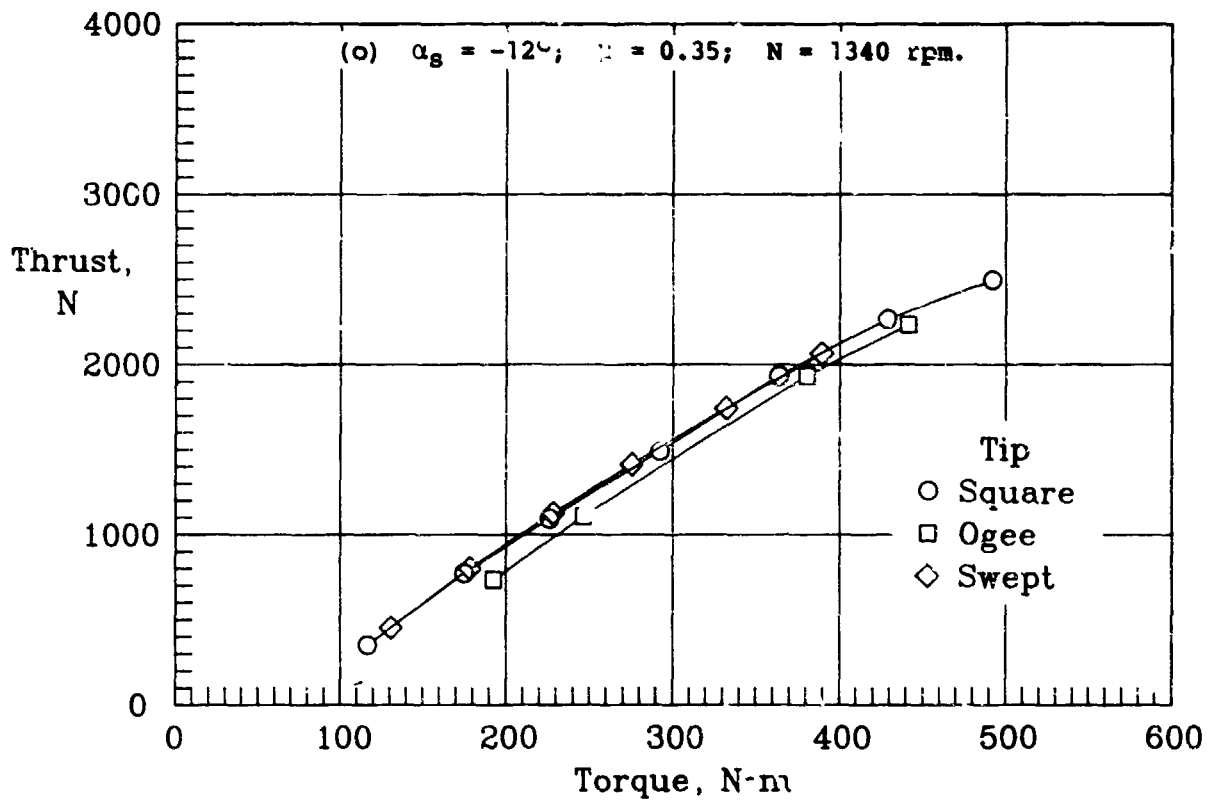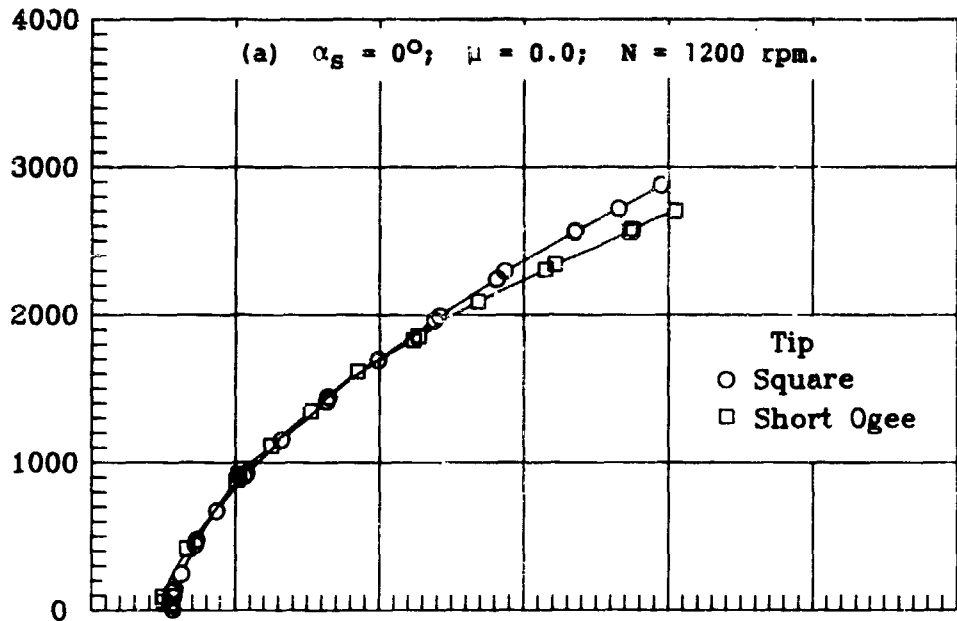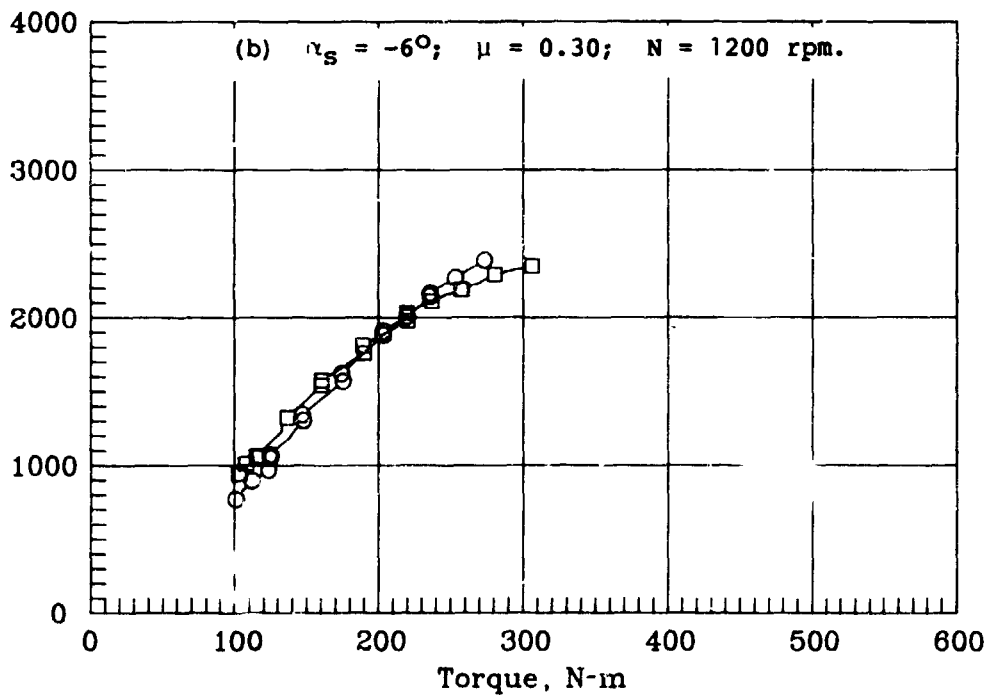
Figure 6.- Concluded.

Figure 7.- Short ogee tip performance.
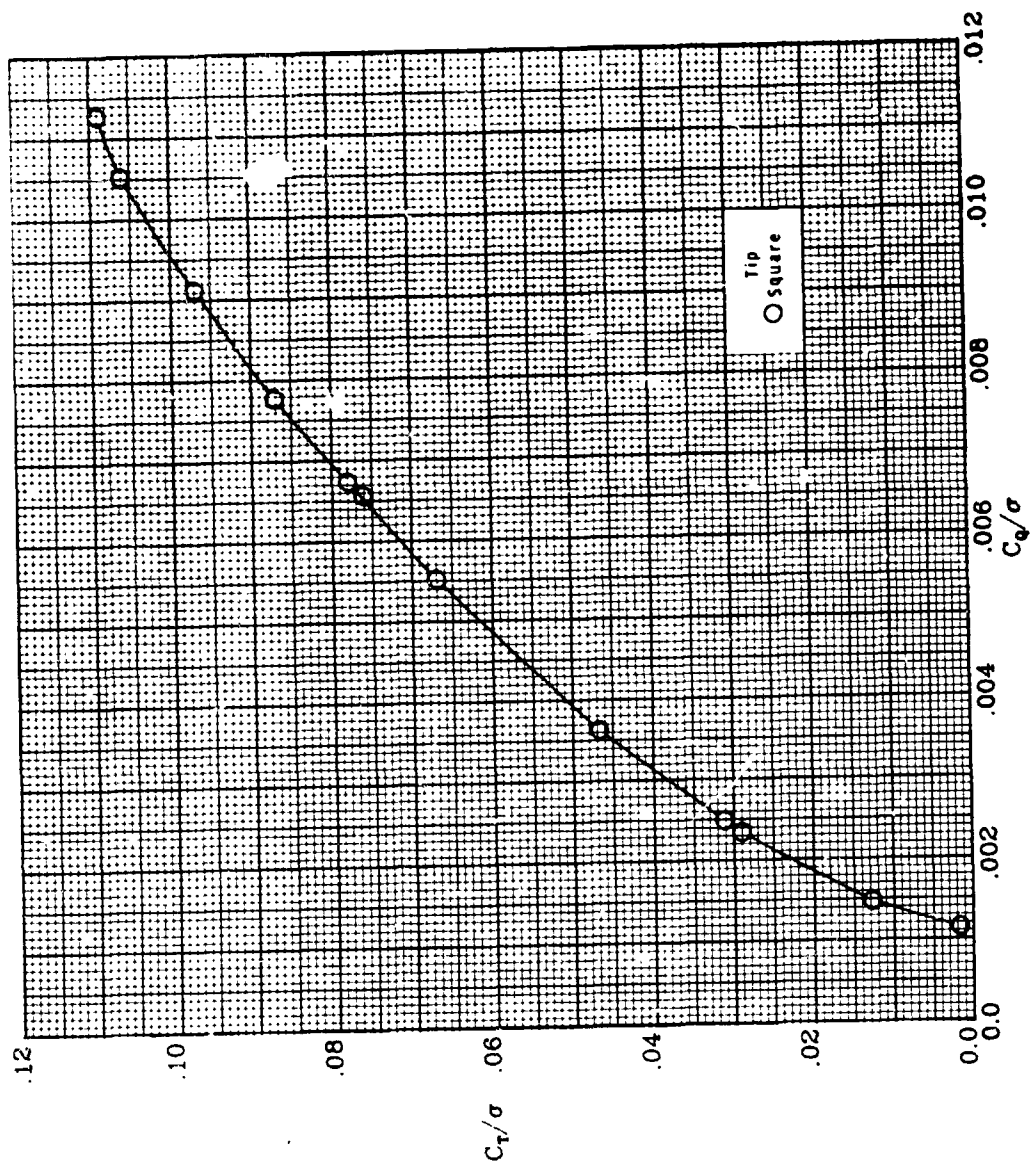
(a) $\mu = 0.0$; $N = 1200$ rpm.

Figure 8.— Square tip performance.
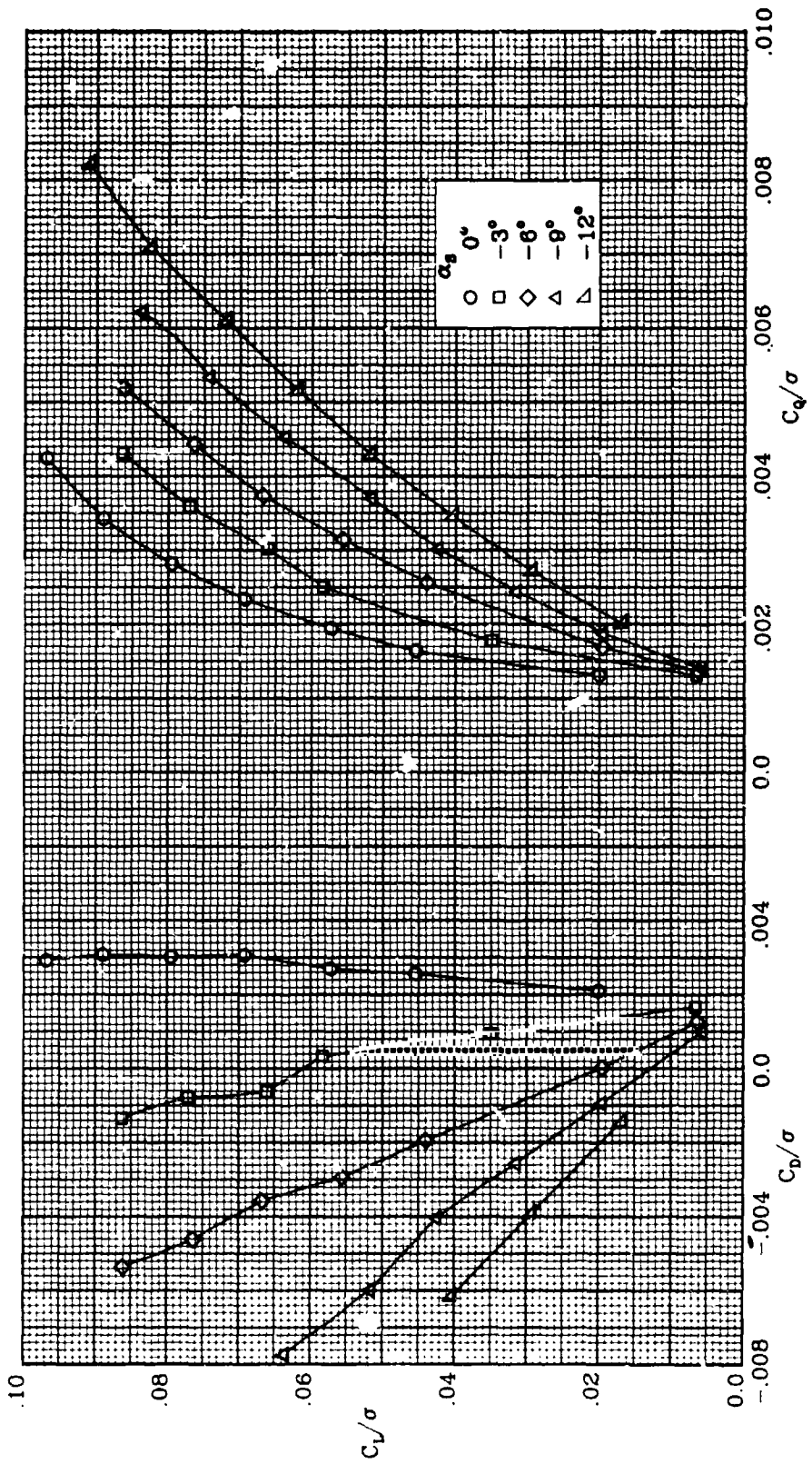
(b) $\mu = 0.20$; $N = 1200$ rpm.
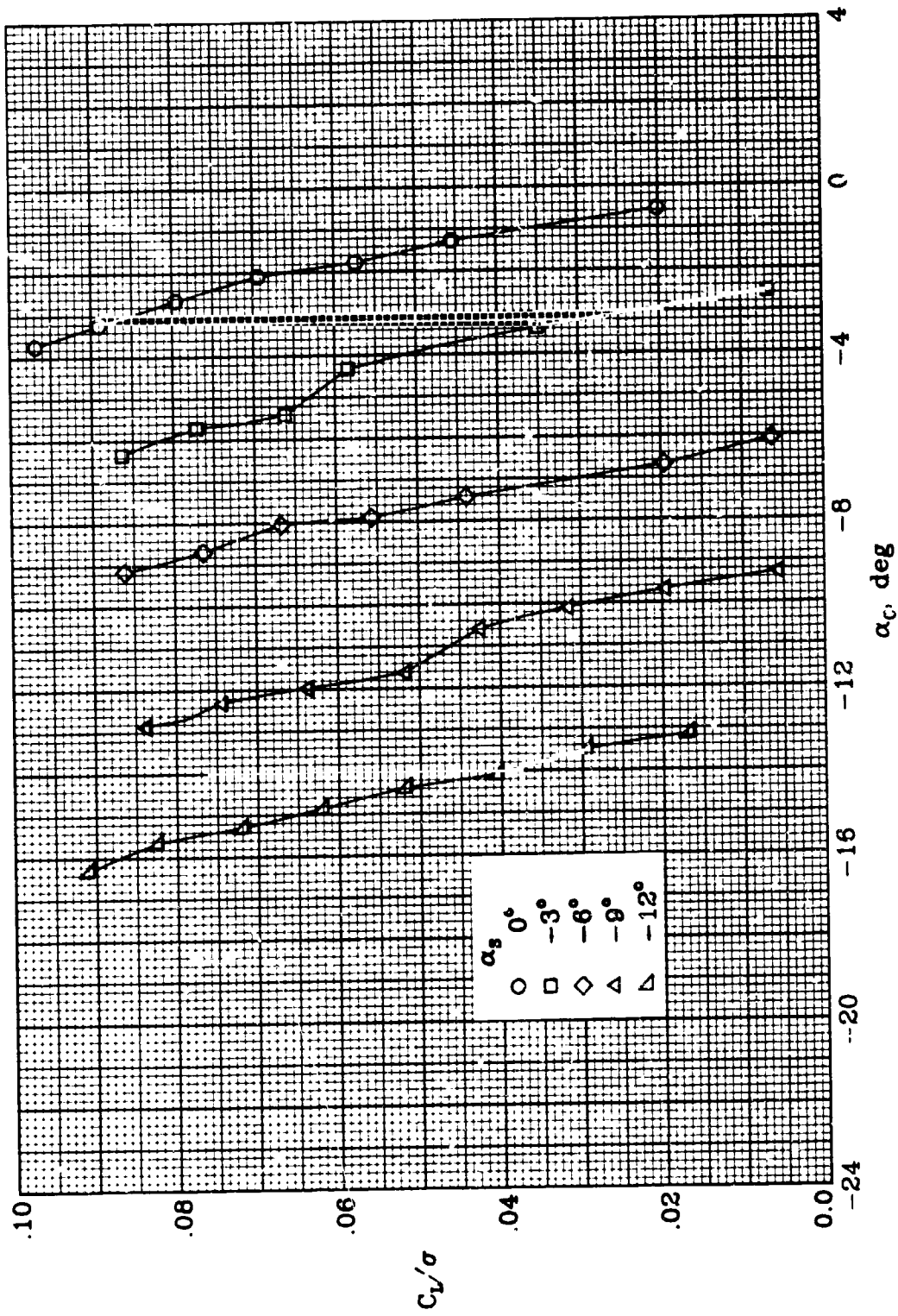
Figure 8.- Continued.

(b) Concluded.
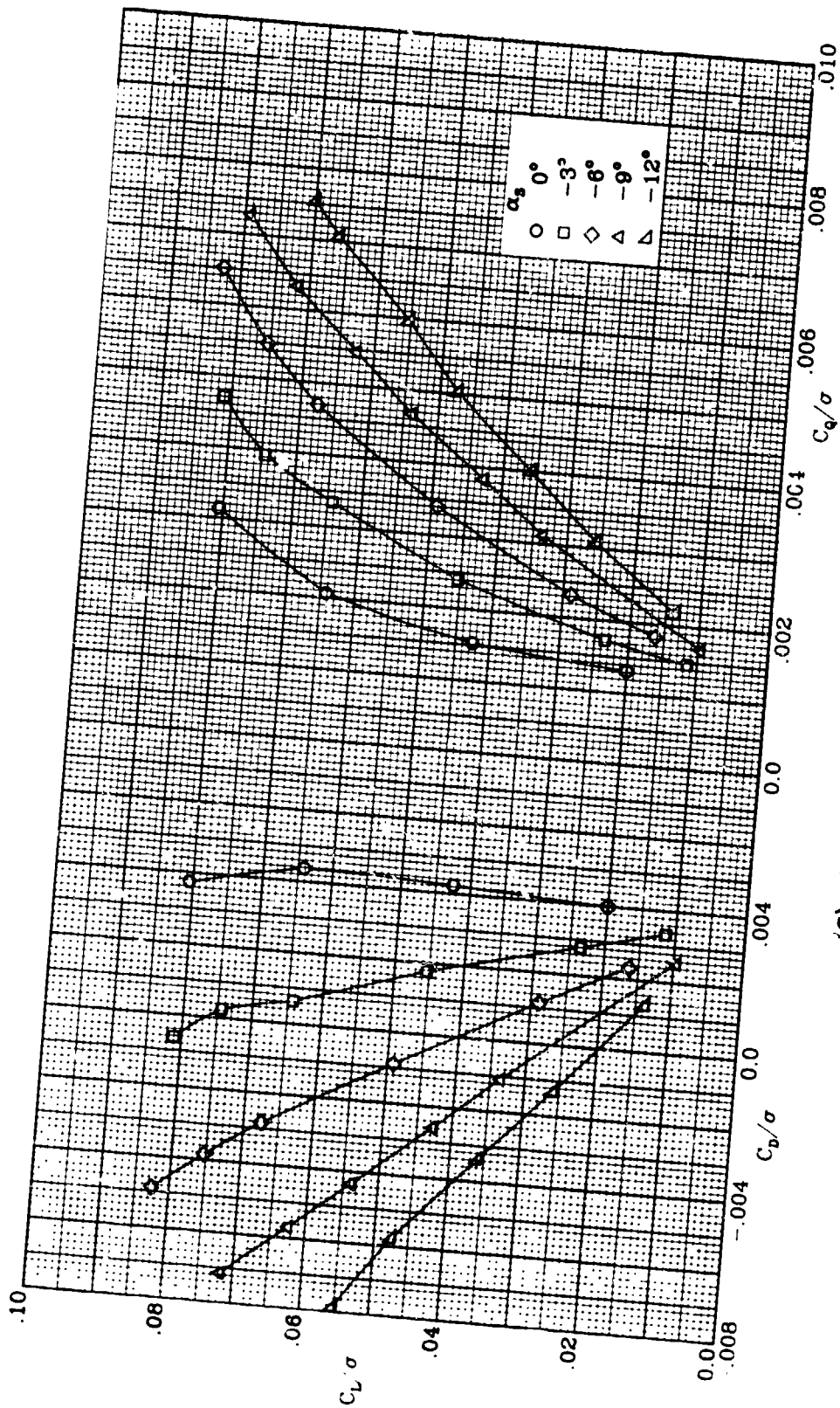
Figure 8.- Continued.

(c) $\mu = 0.30$; $N = 1200$ rpm.
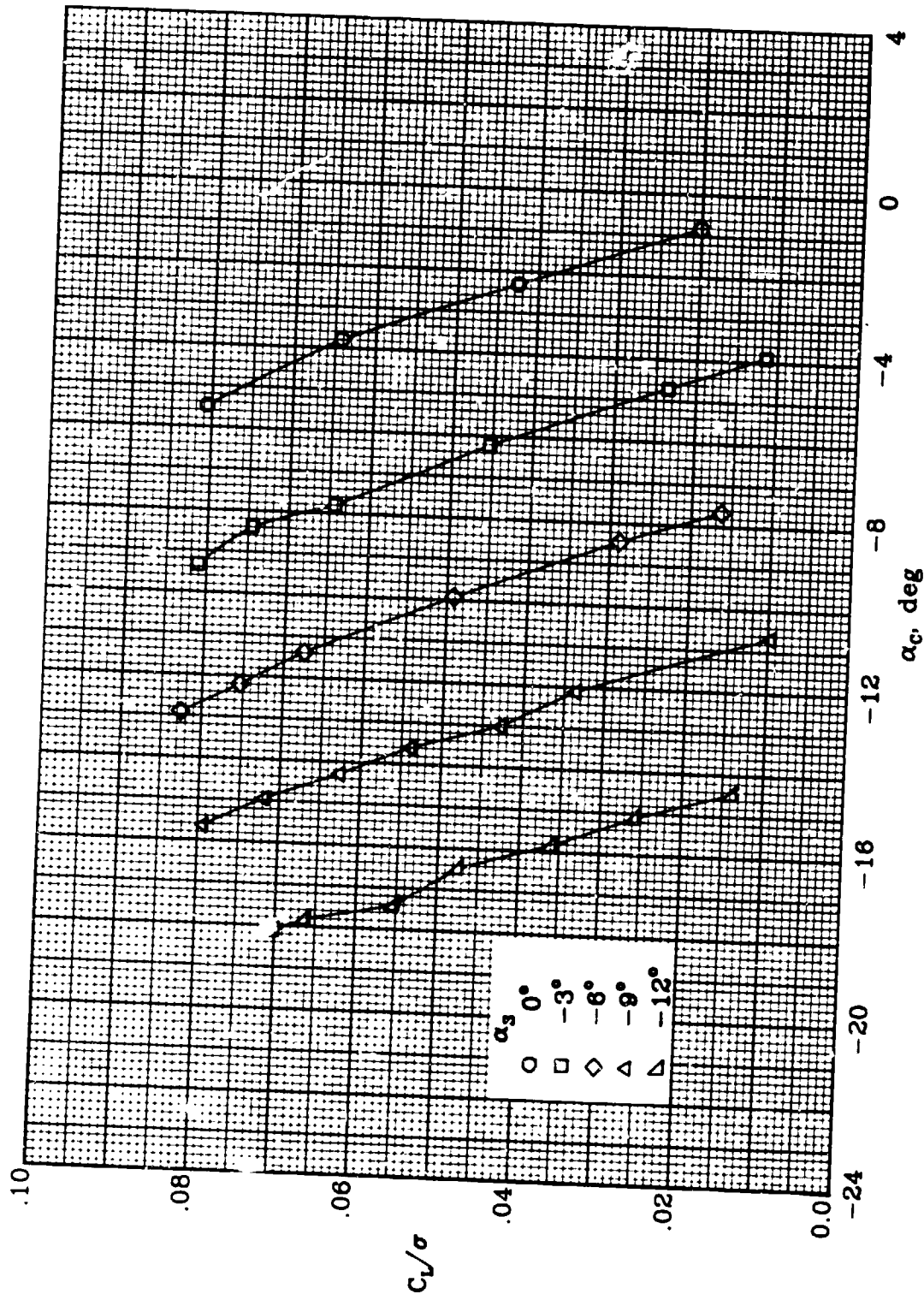
Figure 8.— Continued.

(c) Concluded.
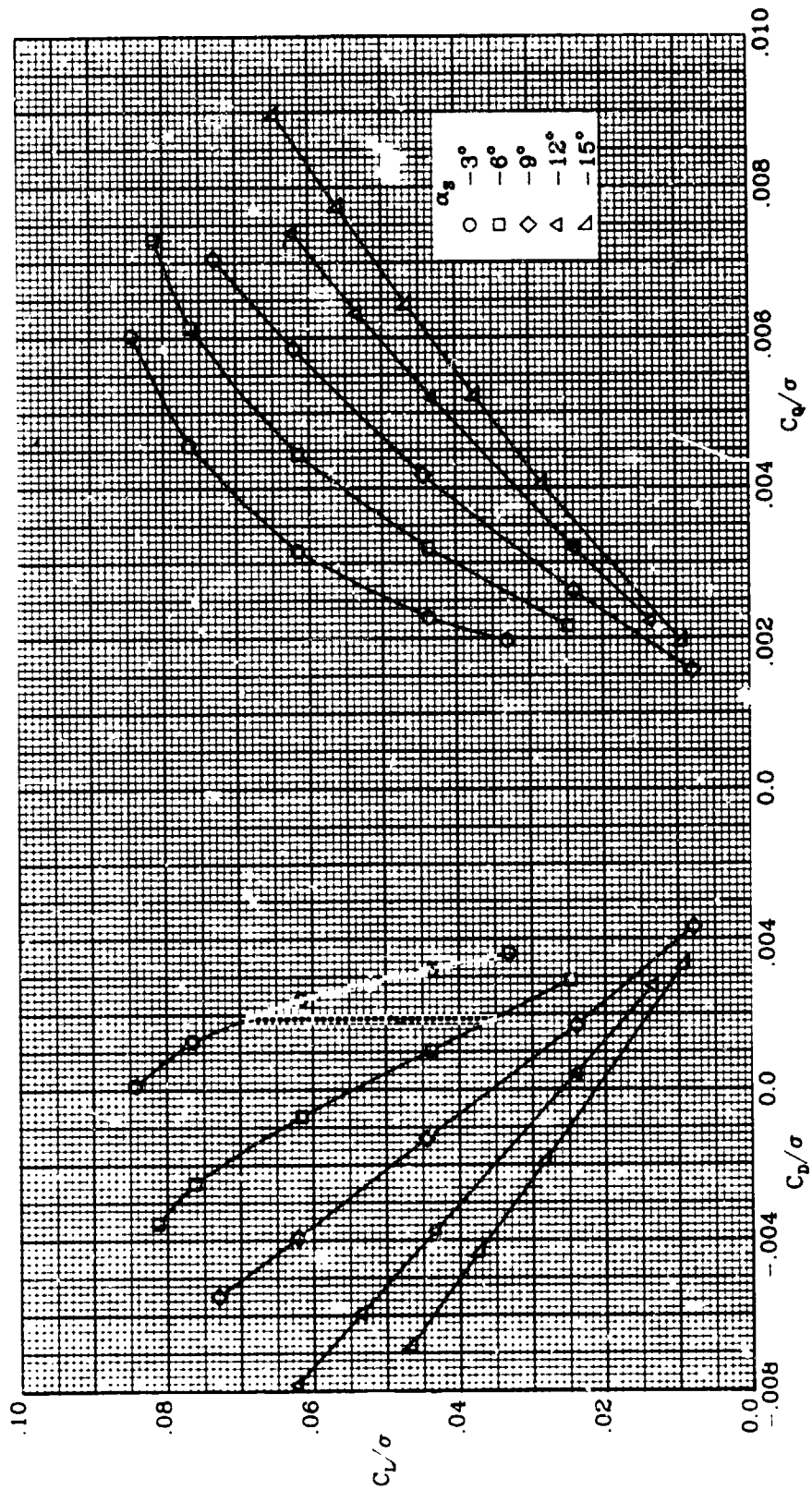
Figure 8.- Continued.

(d) $\mu = 0.35$; N = 1200 rpm.

Figure 8.- Continued.
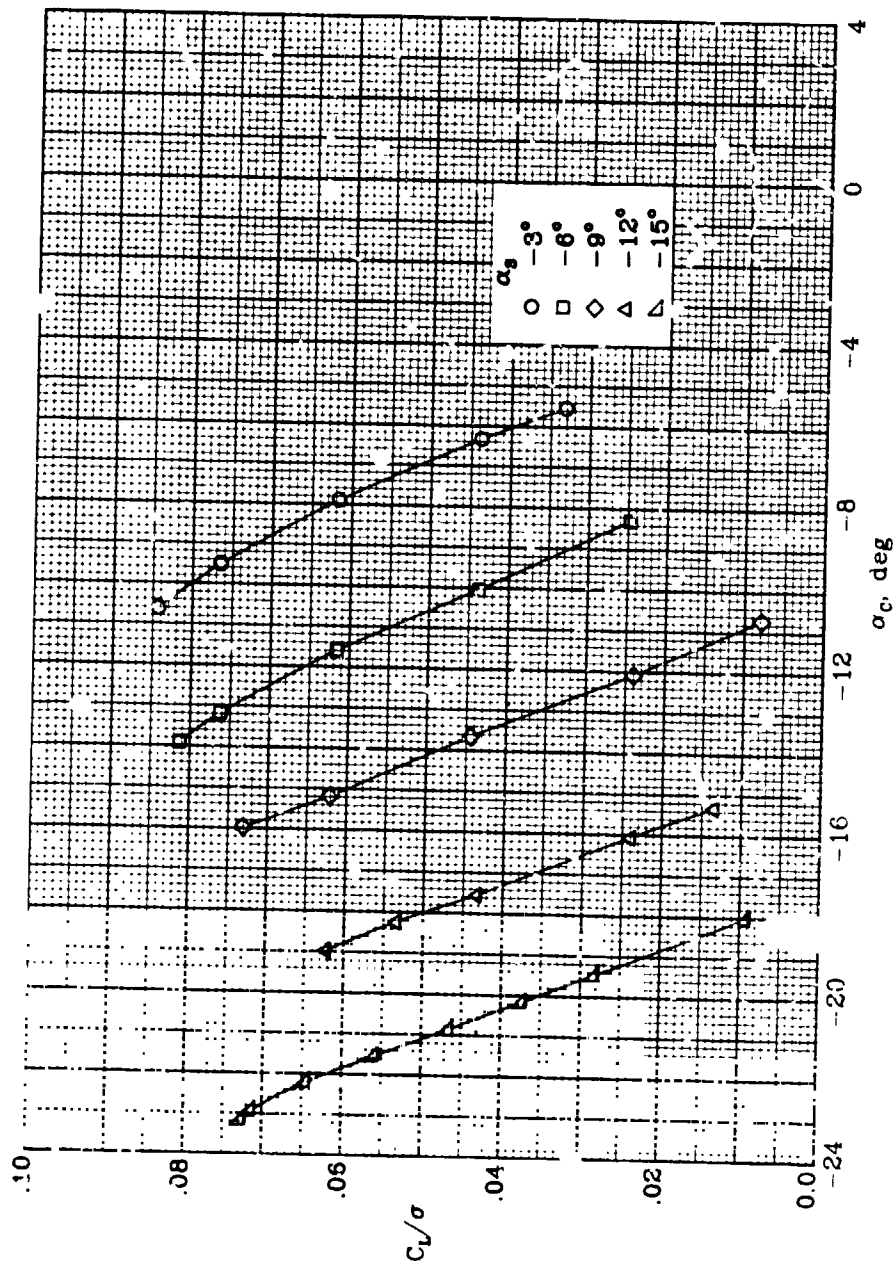
(d) Concluded.
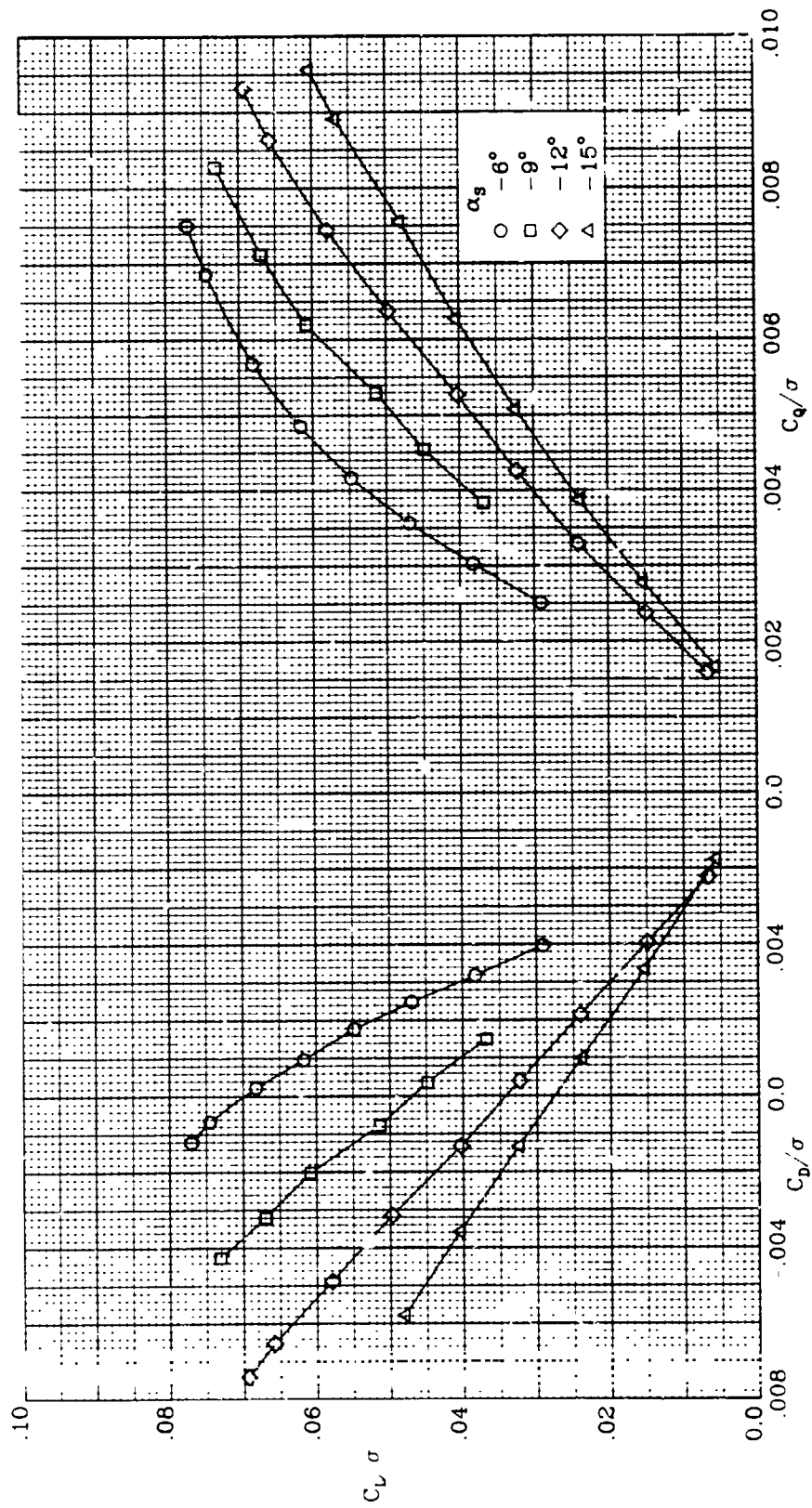
Figure 8.- Continued.

(e) $\mu = 0.40$; $N = 1200$ rpm.

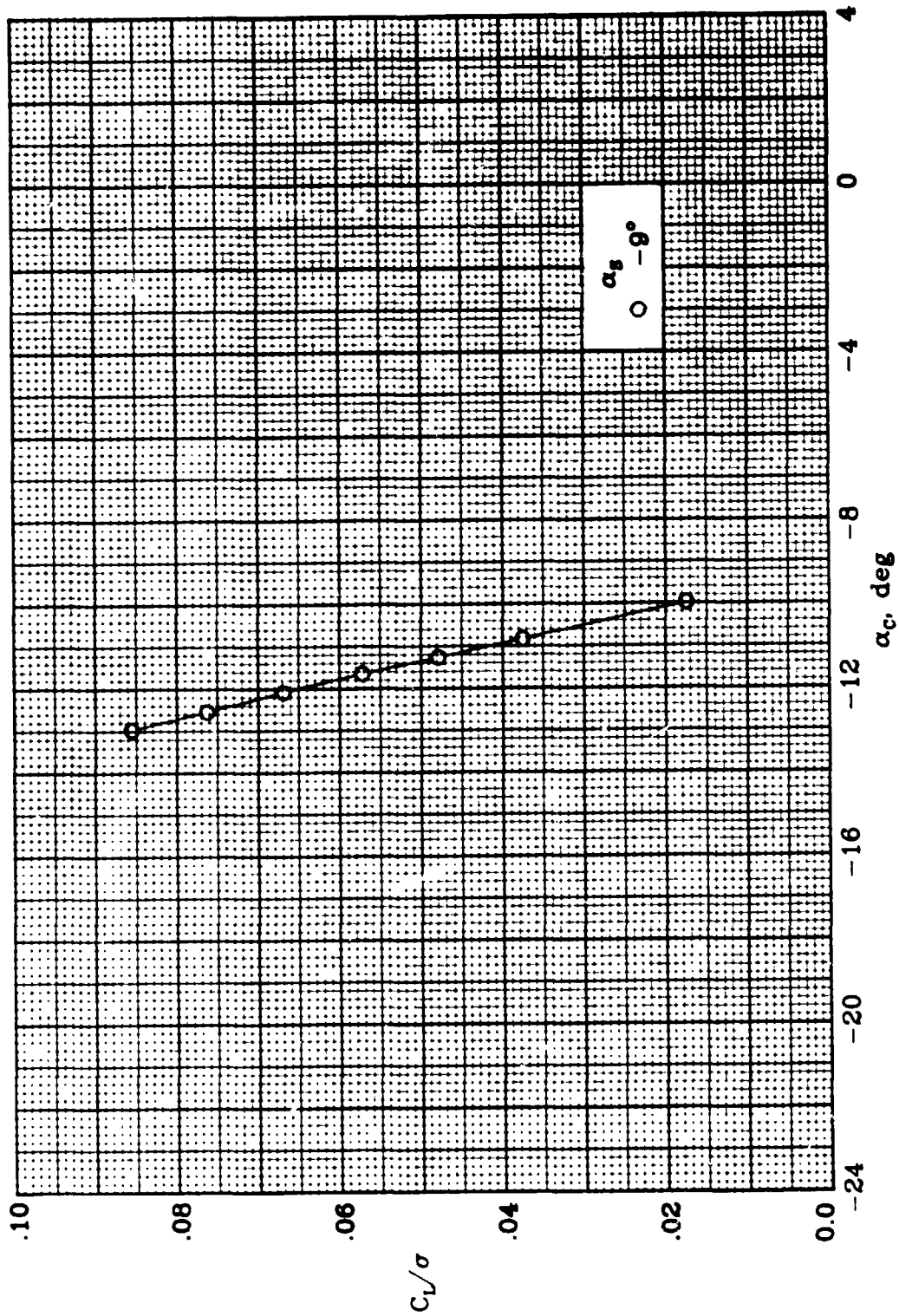Figure 8.- Continued.

40
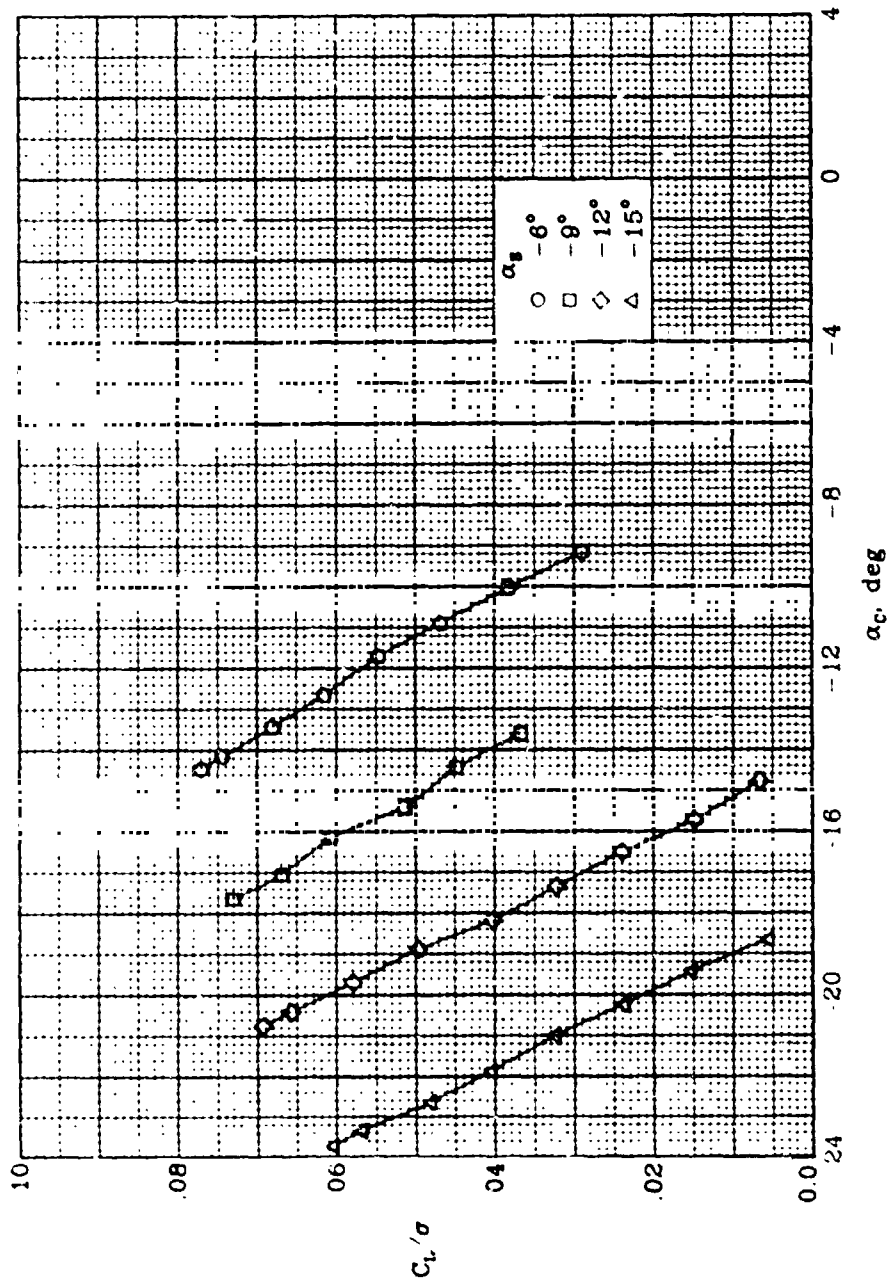
(e) Concluded.

Figure 3.- Continued.
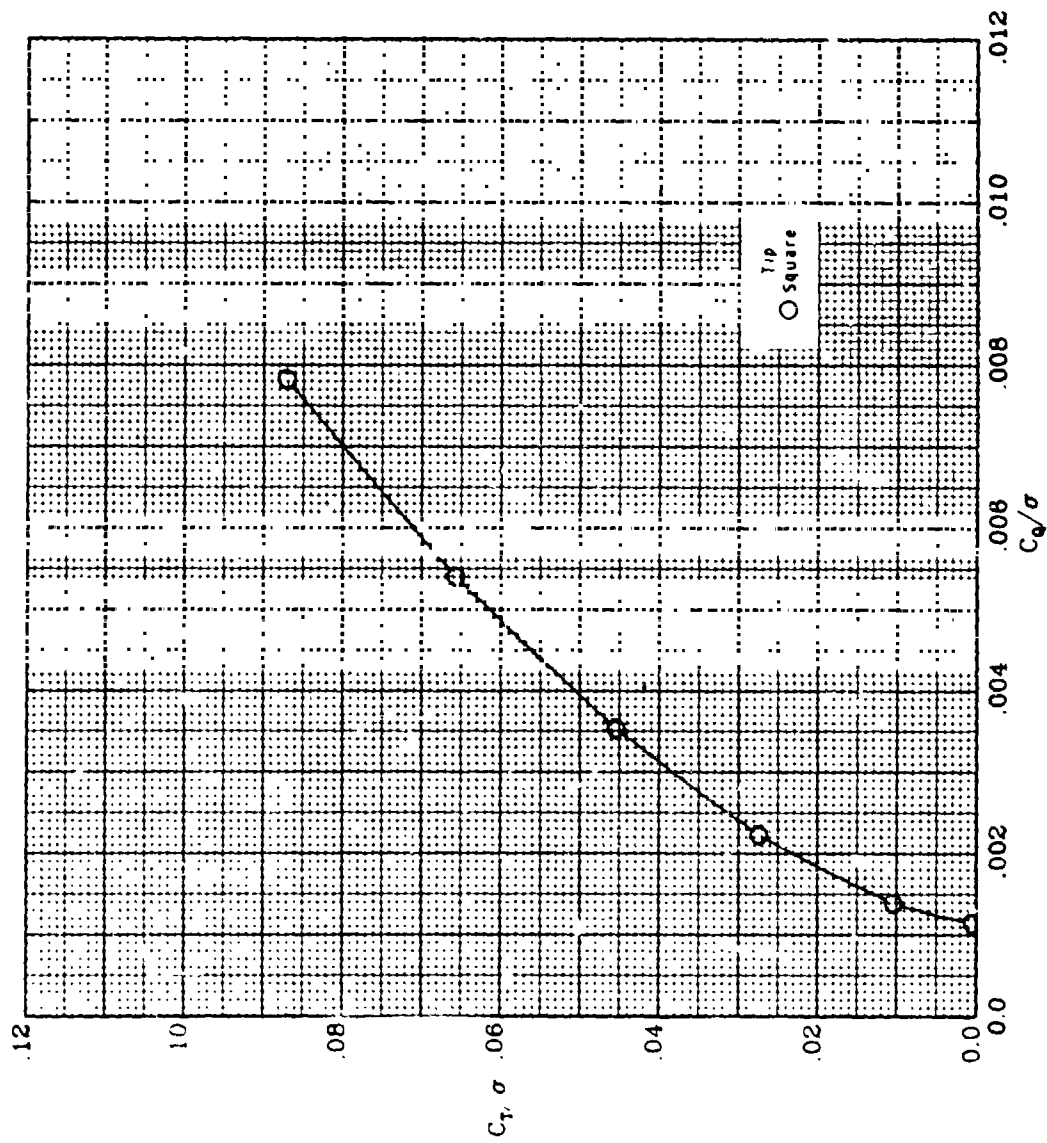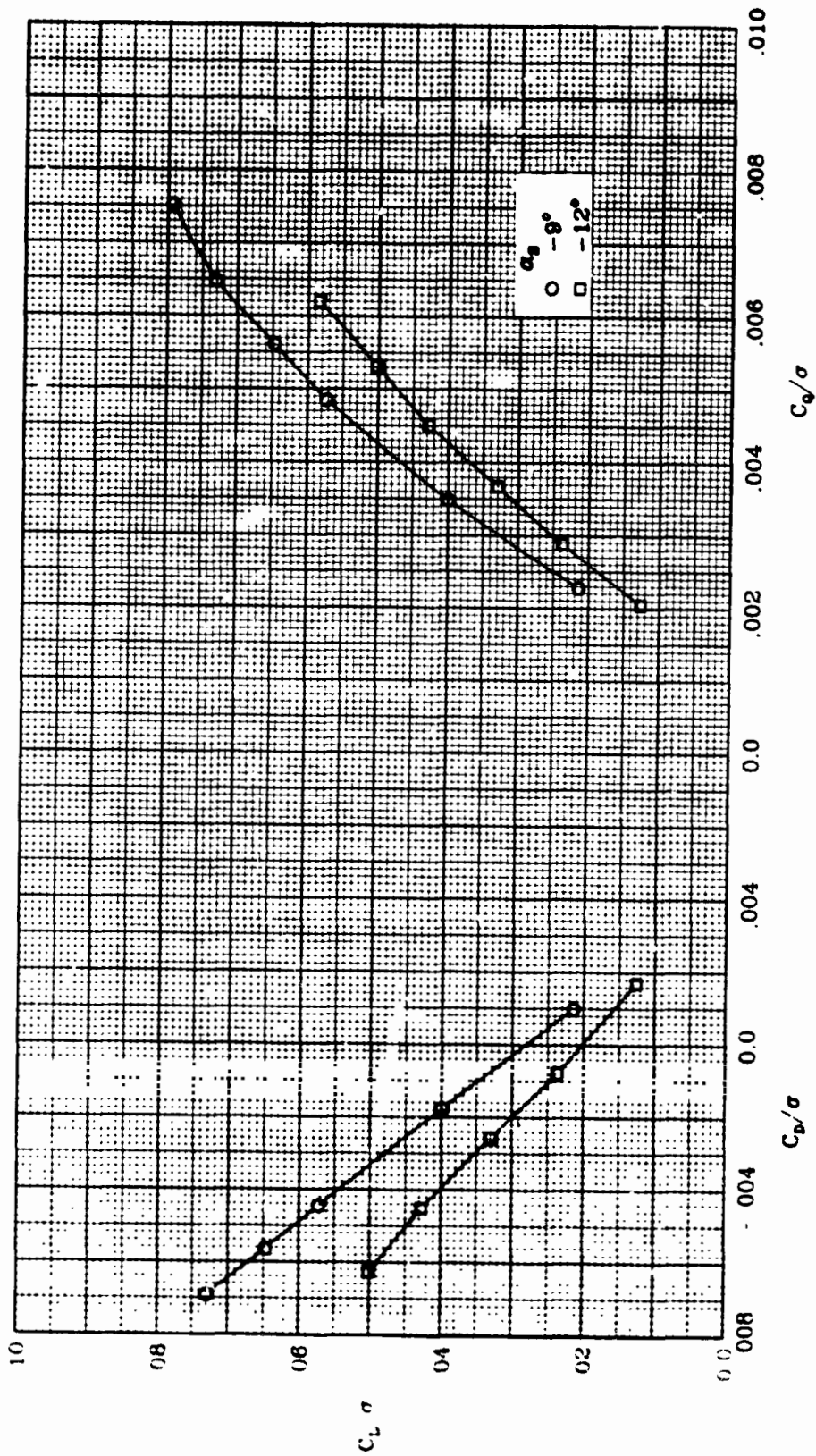
(f) μ = 0.0; N = 1340 rpm.
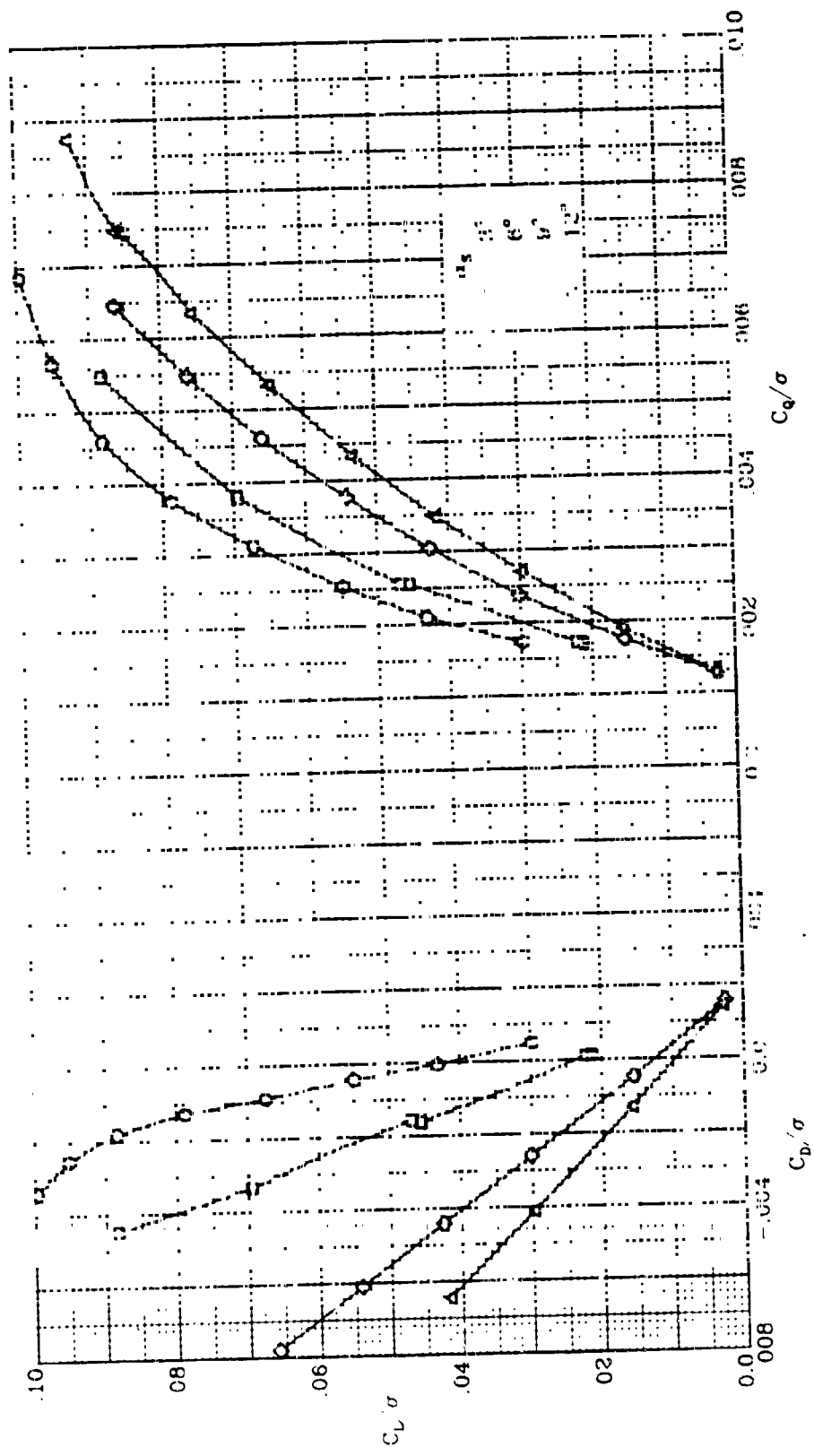
Figure 8.- Continued.

(g) $\mu = 0.20$; N = 1340 rpm.
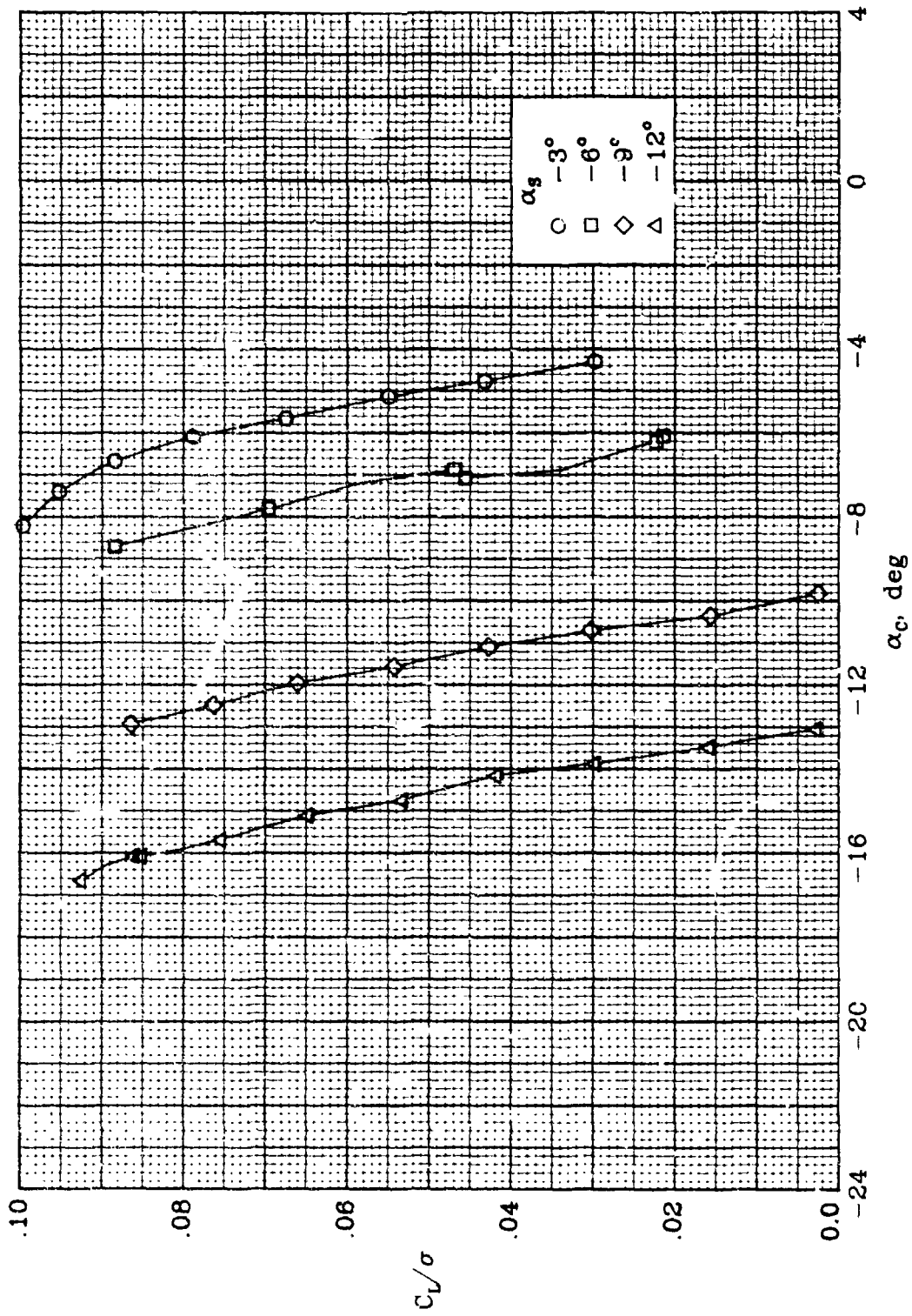
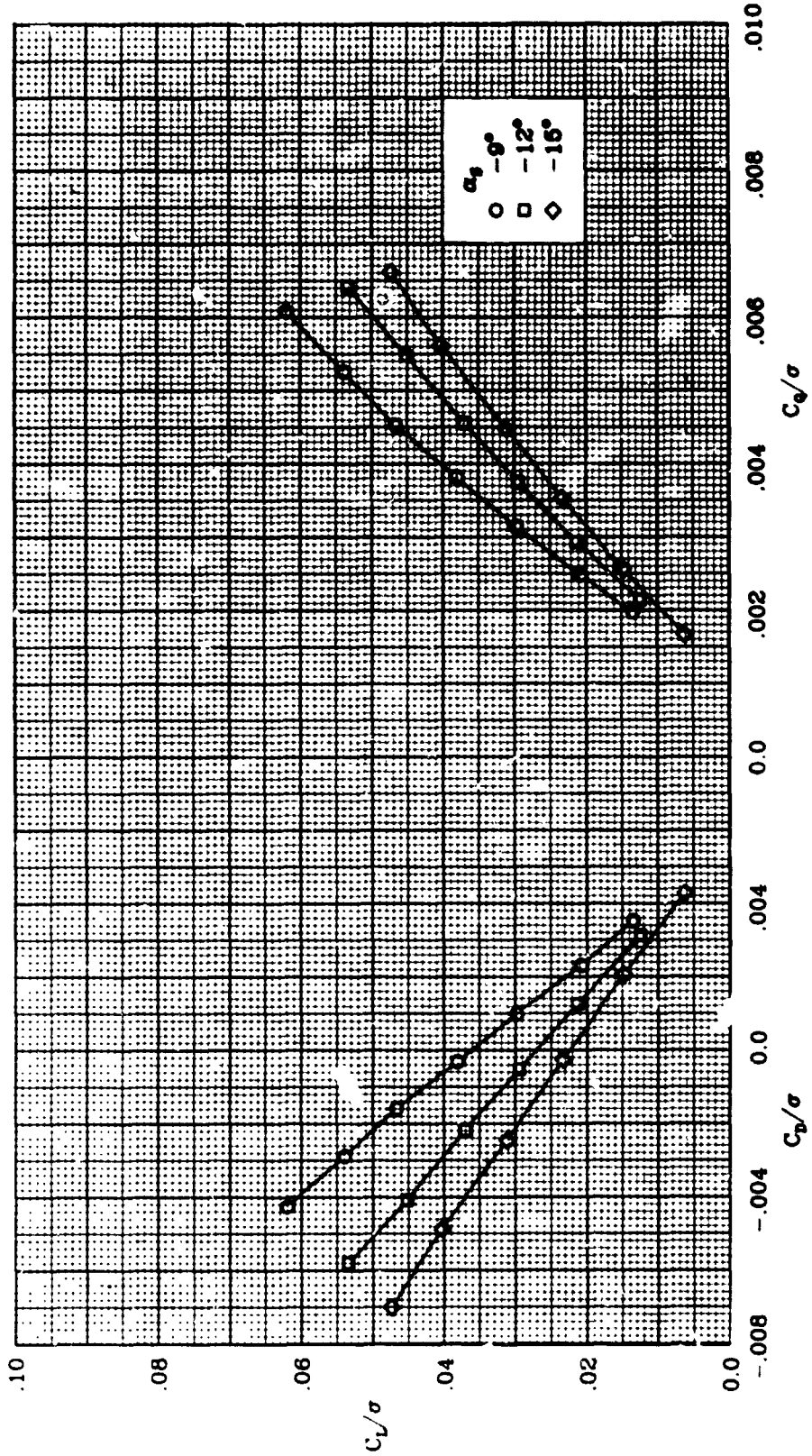Figure 8.- Continued.

(g) Concluded.
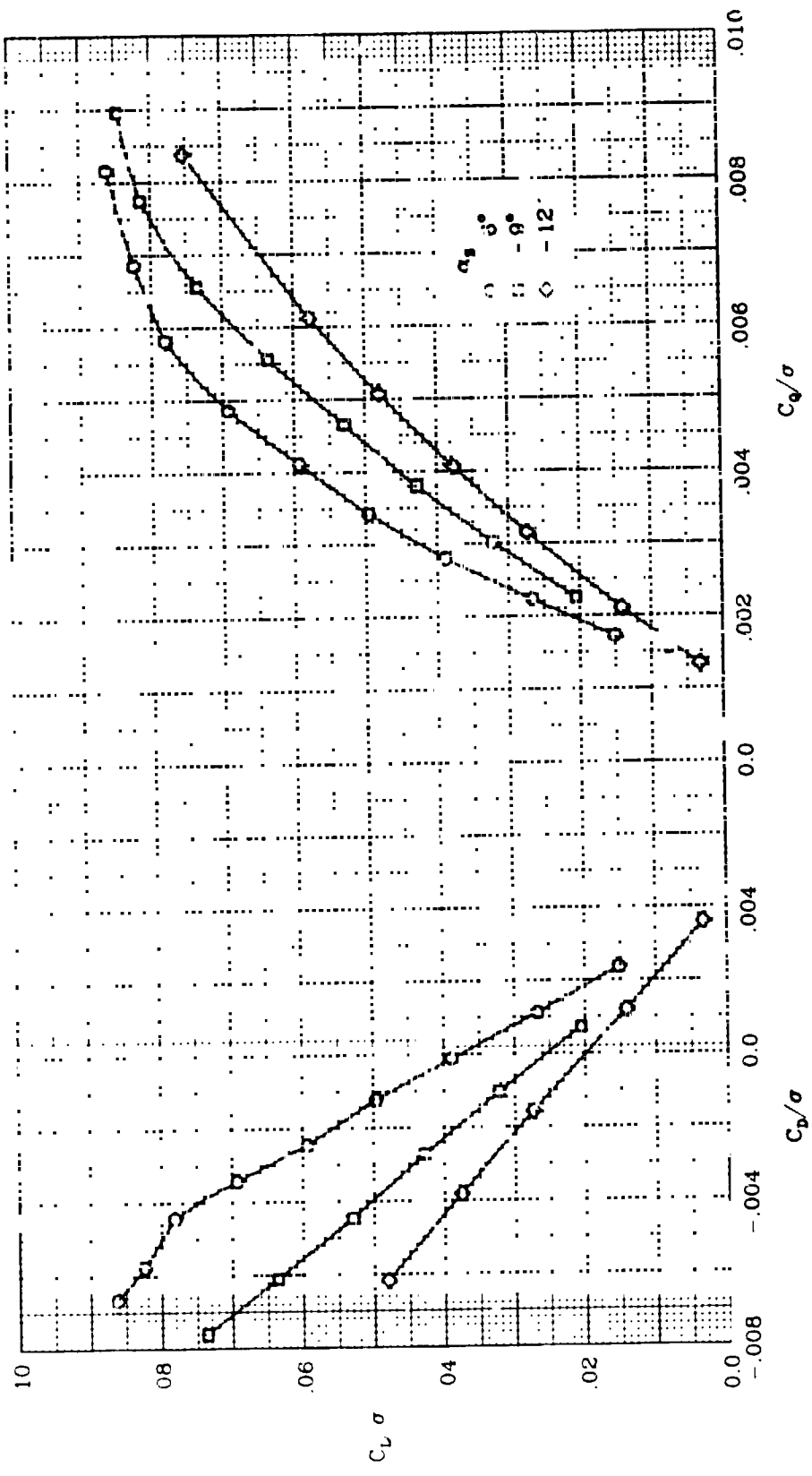
Figure 8.- Continued.

(h) $\mu = 0.30$; $N = 1340$ rpm.
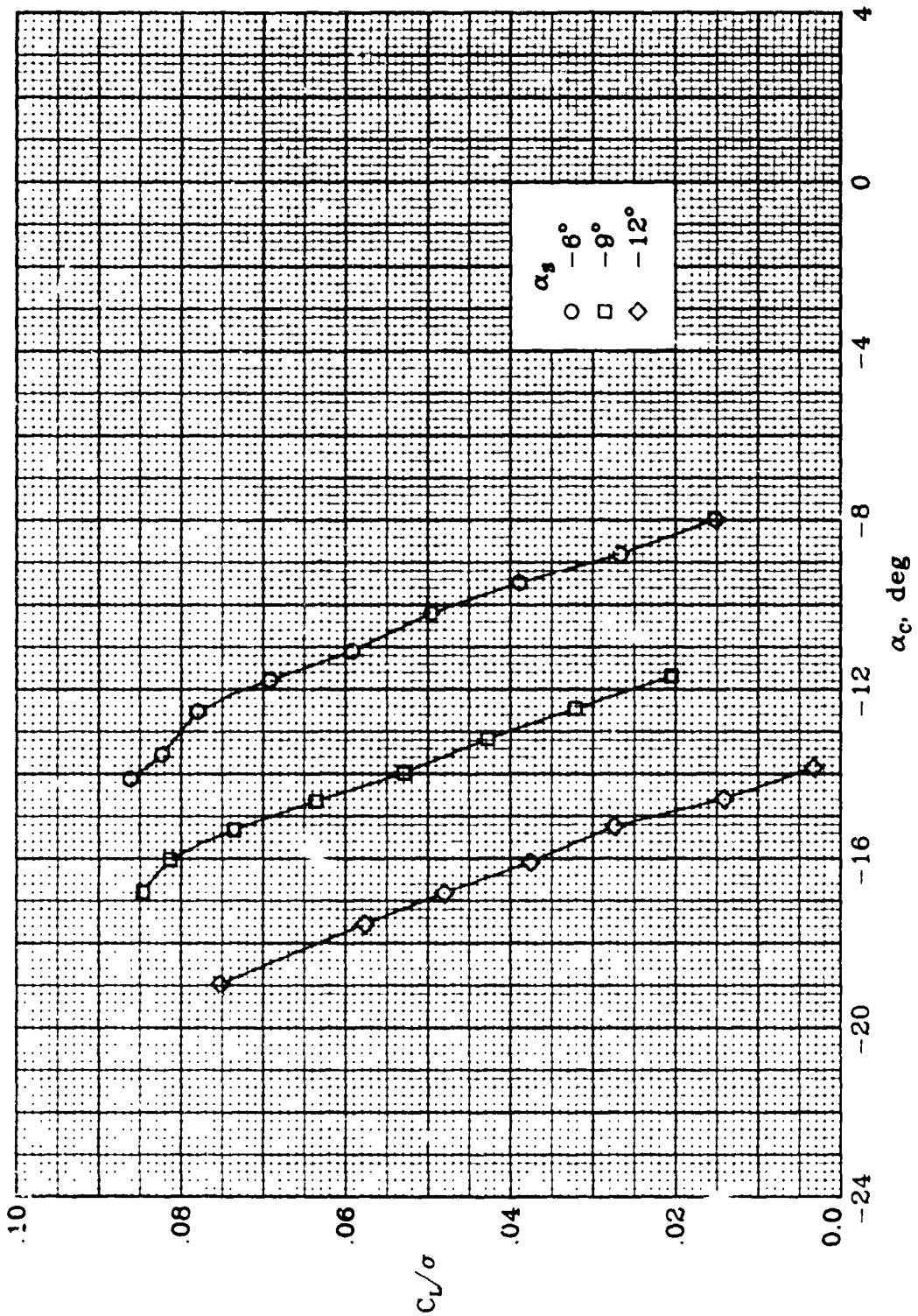
Figure 8.- Continued.

(h) Concluded.
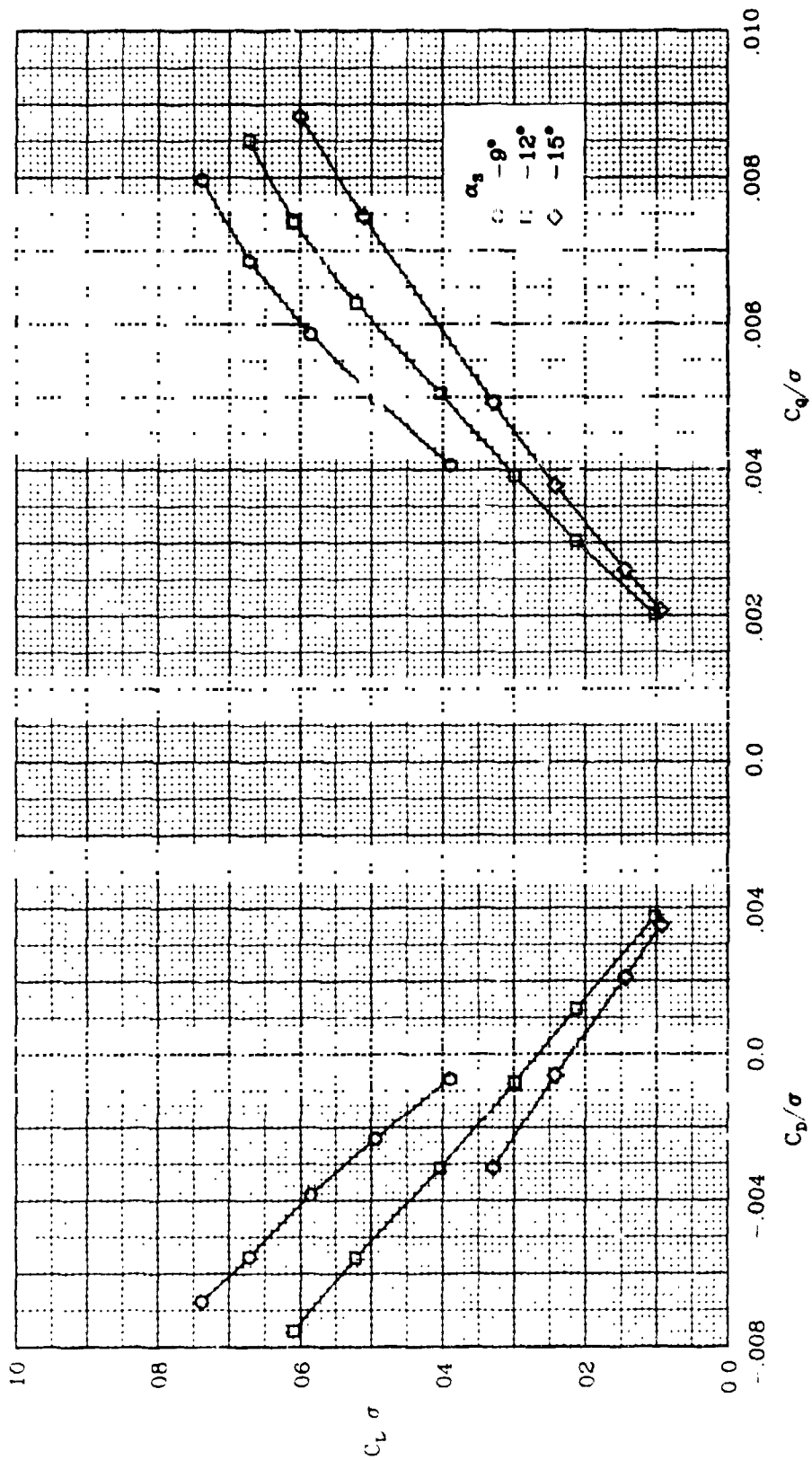
Figure 8.- Continued.

(i) $\mu = 0.35$; $N = 1340$ rpm.

Figure 8.- Continued.

47
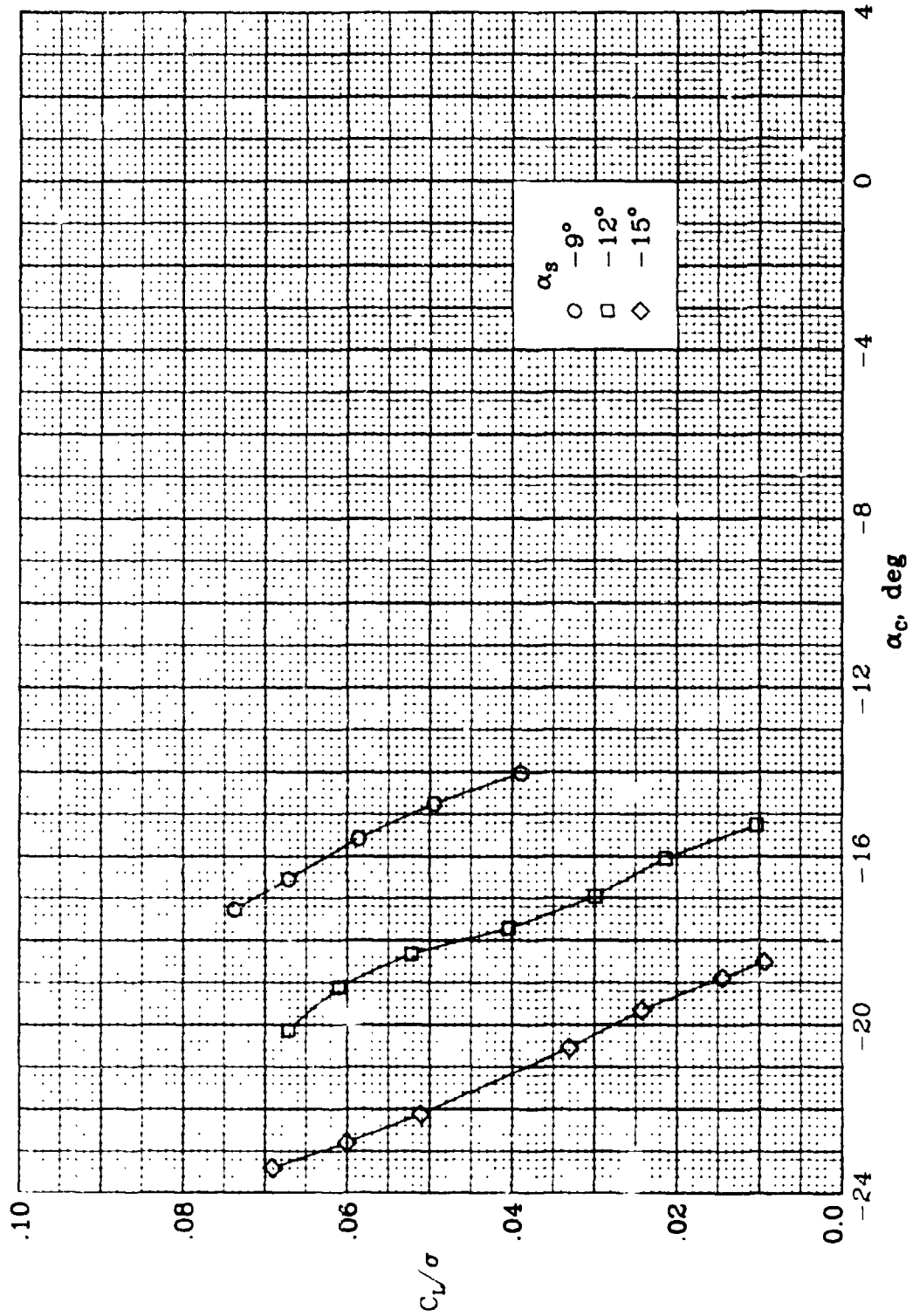
(i) Concluded.

Figure 8.- Concluded.
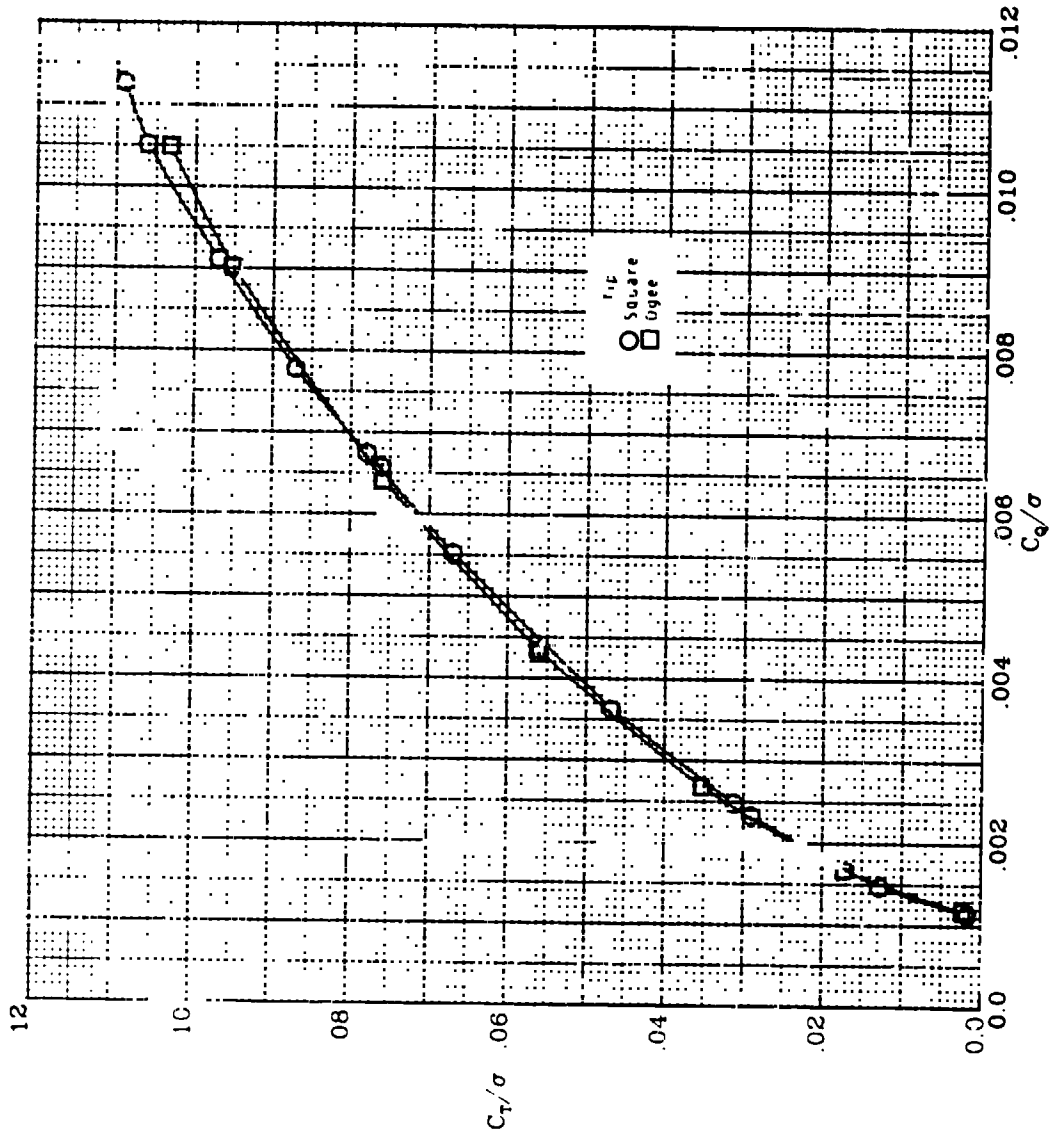
(a) $\mu = 0.0$; $N = 1200$ rpm.

Figure 9.- Ogee tip performance.
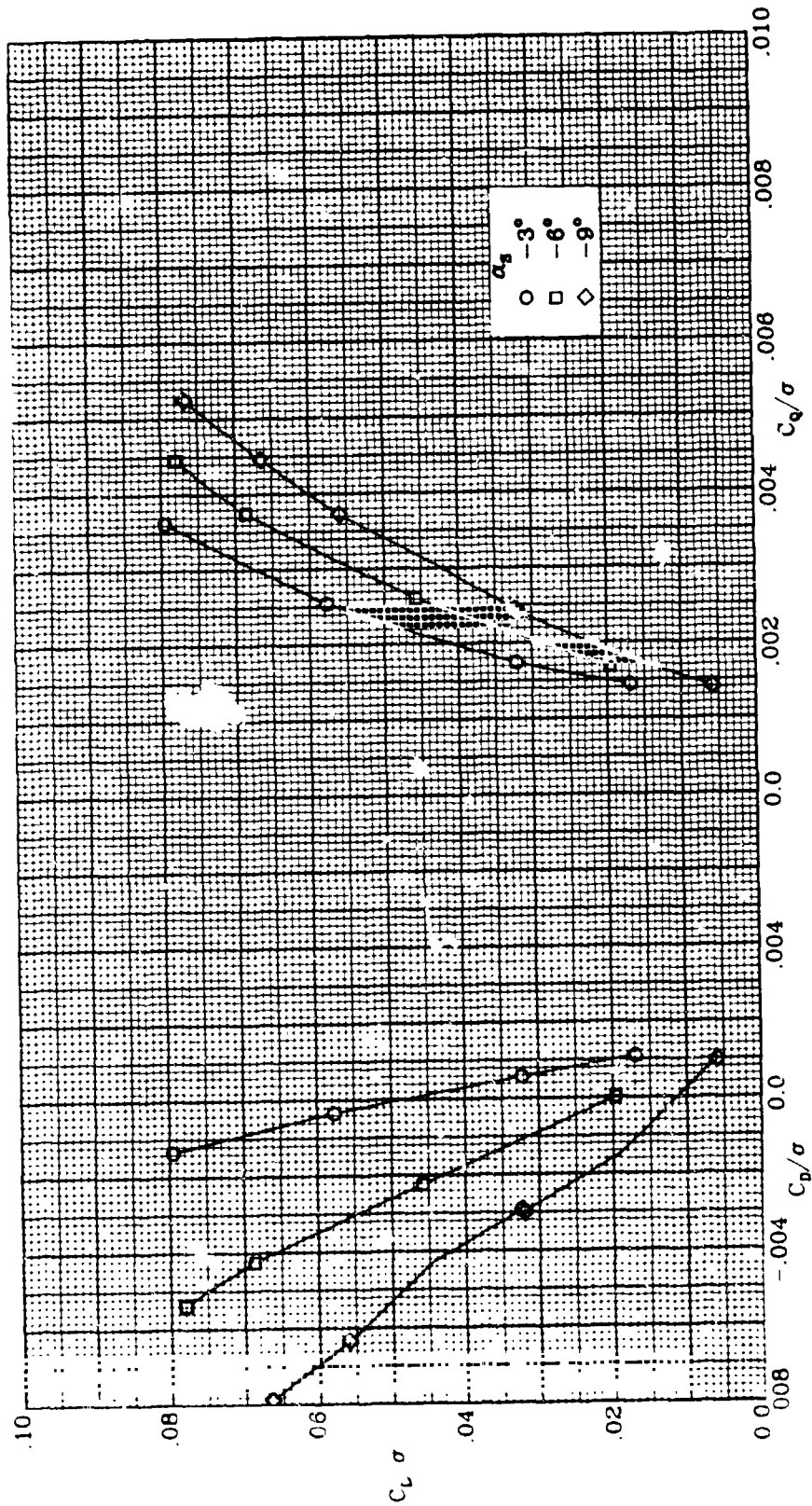
(b) $\mu = 0.20$; $N = 1200$ rpm.
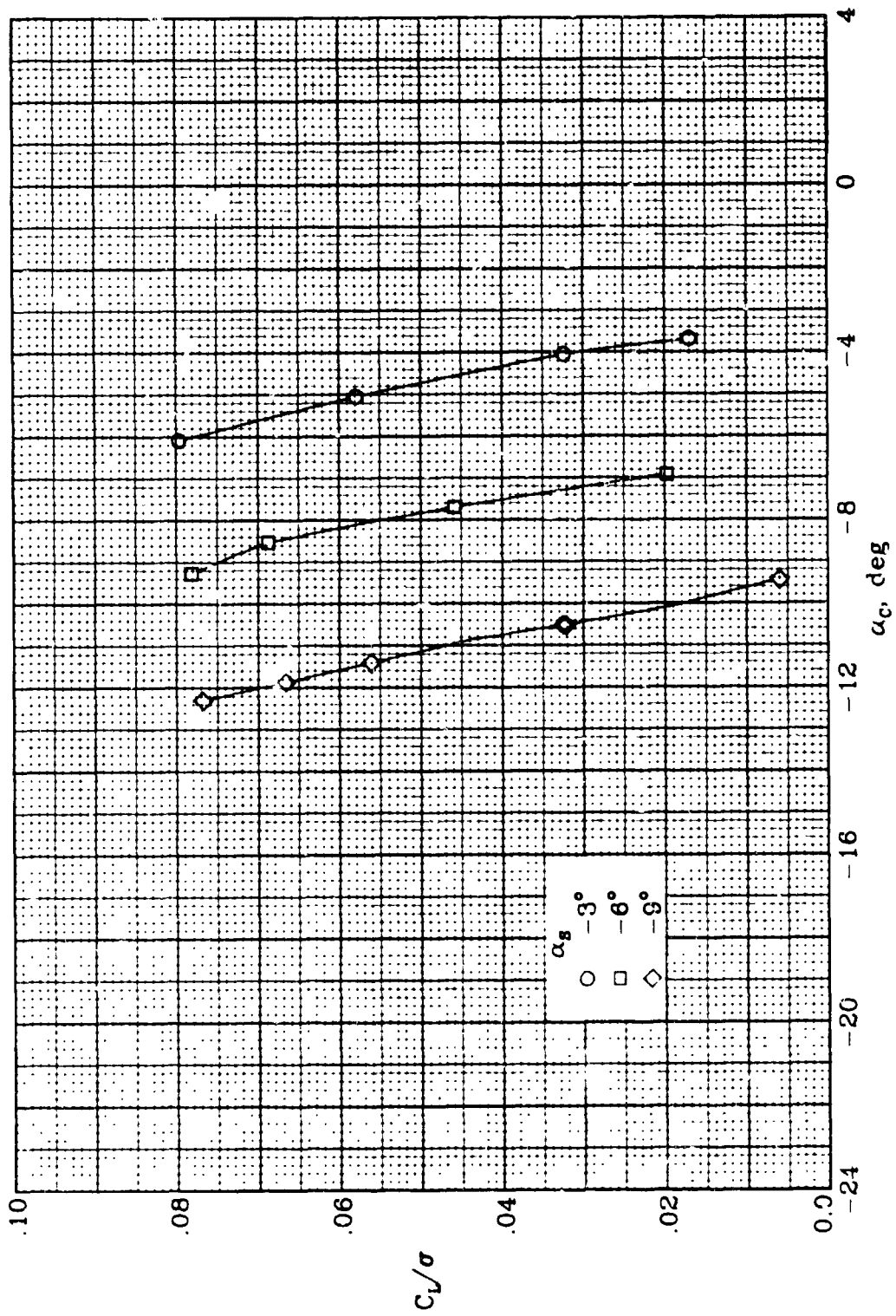
Figure 9.- Continued.

(b) Concluded.
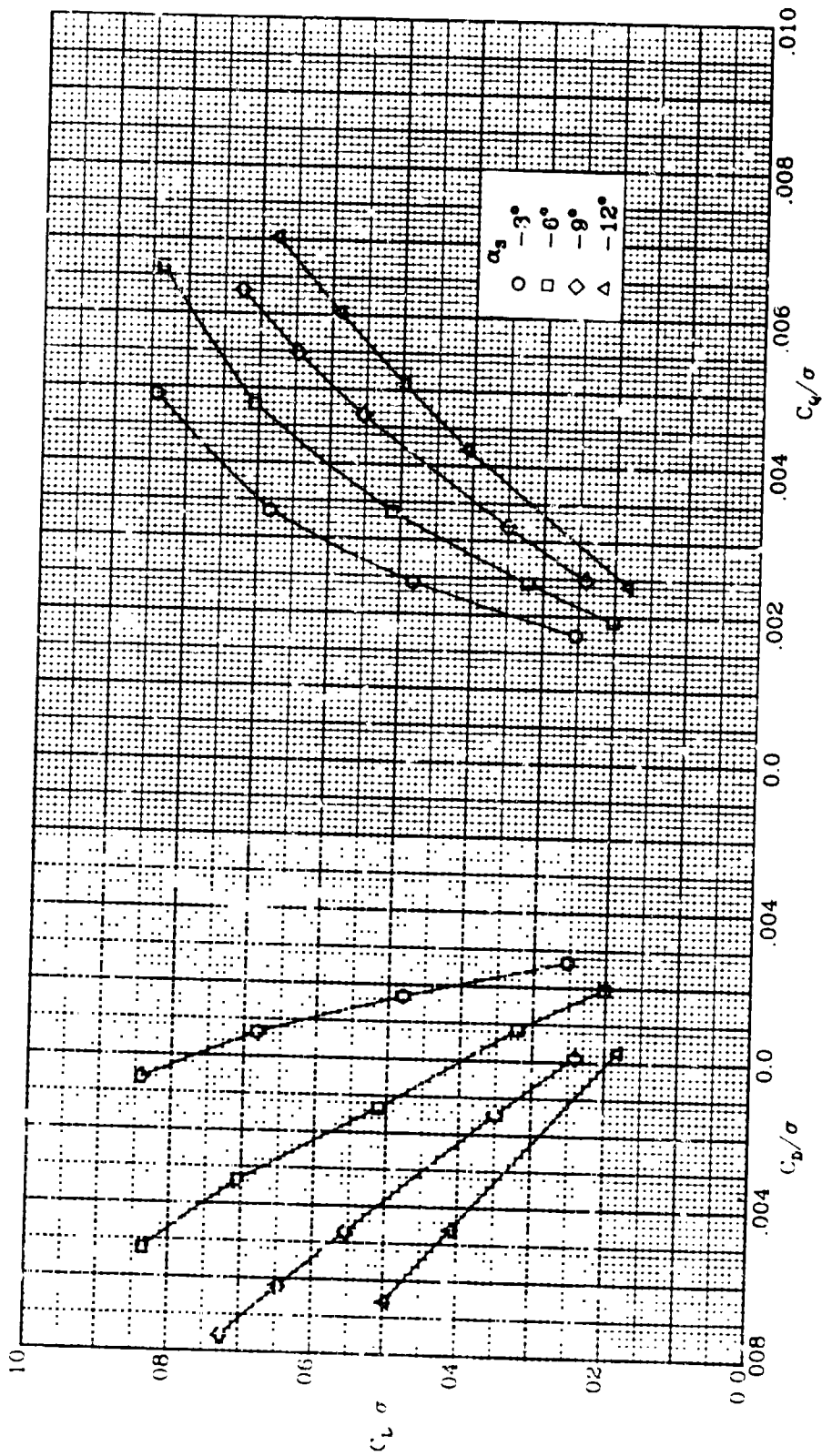
Figure 9.- Continued.
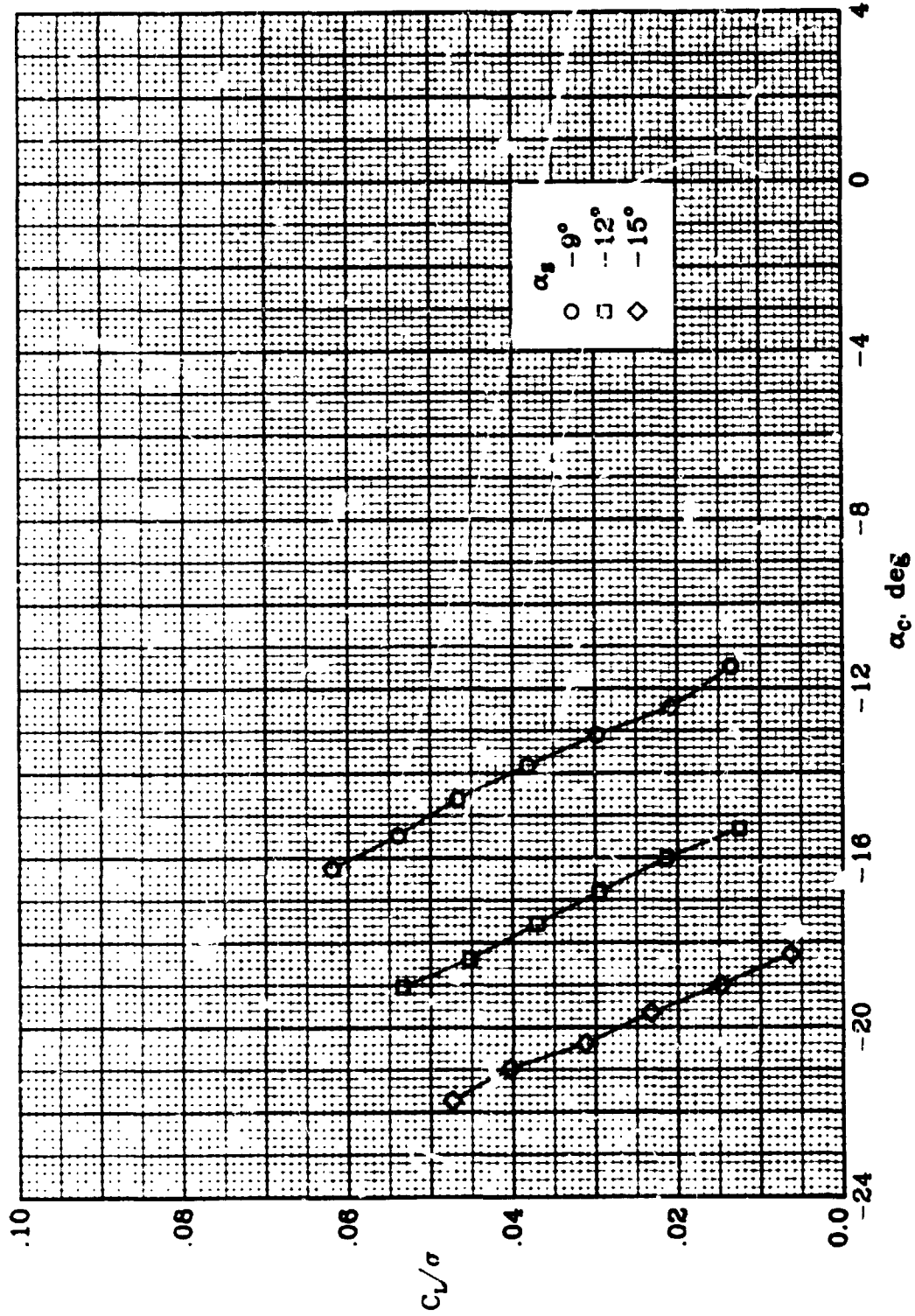
(c) $\mu = 0.30$; $N = 1200$ rpm.

Figure 9.- Continued.

(c) Concluded.
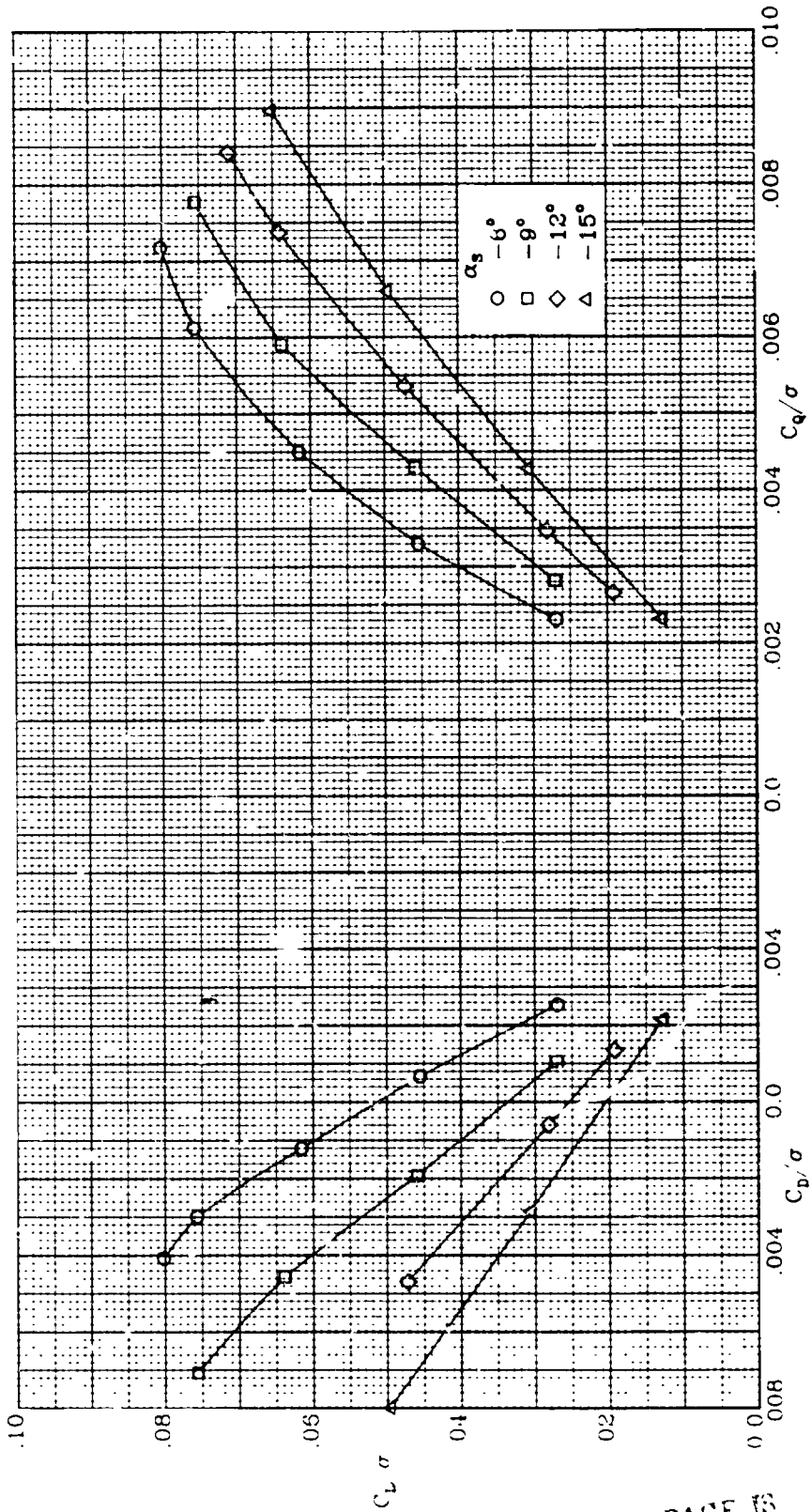
Figure 9.- Continued.

(d) μ = 0.35; N = 1200 rpm.

Figure 9.- Continued.

54
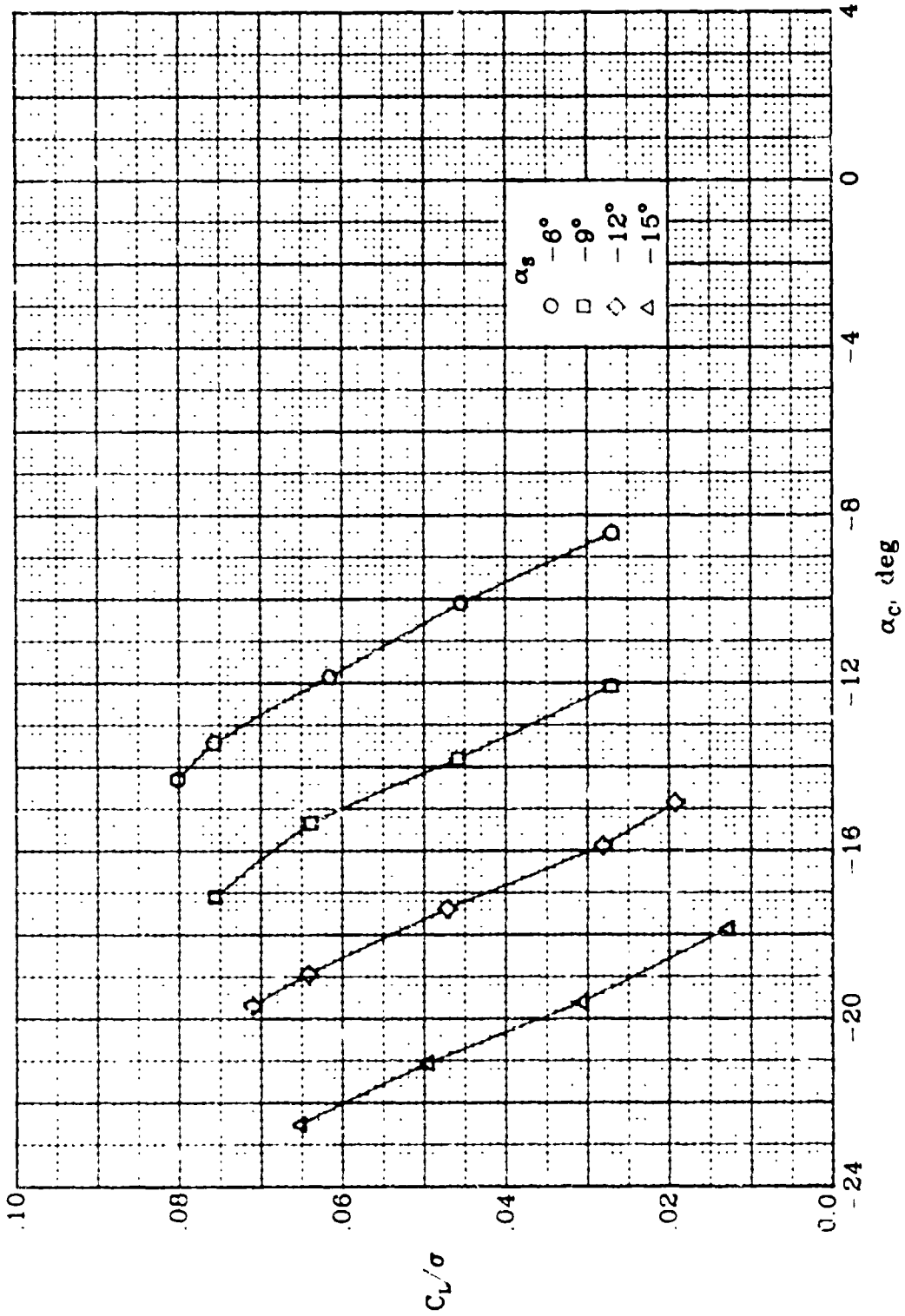
(d) Concluded.

Figure 9.- Continued.

(e) $\mu = 0.40$; $N = 1200$ rpm.

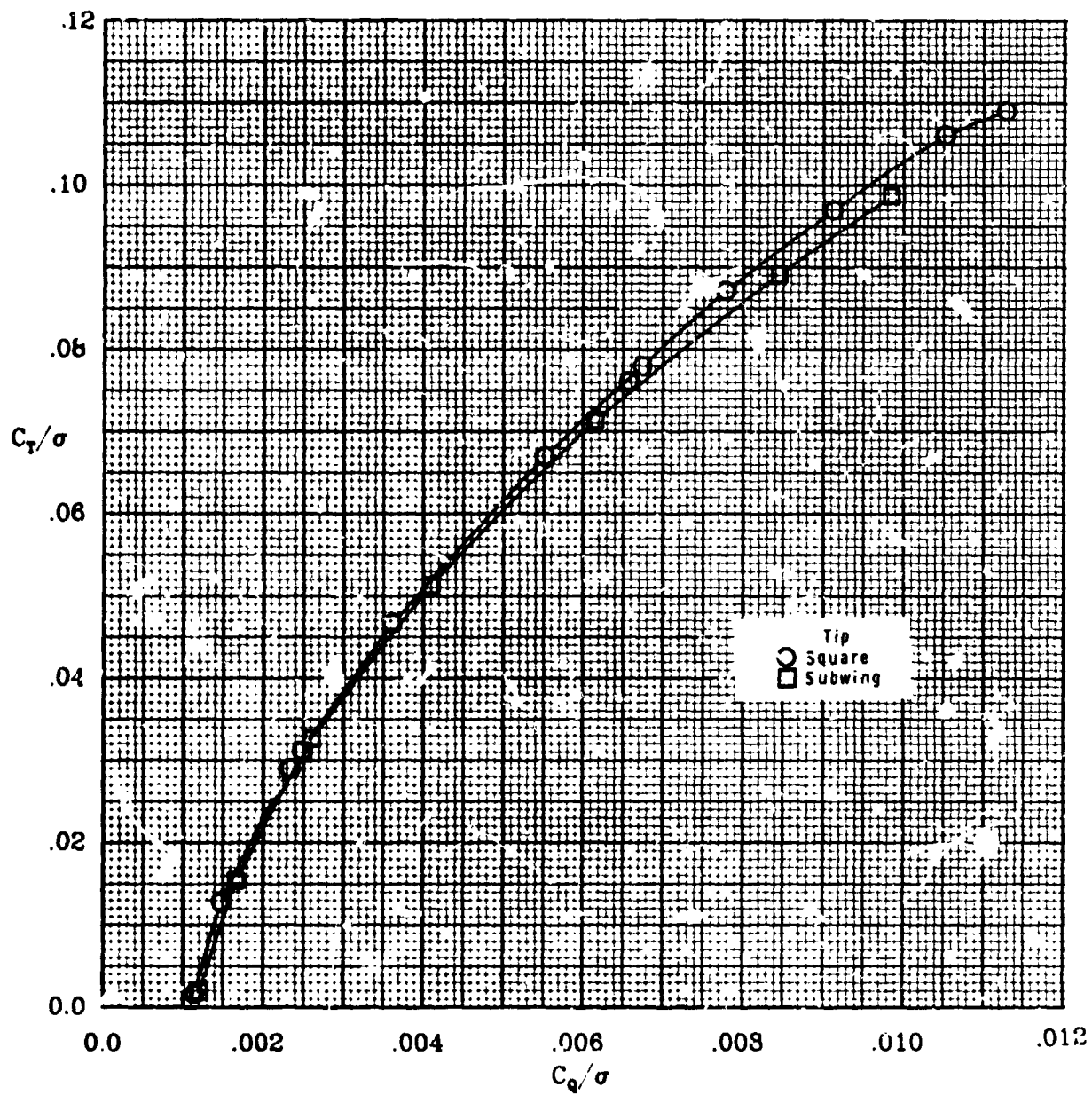Figure 9.- Continued.

56
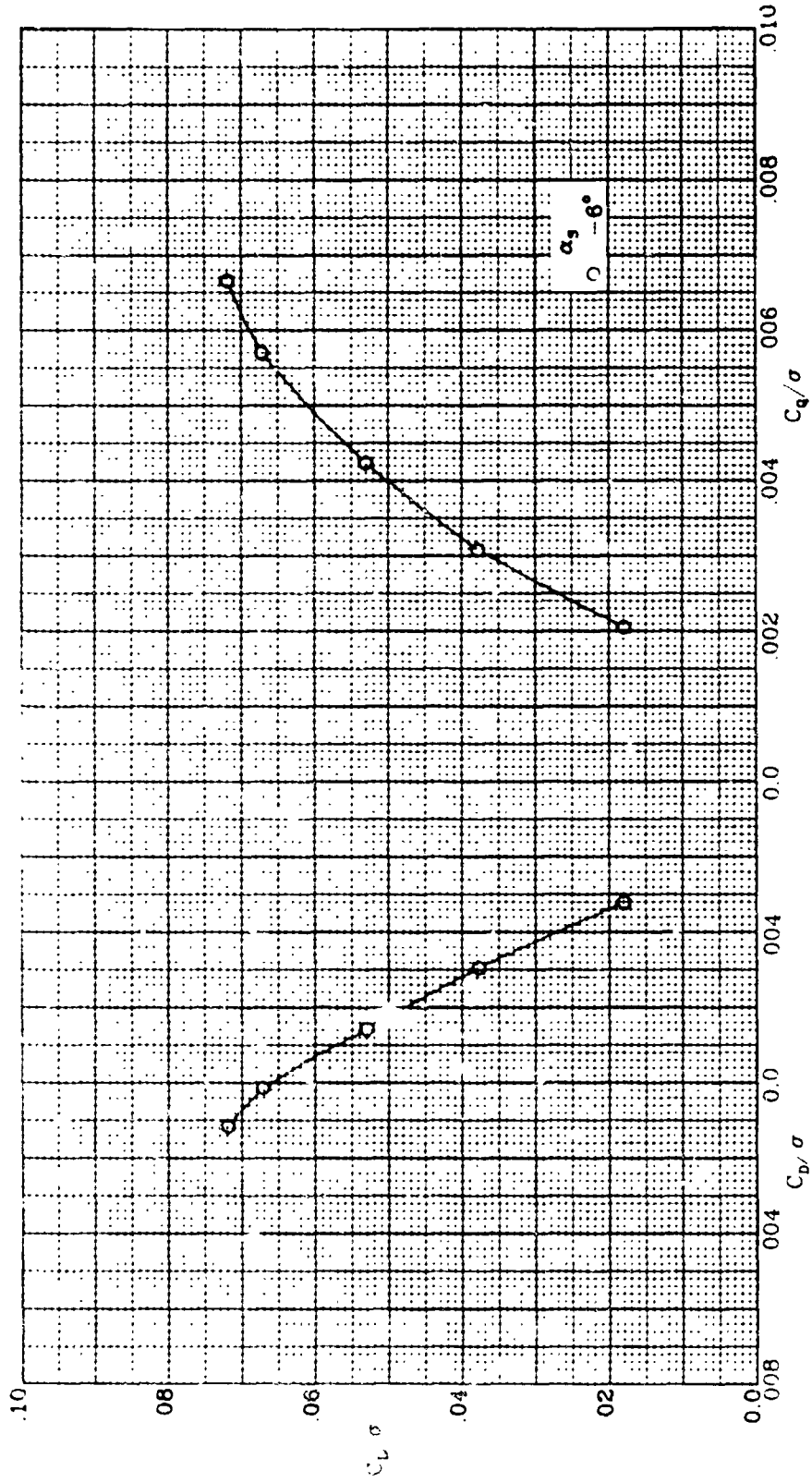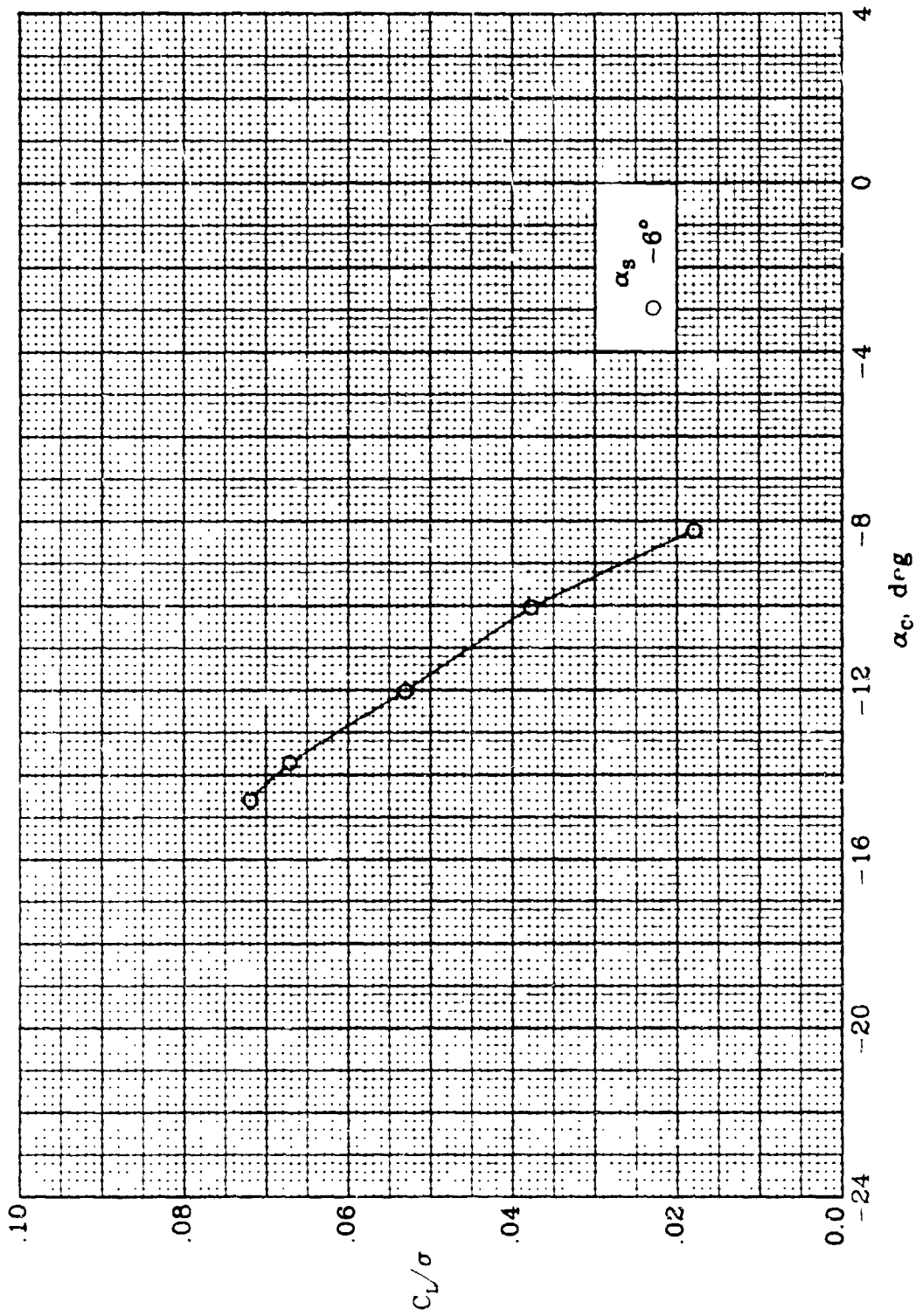
(e) Concluded.
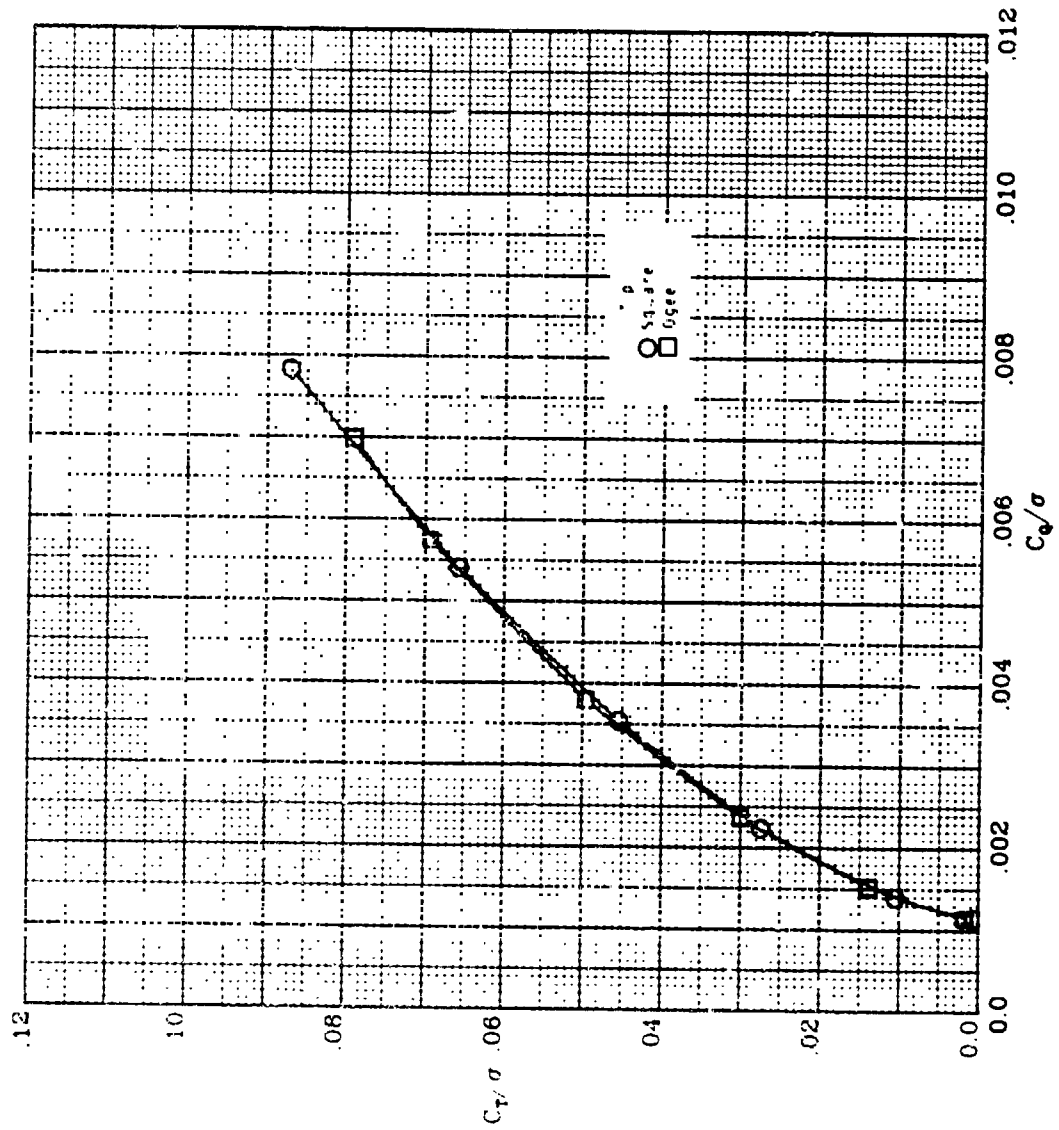
Figure 9.- Continued.

(f) $\mu = 0.0$; $N = 1340$ rpm.
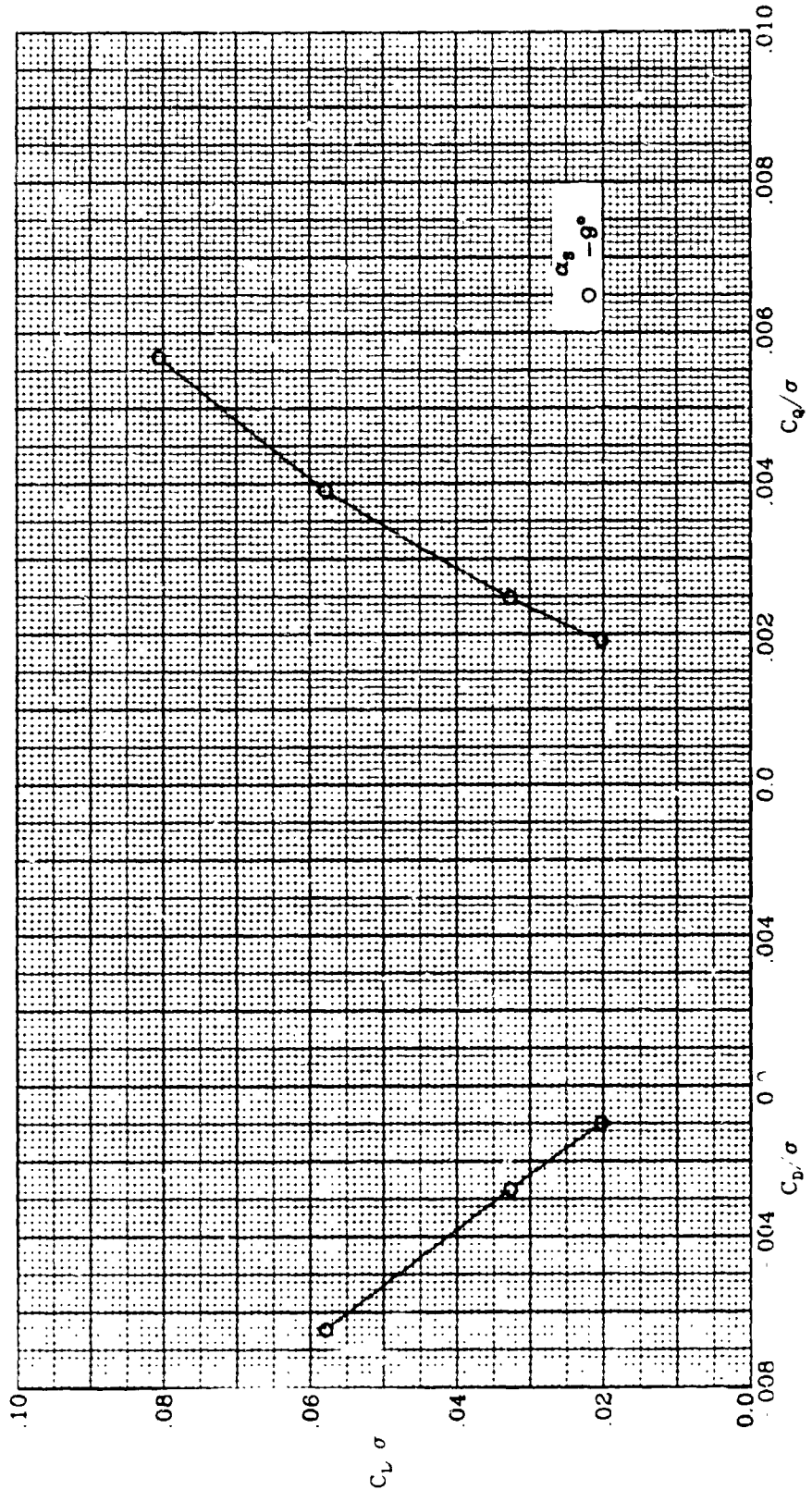
Figure 9.- Continued.

(g) $\mu = 0.20$; $N = 1340$ rpm.
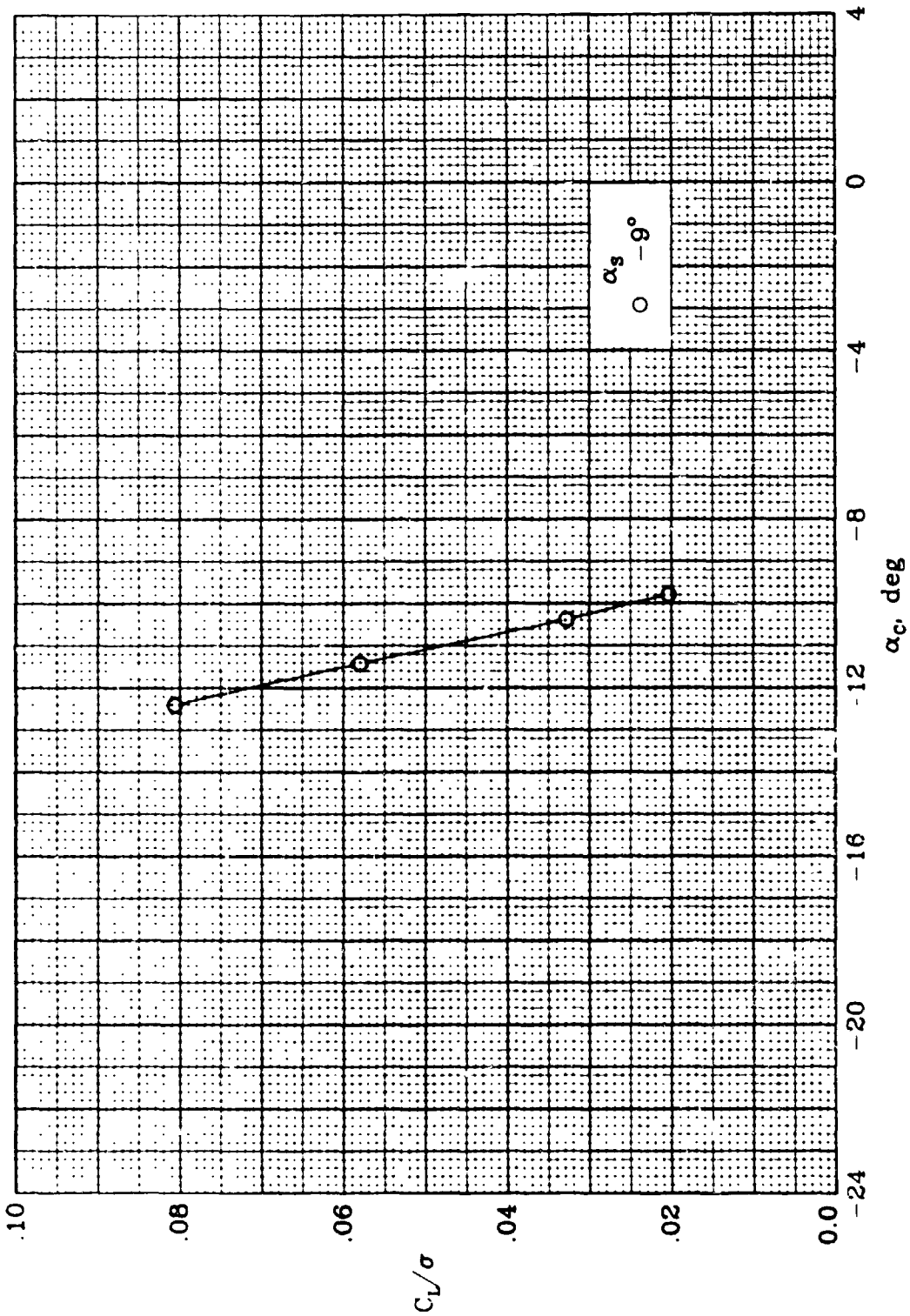
Figure 9.- Continued.

(g) Concluded.
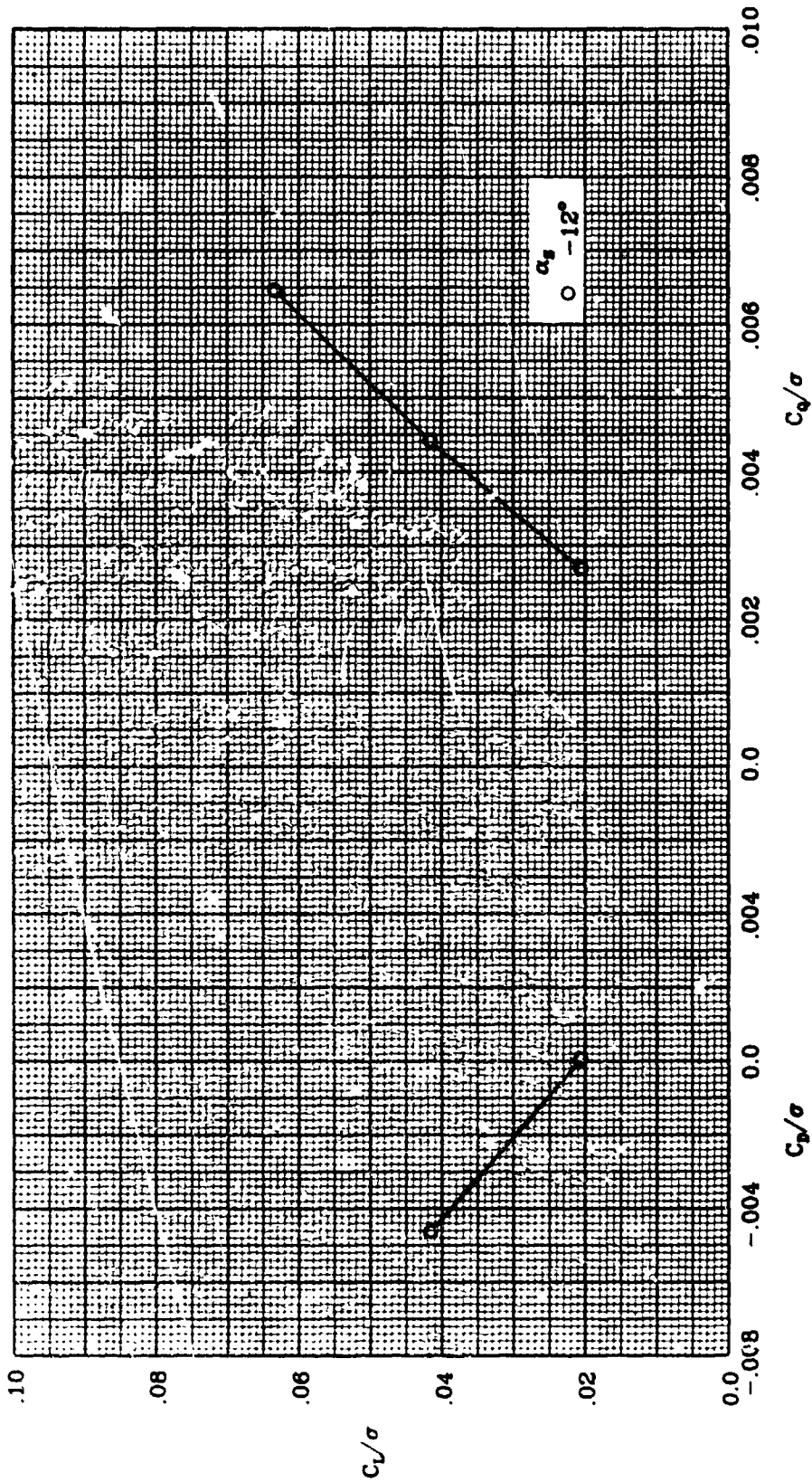
Figure 9.- Continued.

(h) $\mu = 0.30$; $N = 1340$ rpm.
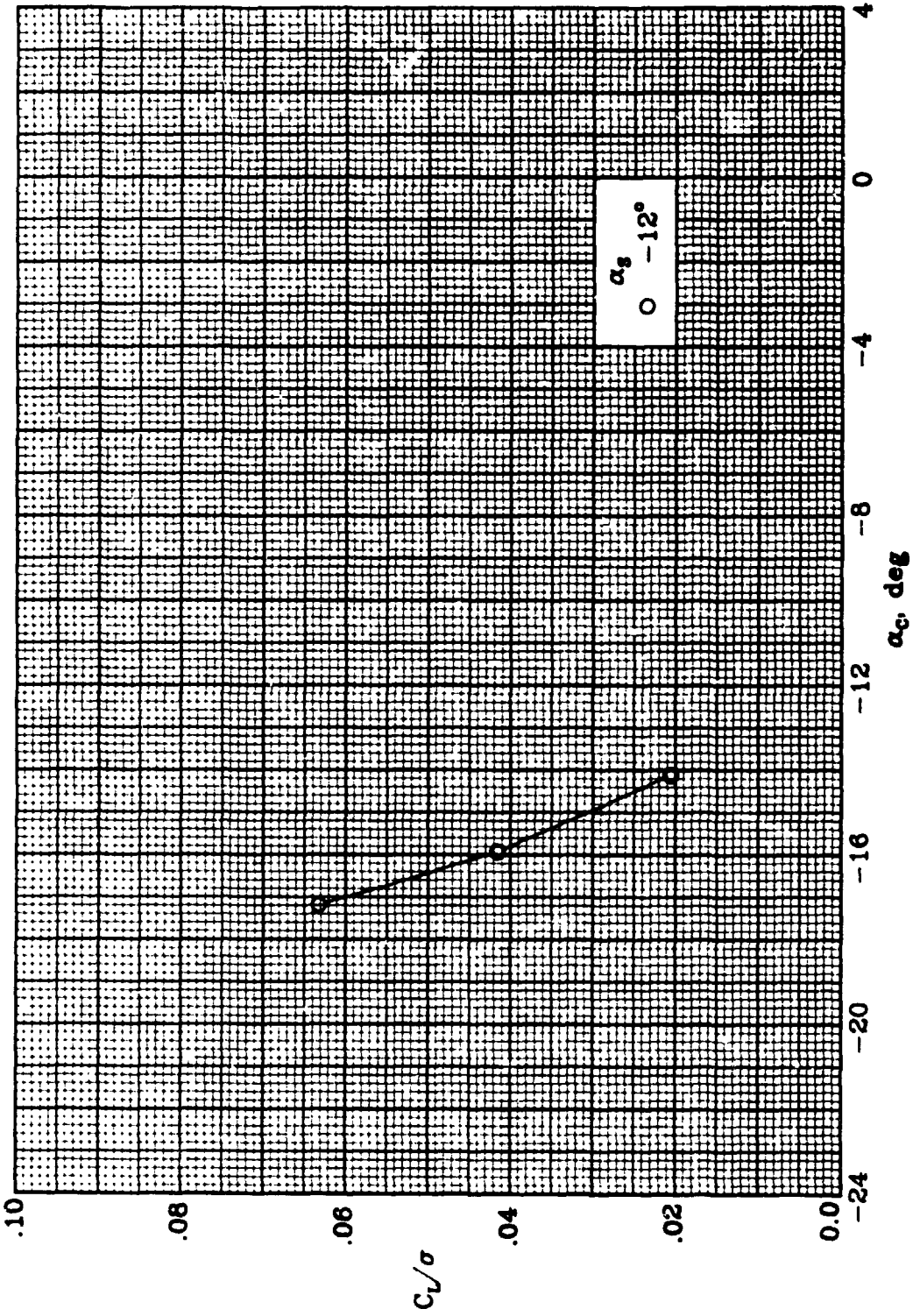
Figure 9.— Continued.

(h) Concluded.
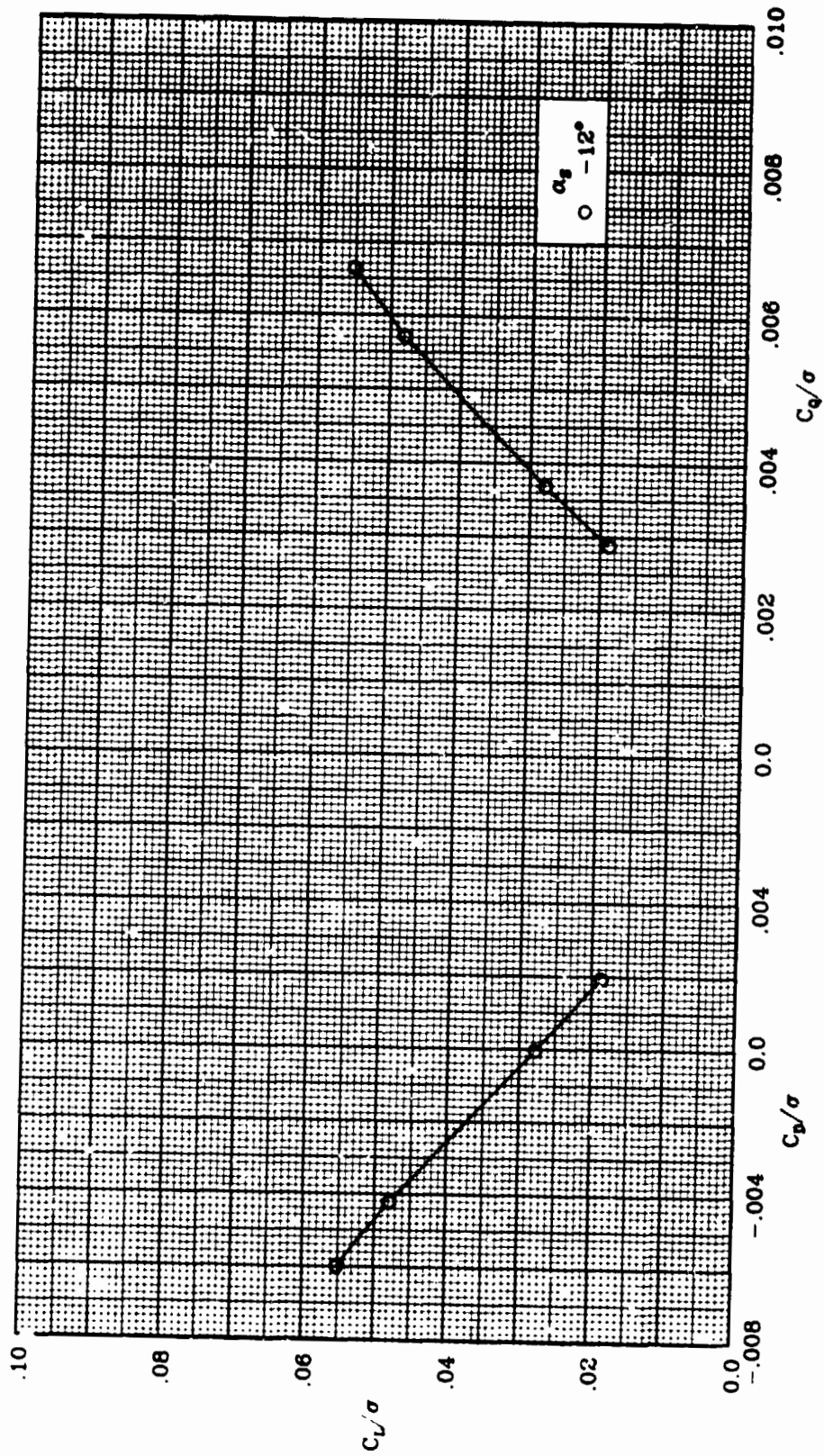
Figure 9.- Continued.

(i) $\mu = 0.35$; N = 1340 rpm.

Figure 9.- Continued.
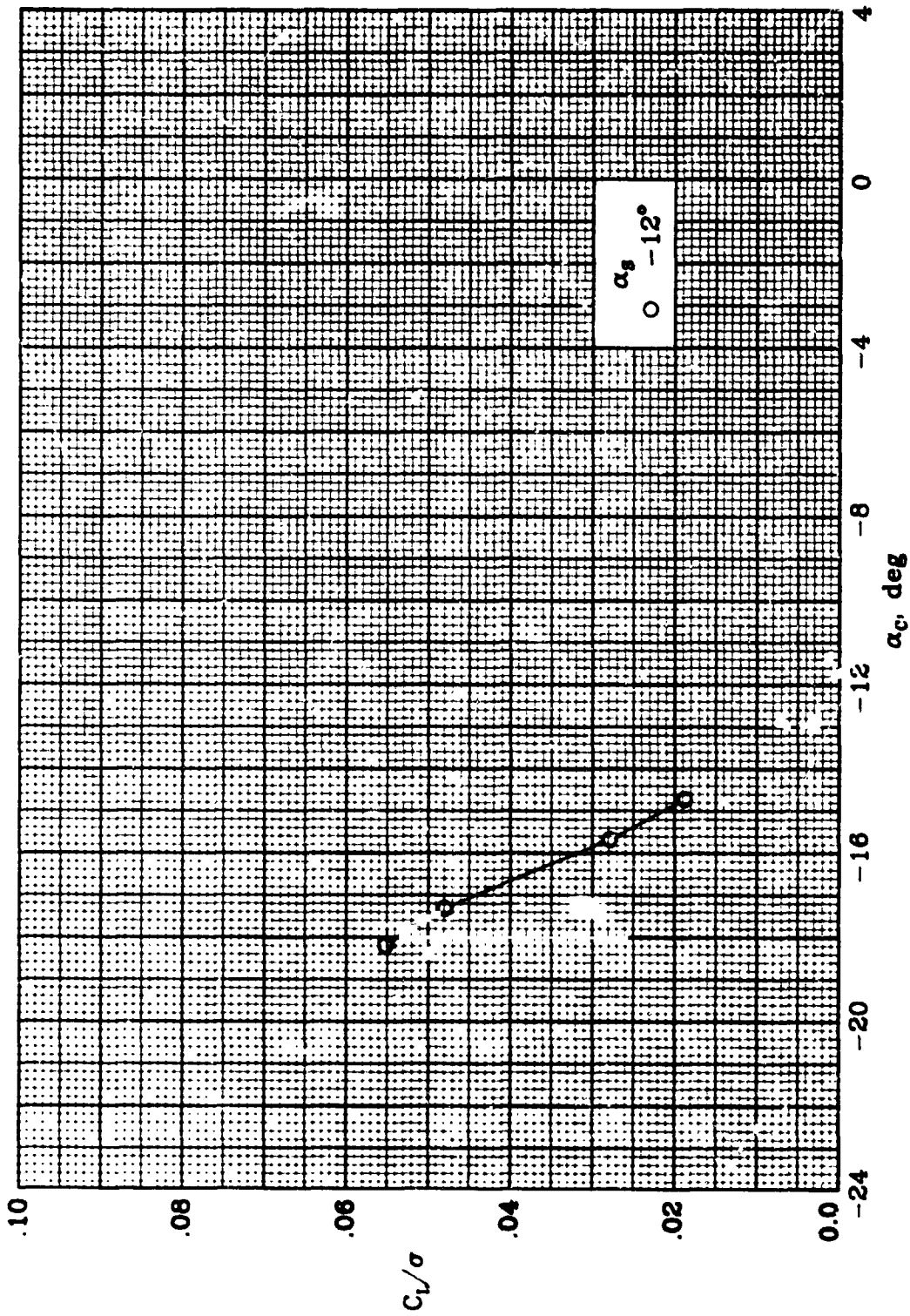
(i) Concluded.

Figure 9.- Concluded.
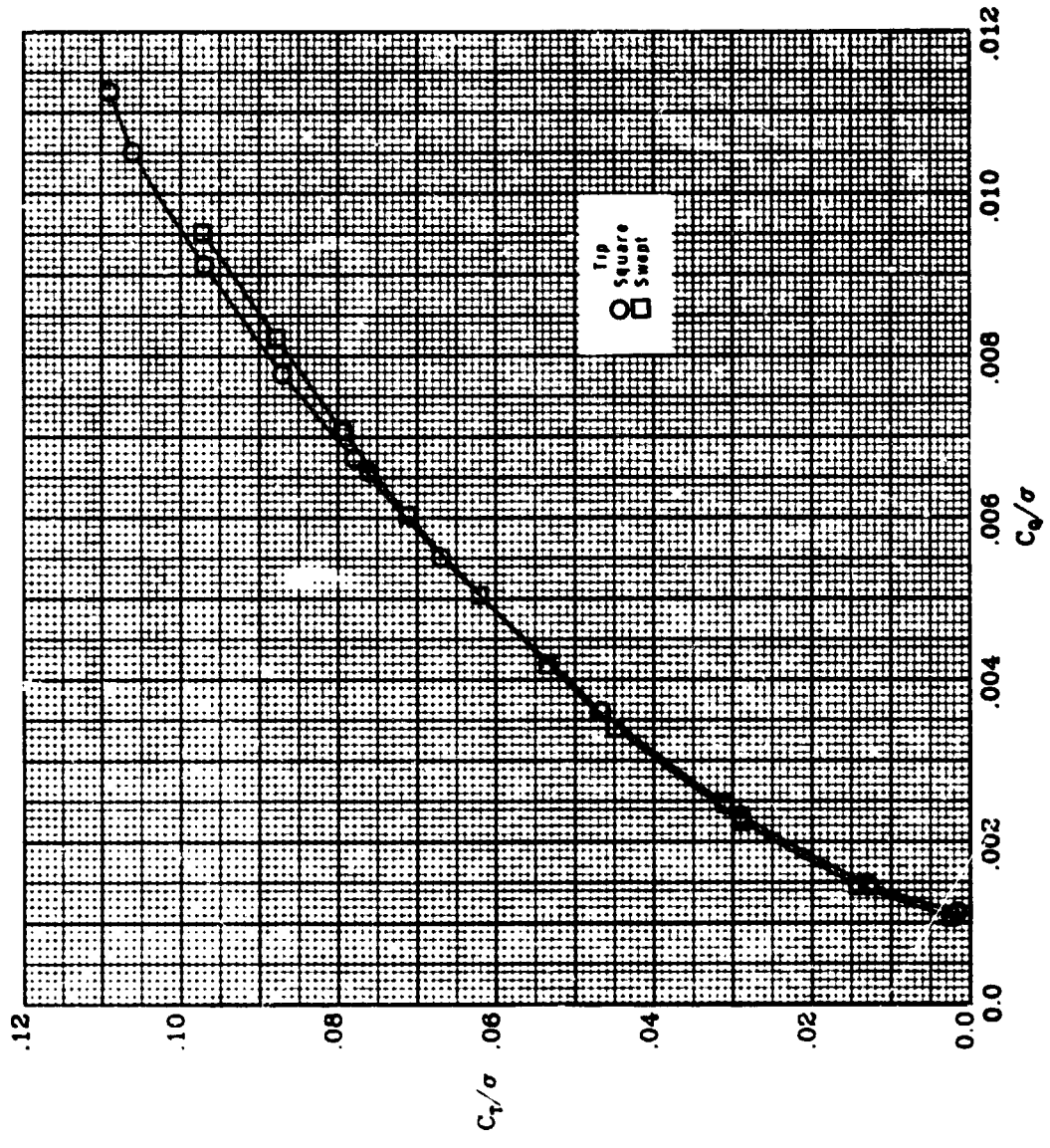
(a) $\mu = 0.0$; $N = 1200$ rpm.

Figure 10.- Swept tip performance.
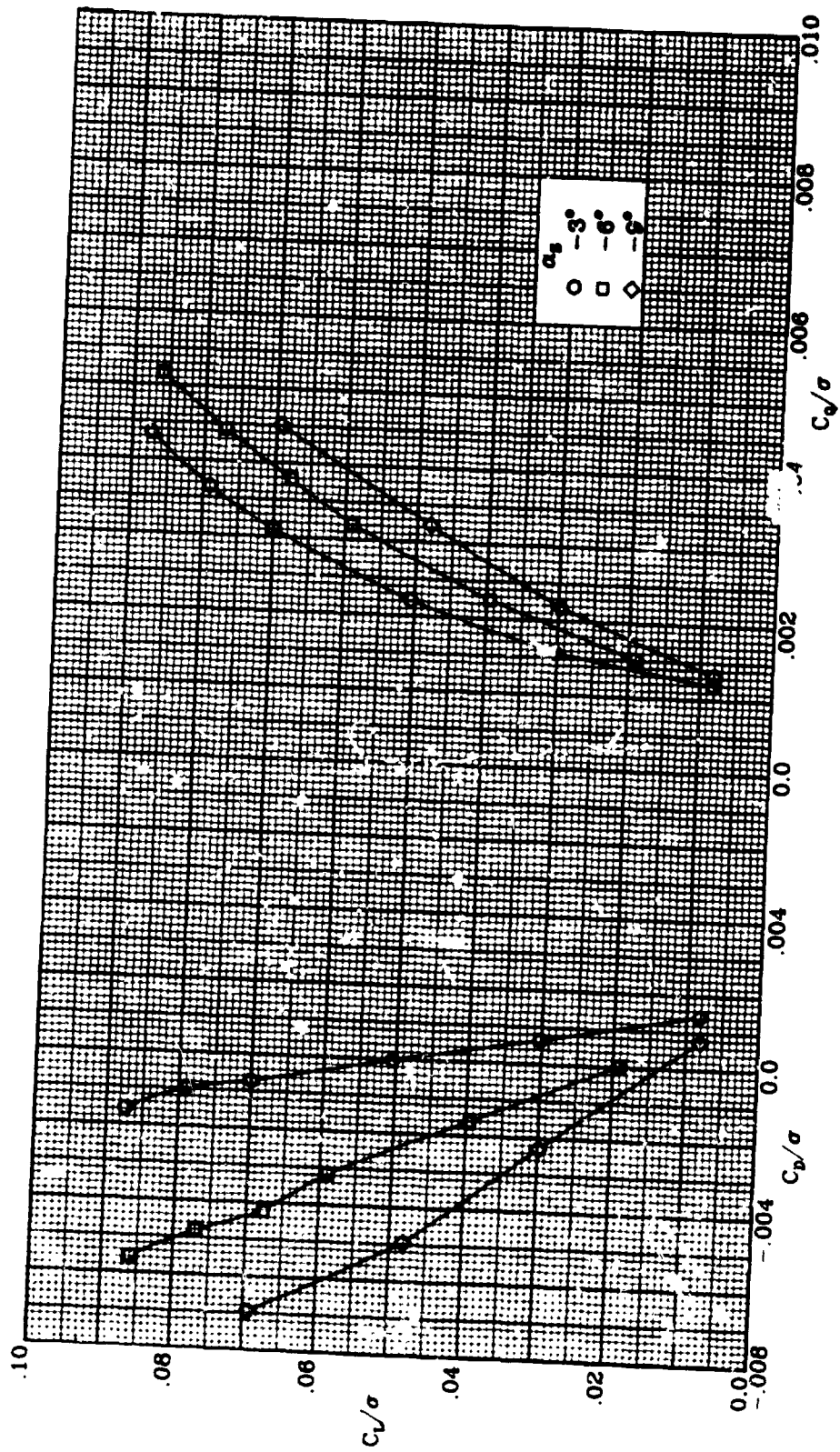
(b) $\mu = 0.20$; $N = 1200$ rpm.
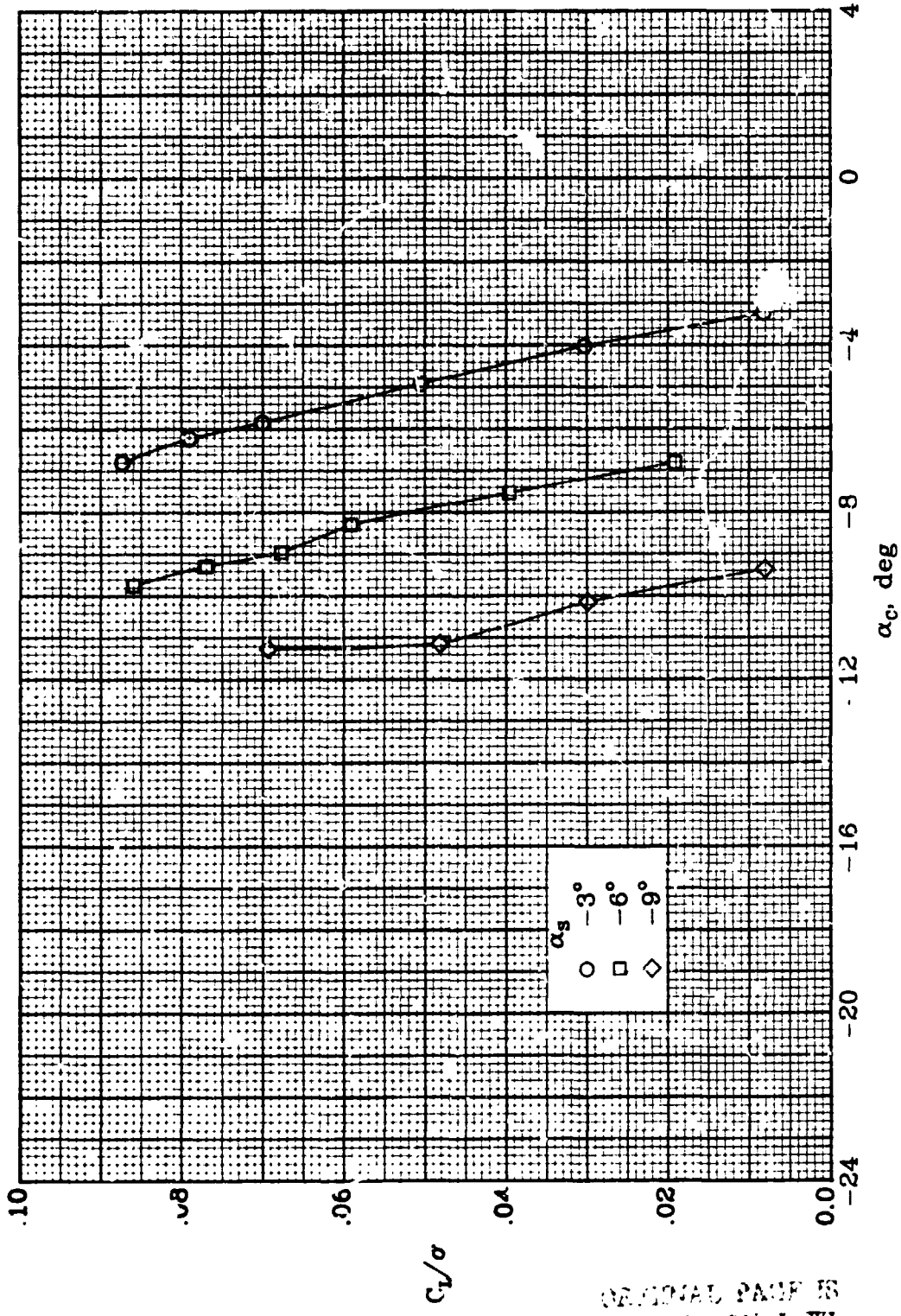
Figure 10.- Continued.

(b) Concluded.

Figure 10.- Continued.
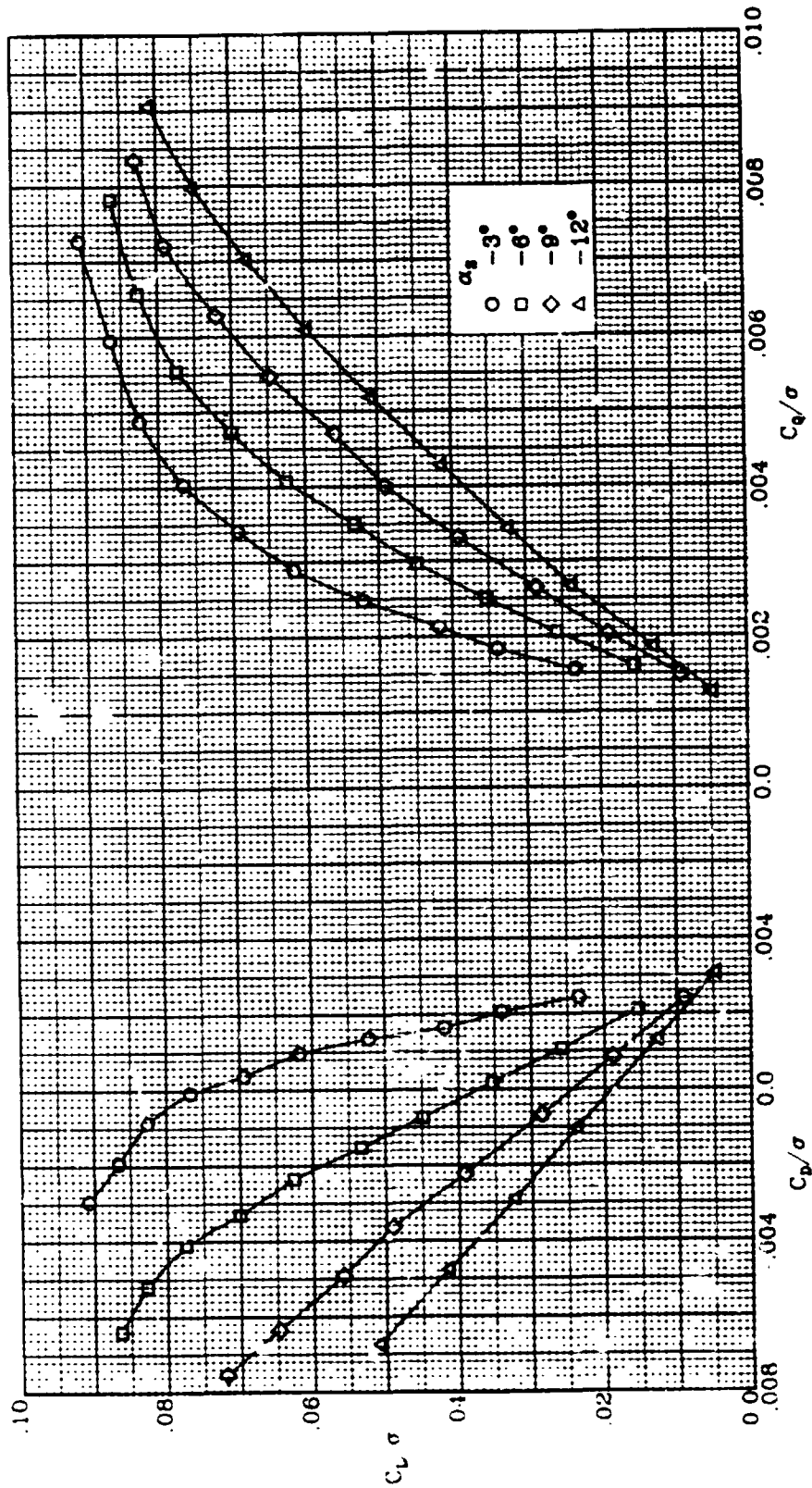
(c) $\mu = 0.30$; $N = 1200$ rpm.

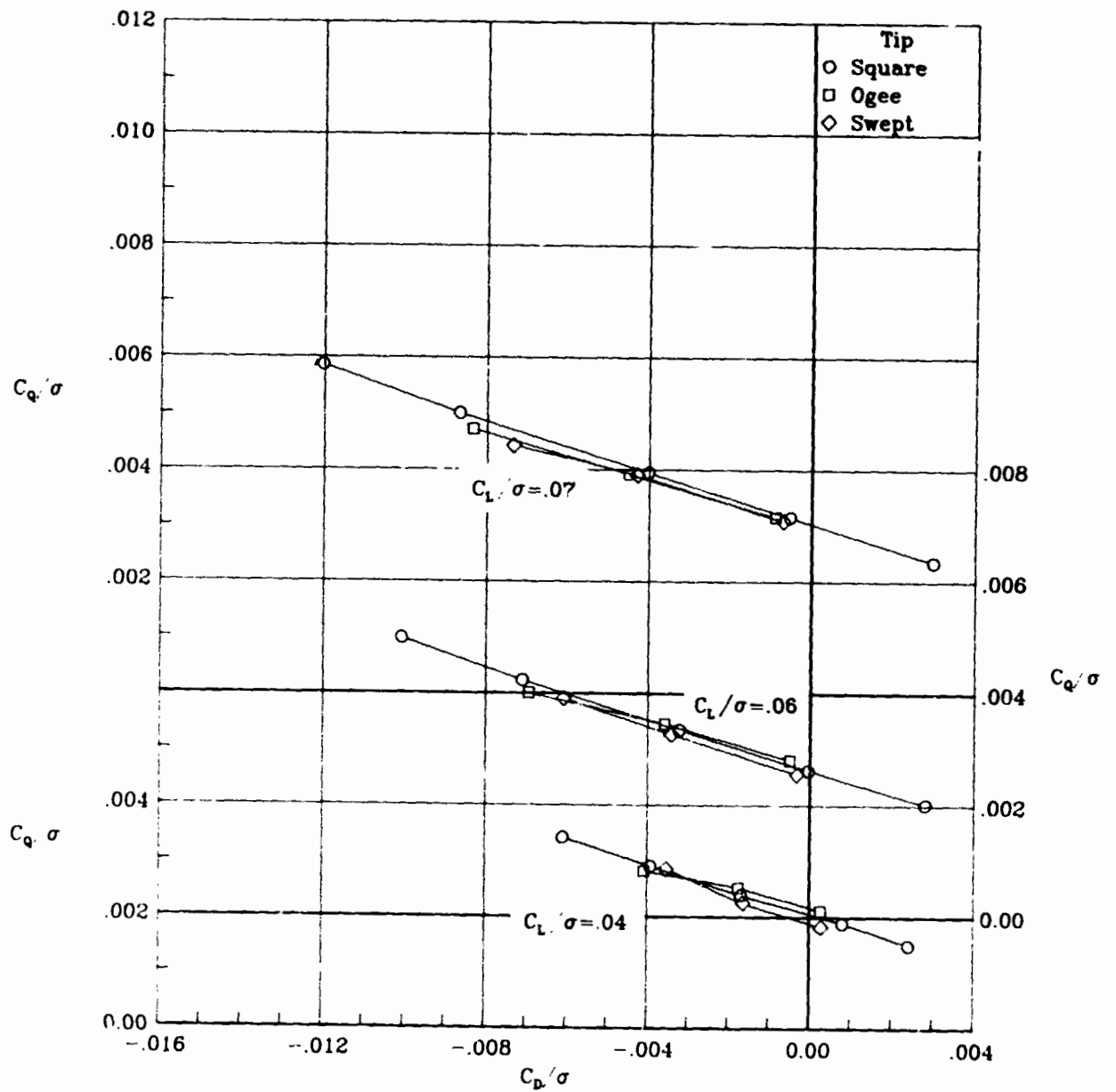Figure 10.- Continued.
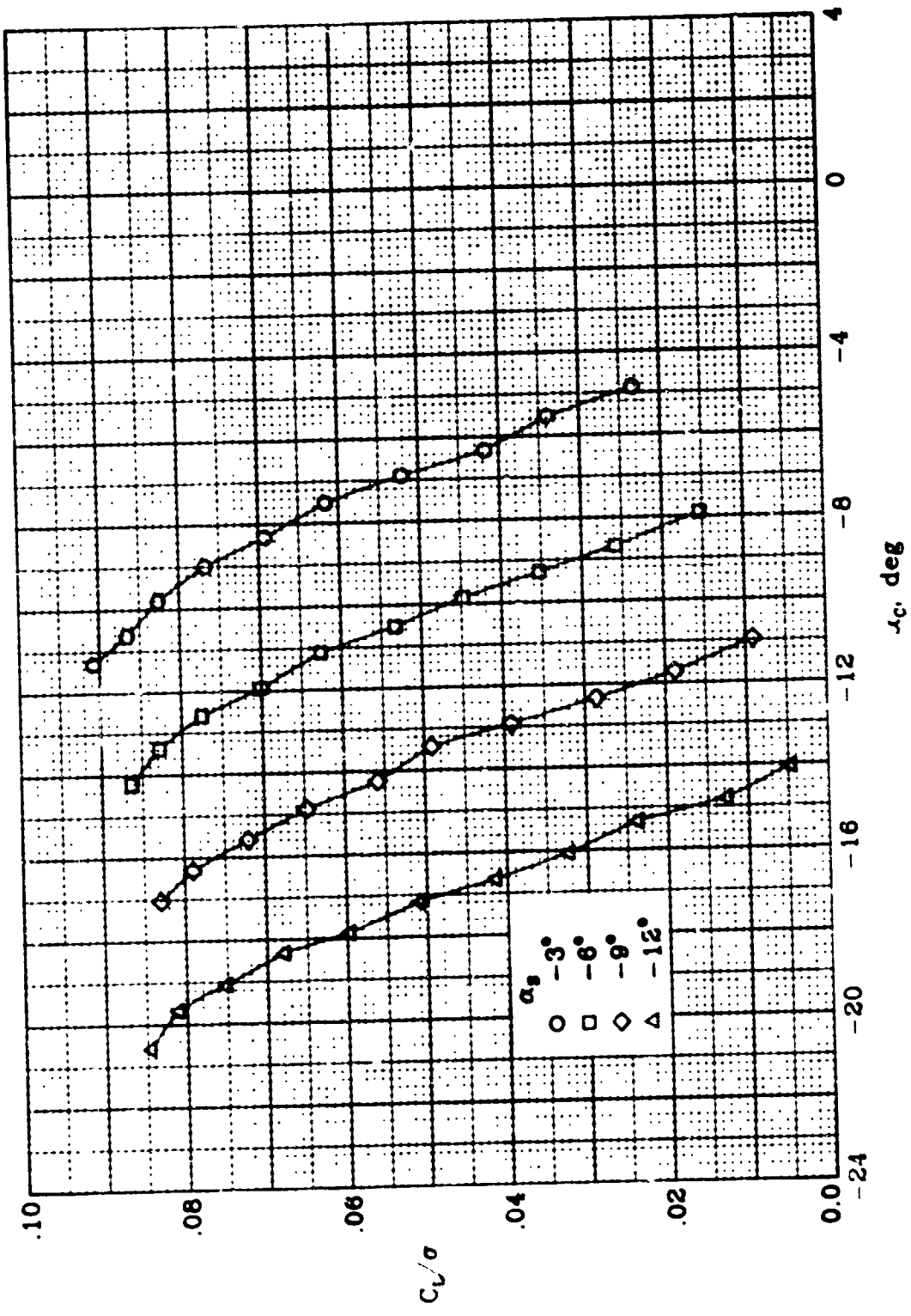
(c) Concluded.
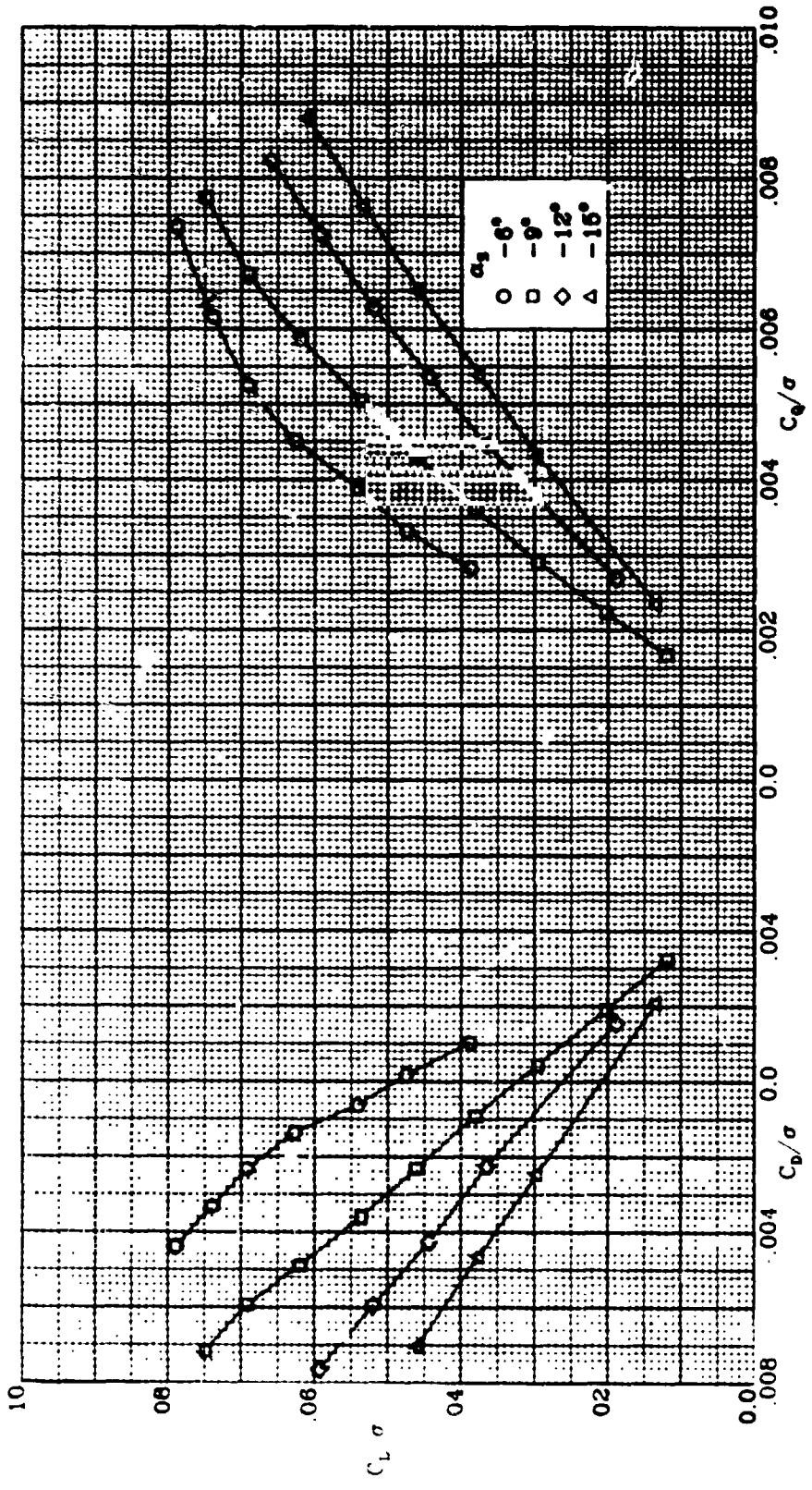
Figure 10.- Continued.

(d) $\mu = 0.?5$; N = 1200 rpm.

Figure 10.- Continued.

(d) Concluded.
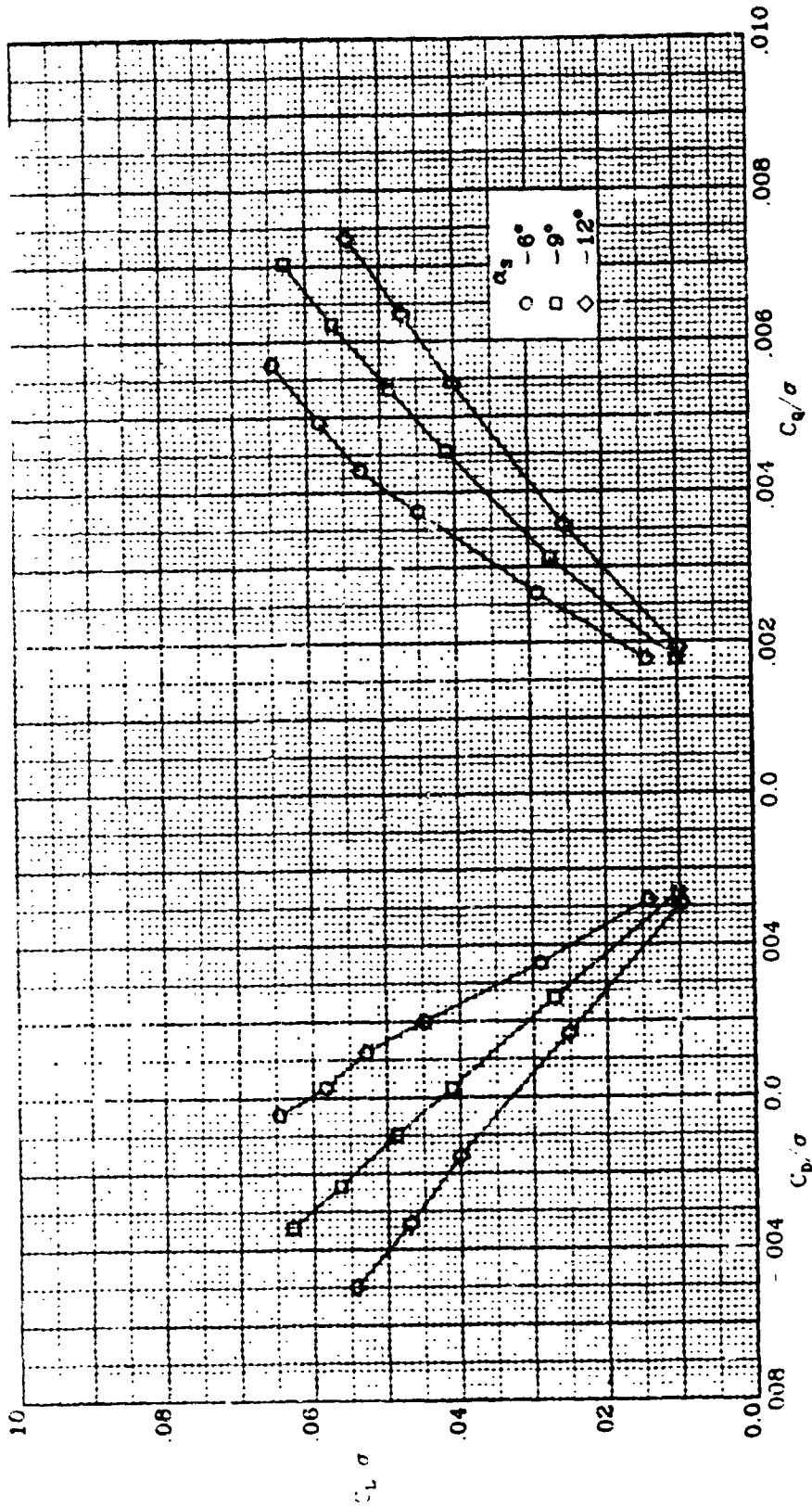
Figure 10.- Continued.

(e) $\mu = 0.40$; $N = 1200$ rpm.
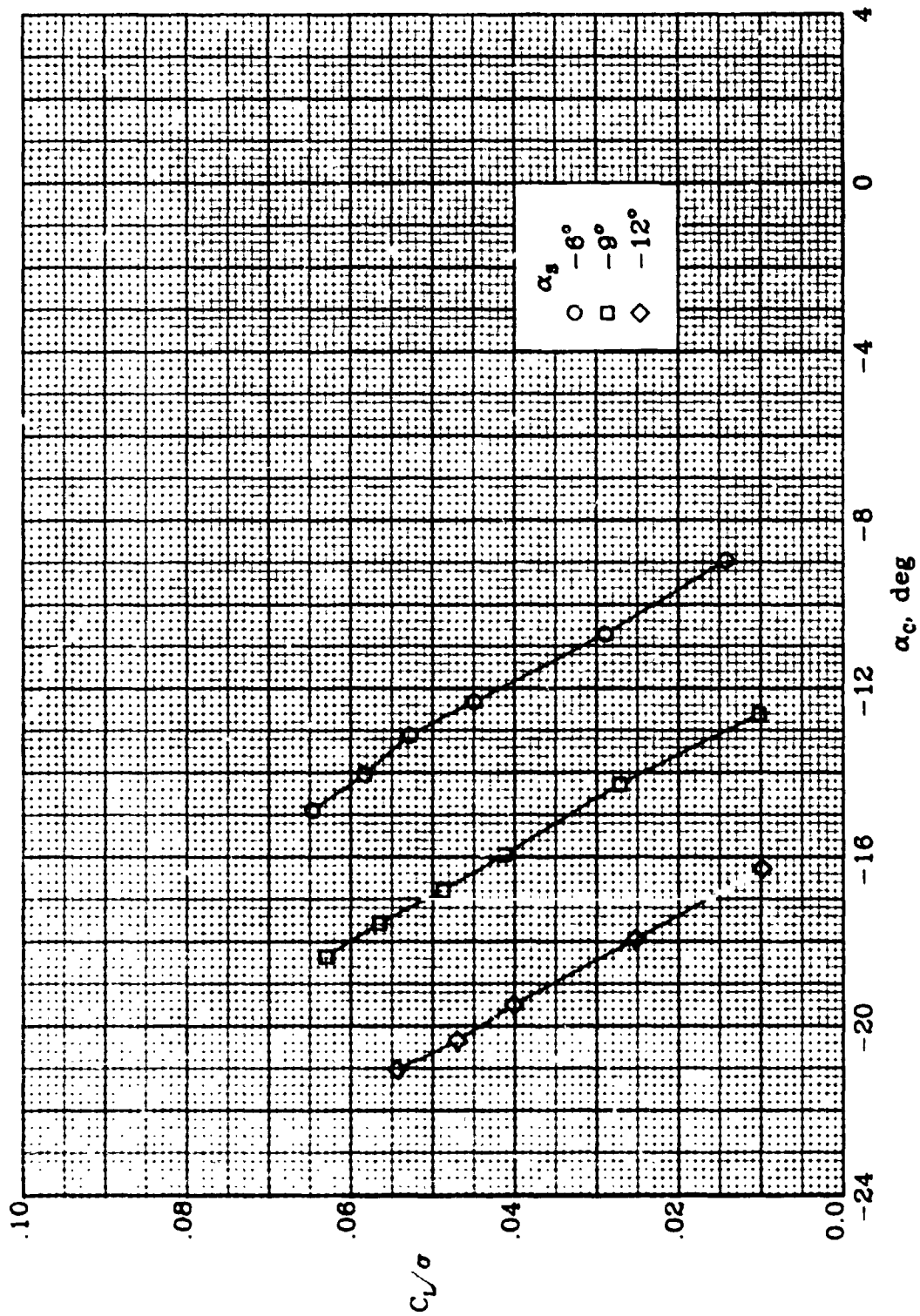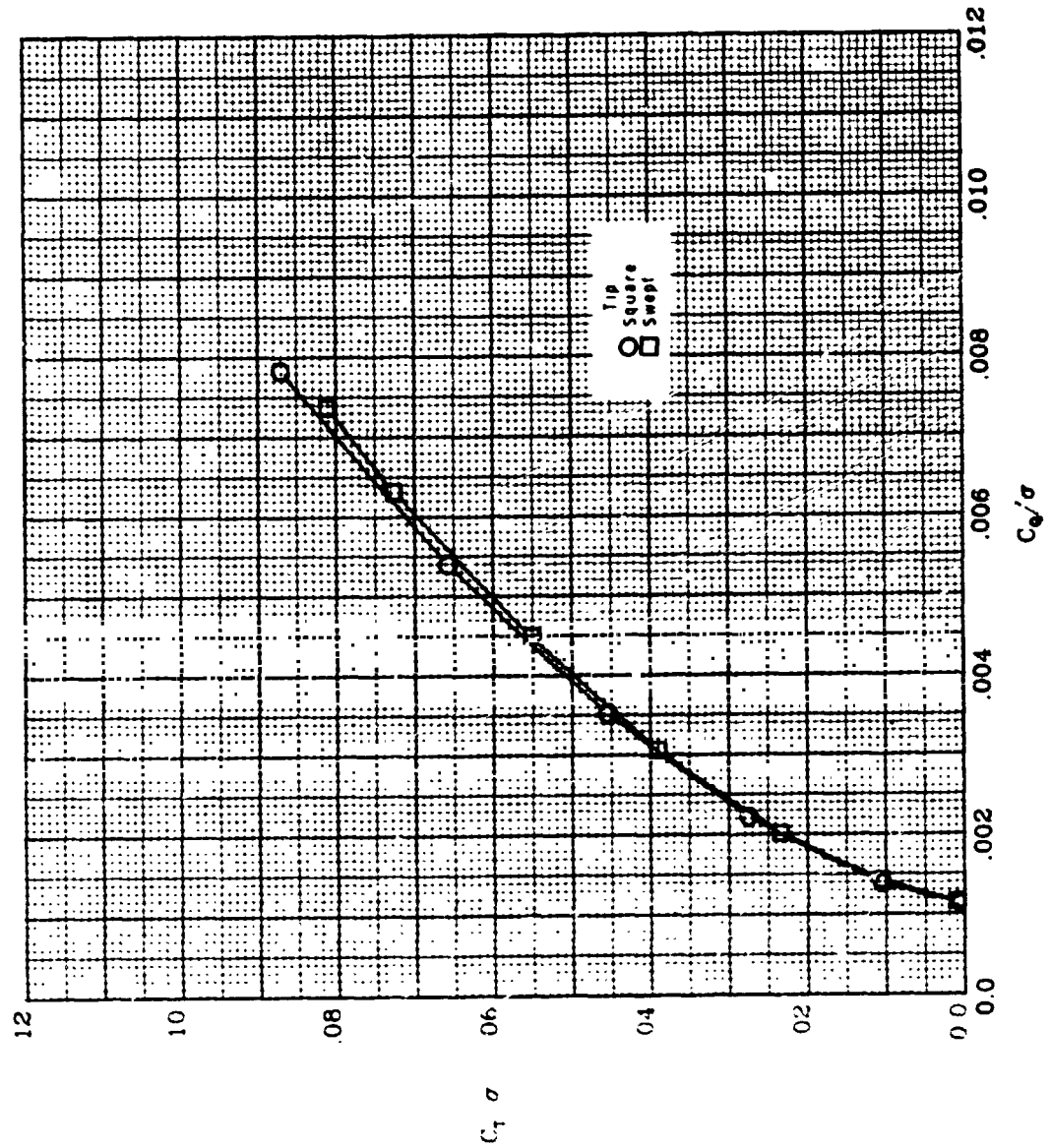
Figure 10.- Continued.

72

(e) Concluded.

Figure 10.- Continued.

(f) $\mu = 0.0$; $N = 1340$ rpm.

Figure 10.- Continued.

74
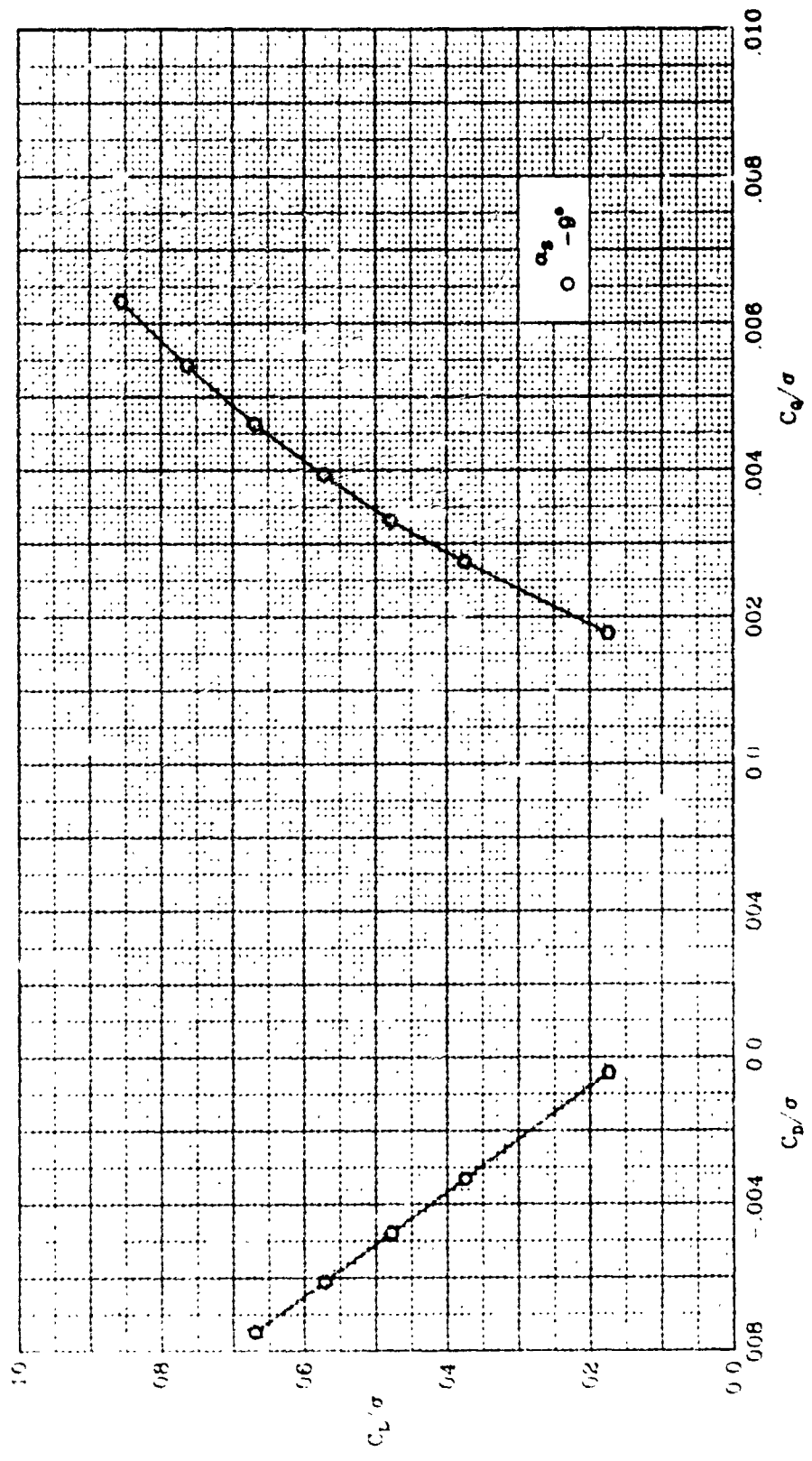
(g) $\mu = 0.20$; $N = 1340$ rpm.

Figure 10.- Continued.

(g) Concluded.

Figure 10.- Continued.

(h) $\mu = 0.30$; $N = 1340$ rpm.
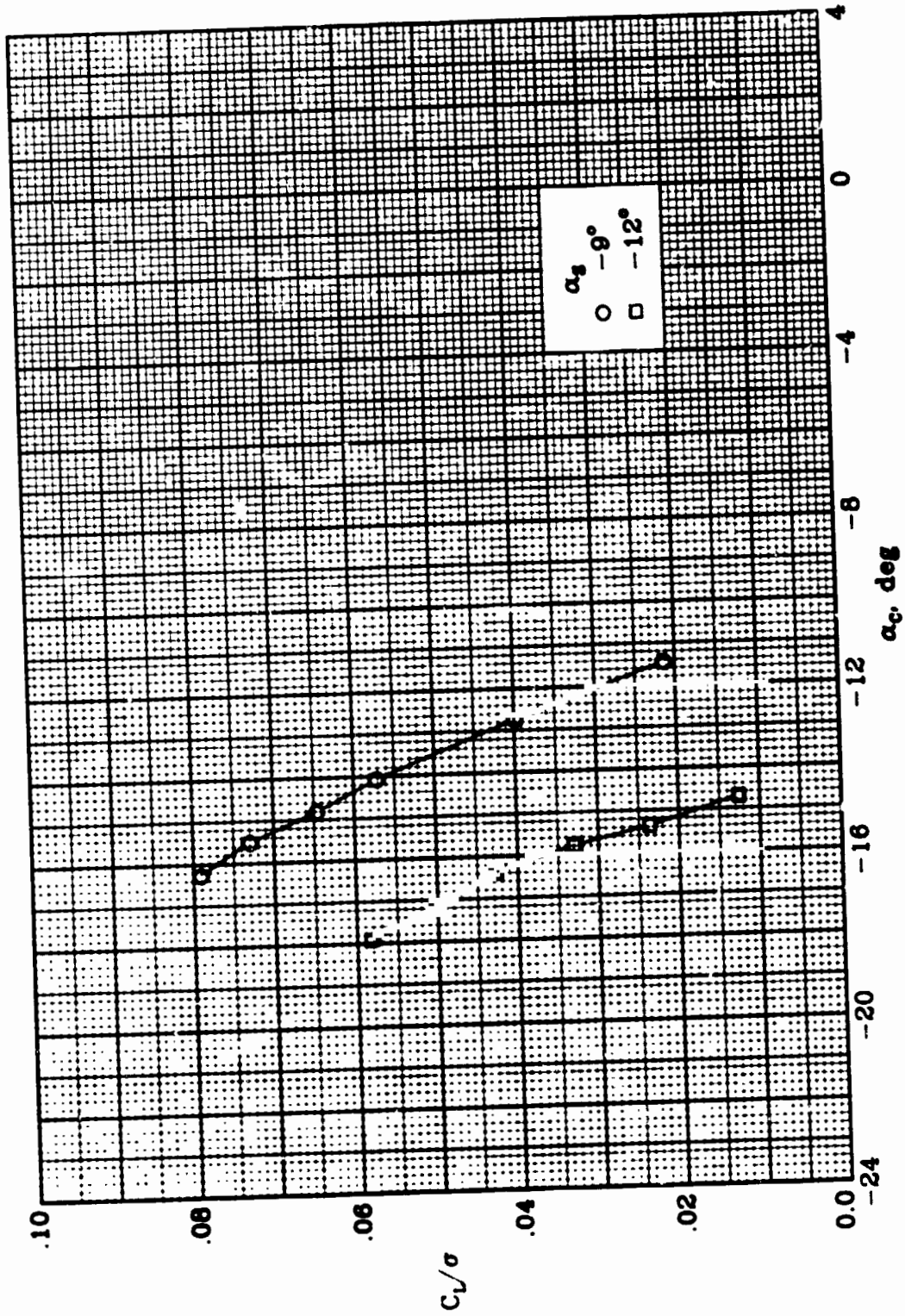
Figure 10.- Continued.

(h) Concluded.

Figure 10.- Continued.

(i) $\mu = 0.35$; $N = 1340$ rpm.

Figure 10.- Continued.

(l) Concluded.

Figure 10.- Concluded.

Figure 11.- Subwing tip performance at $\mu = 0.0$ and $N = 1200$ rpm.
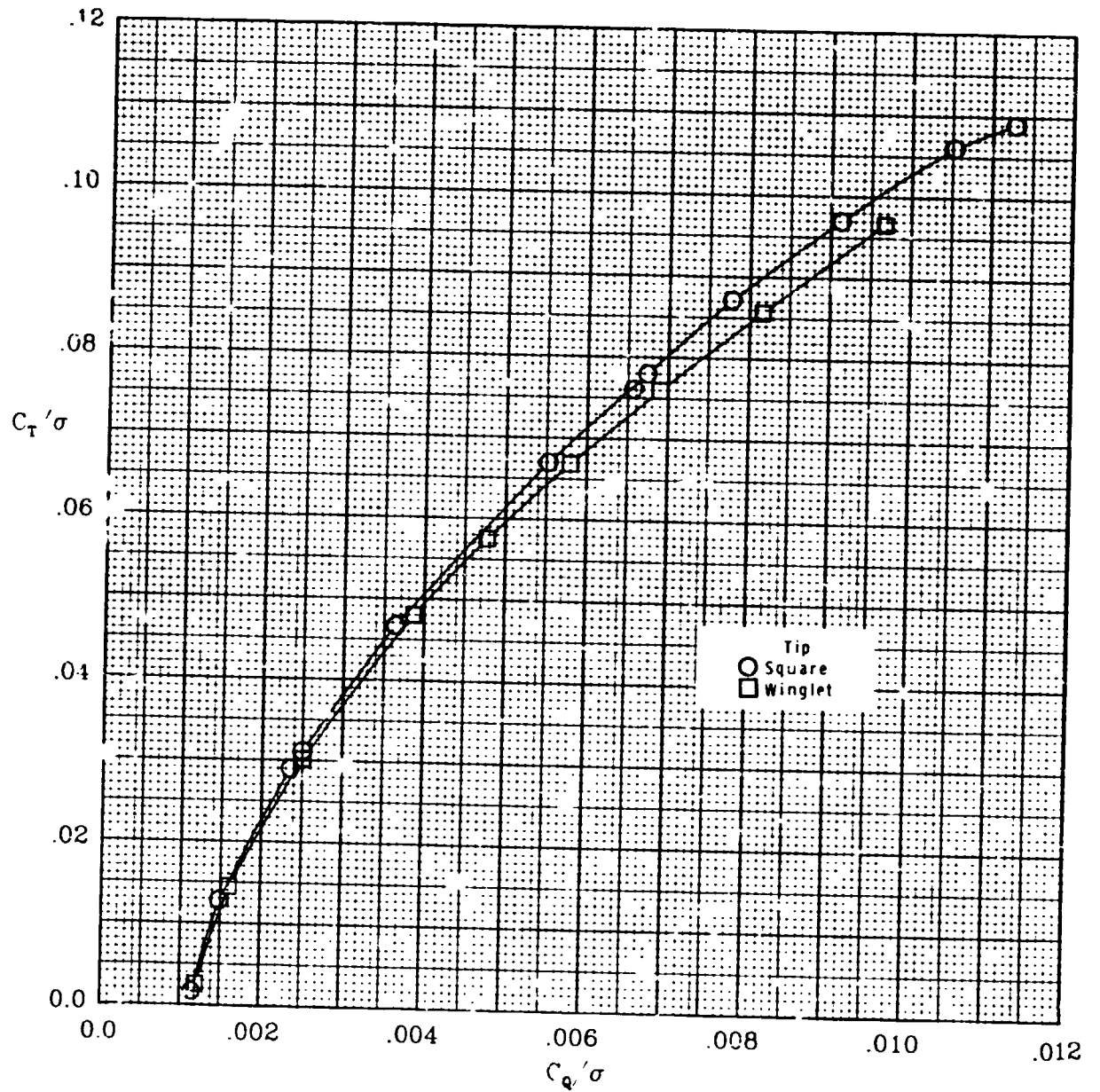
Figure 12.- Winglet tip performance at $\mu = 0.0$ and $N = 1200$ rpm.
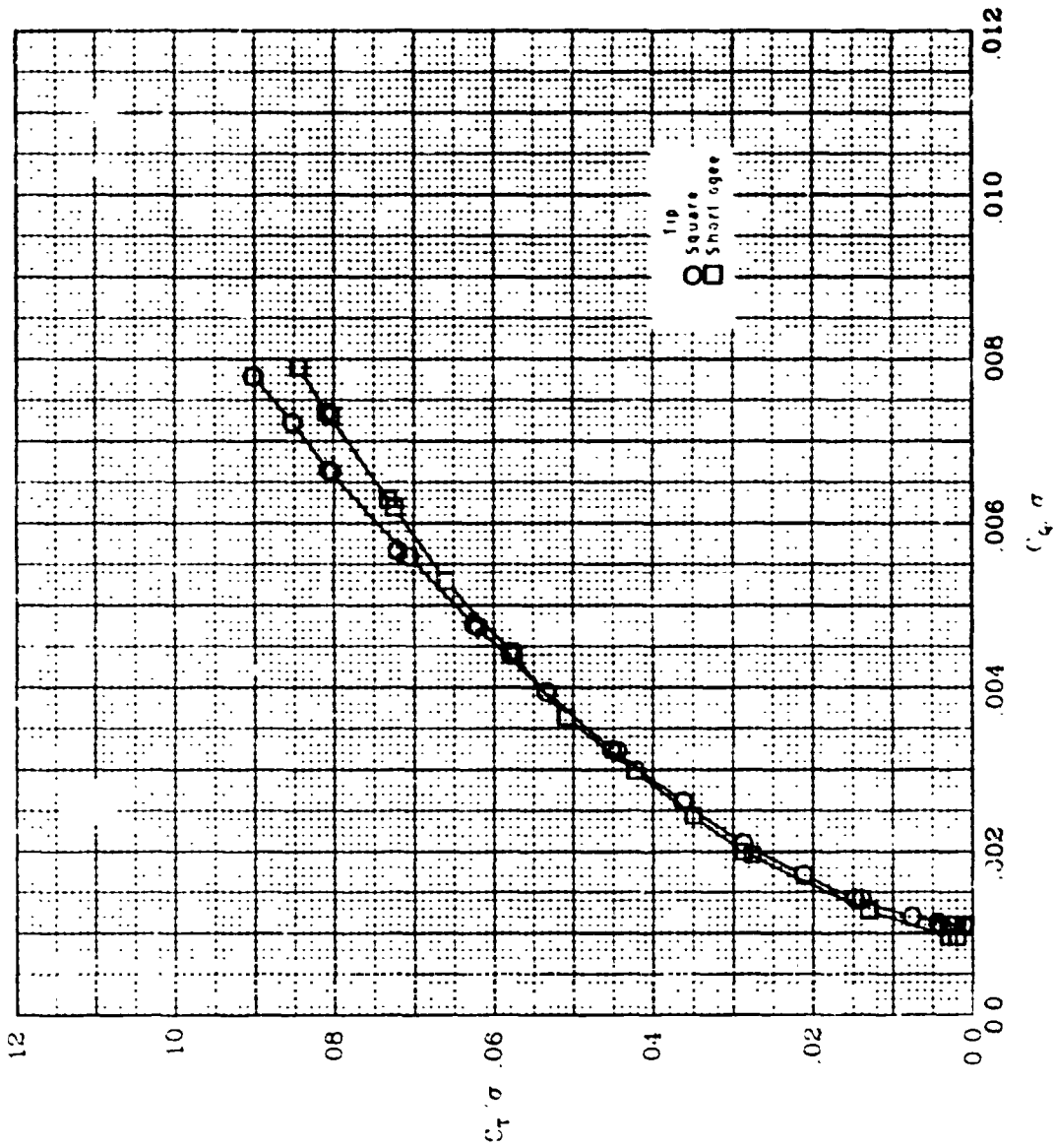
(a) $\mu = 0.0$; $N = 1200$ rpm.

Figure 13.- Short ogee tip performance.

83
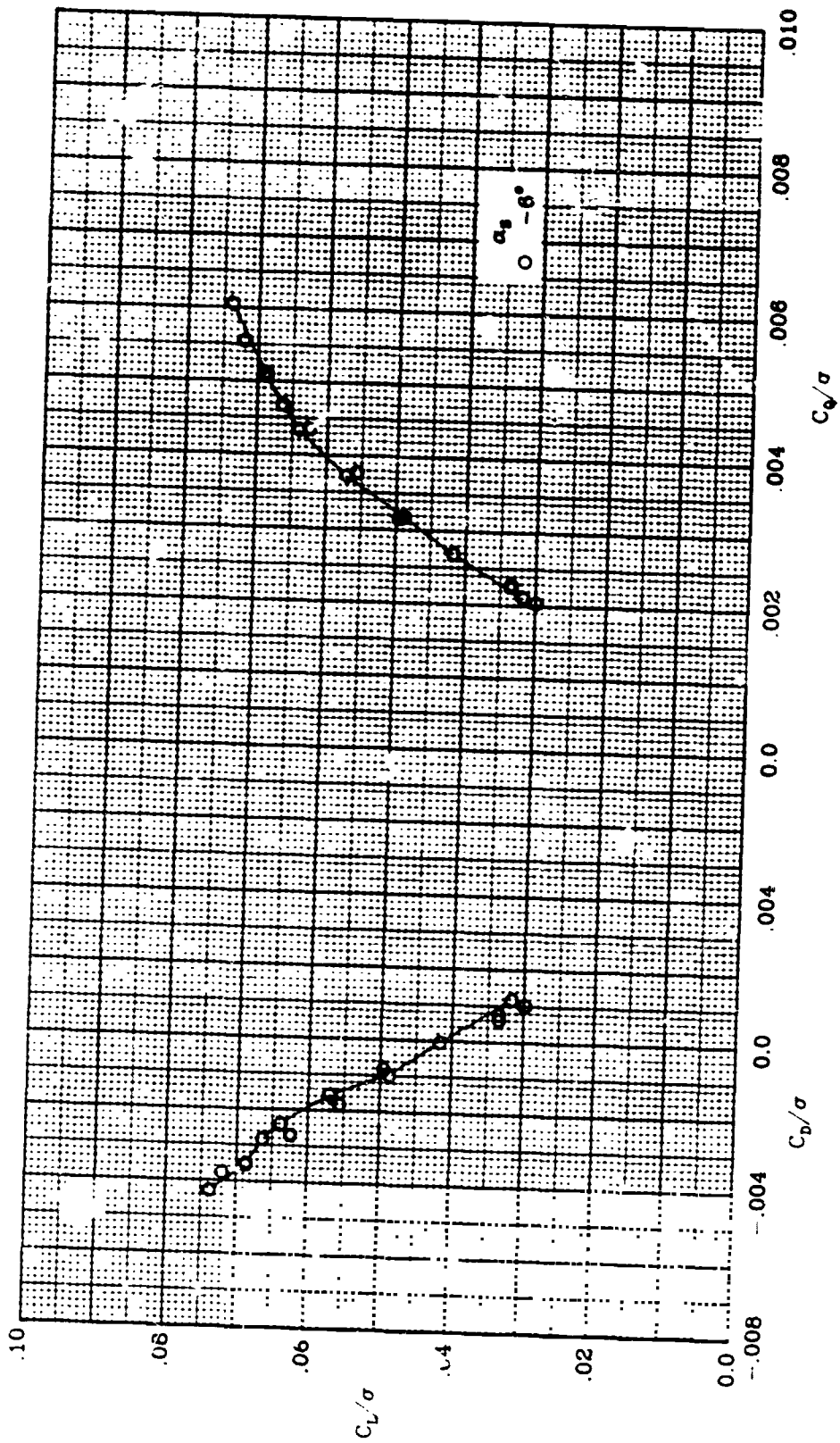
(b) $\mu = 0.30$; $N = 1200$ rpm.

Figure 13.- Continued.
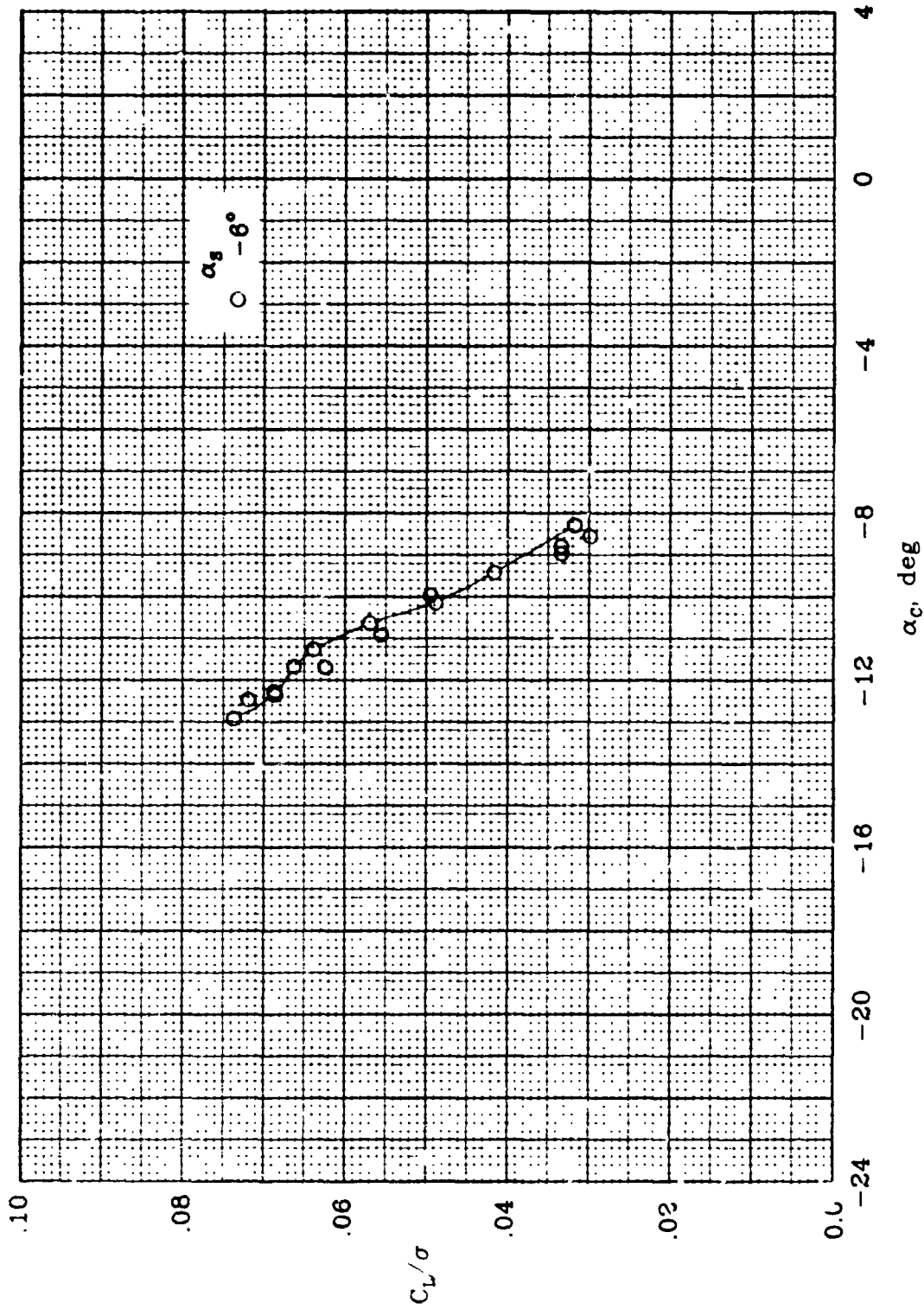
(b) Concluded.

Figure 13.- Concluded.

(a) $\mu = 0.20$; N = 1200 rpm.

Figure 14.- Comparison of tip performance.
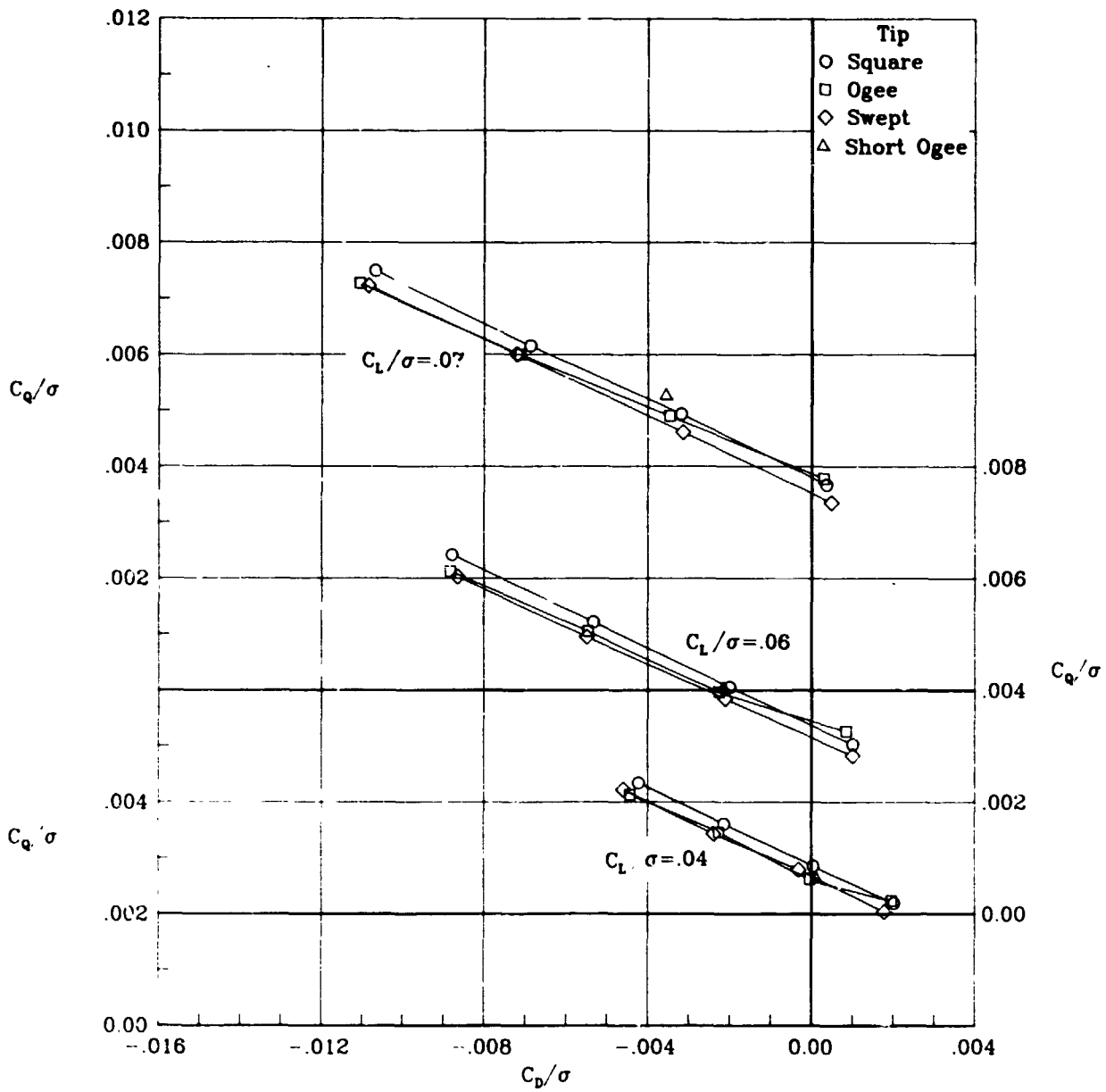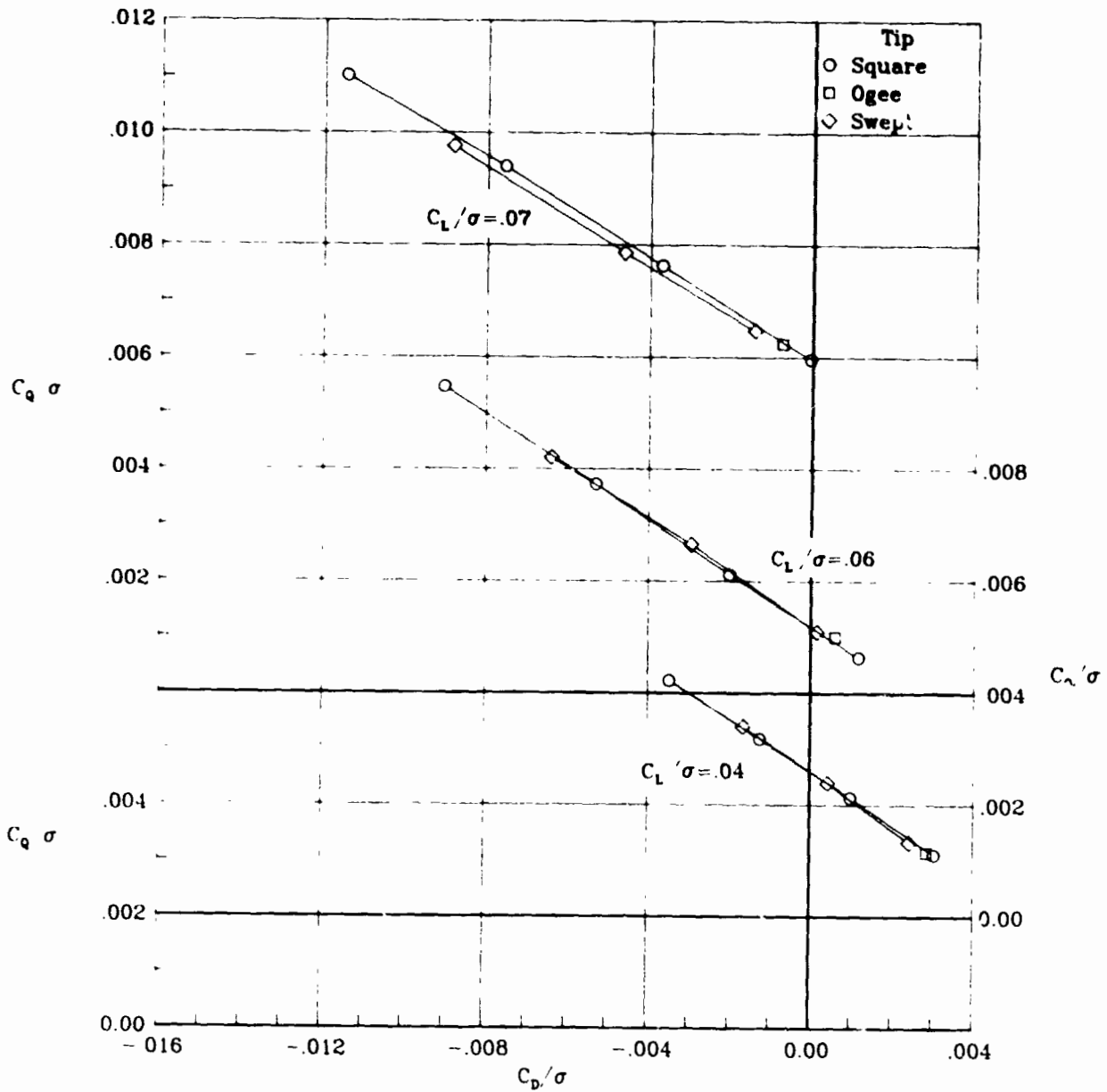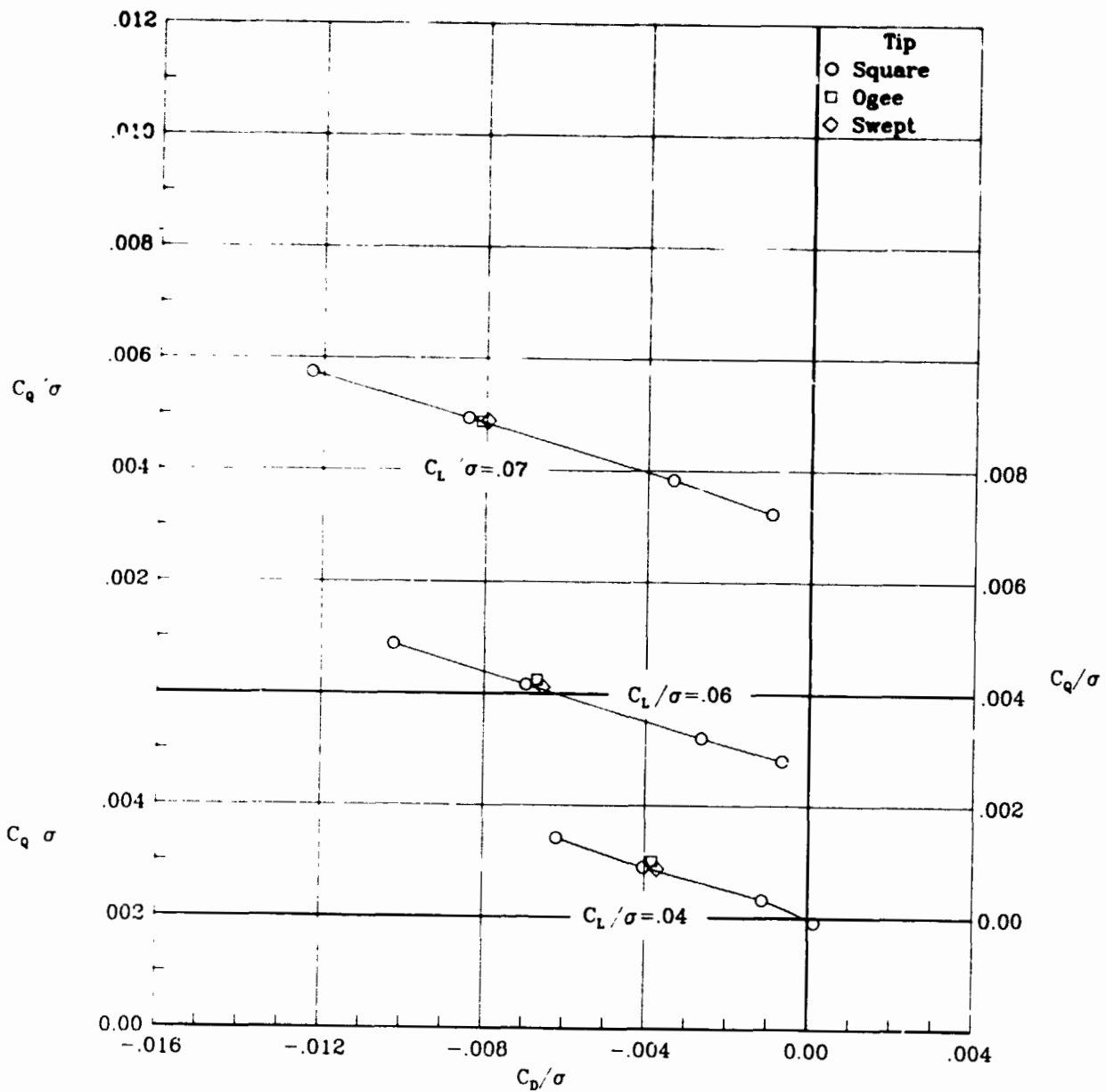
(b) μ = 0.30; N = 1200 rpm.

Figure 14.- Continued.
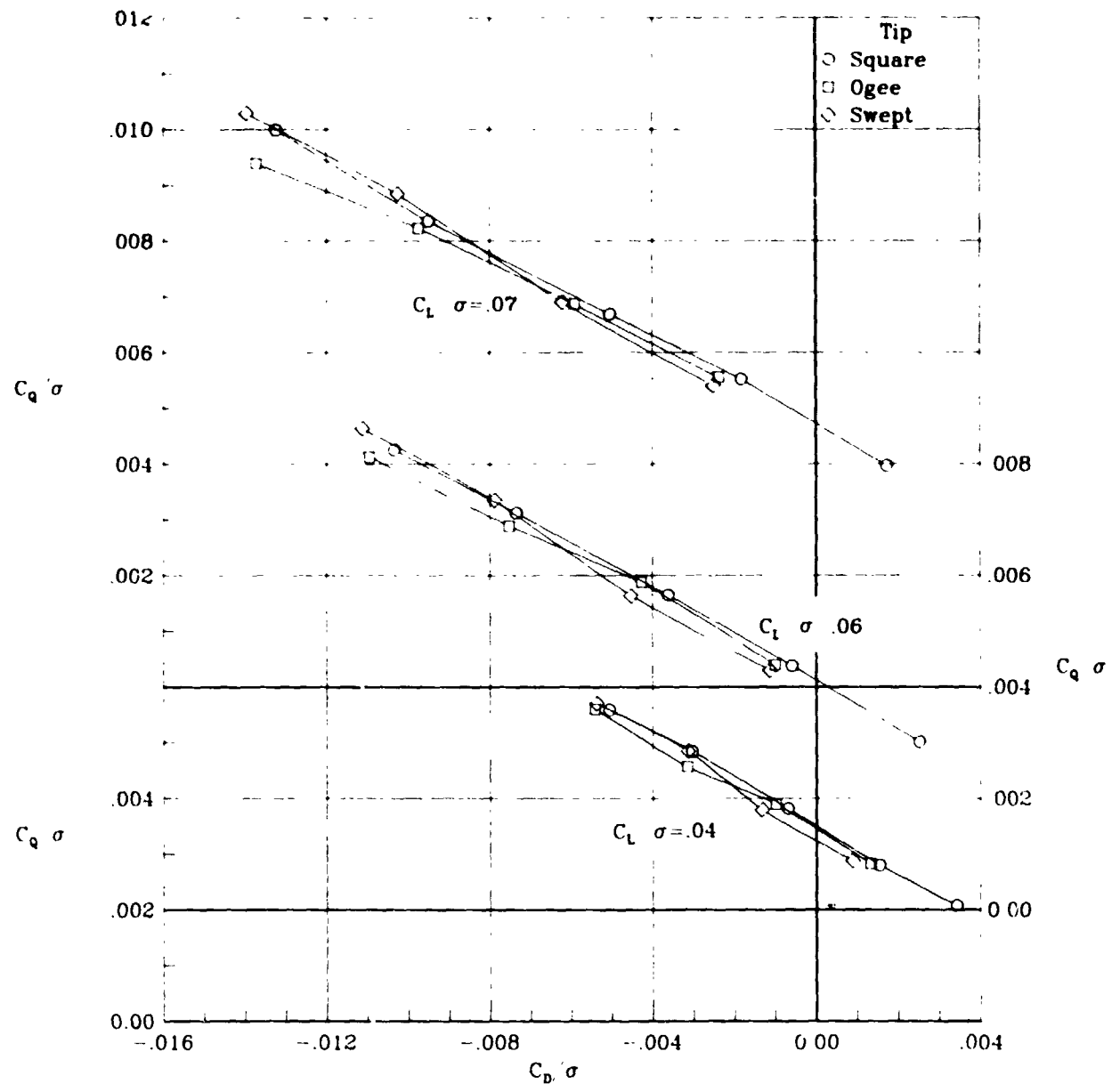
(c) μ = 0.35; N = 1200 rpm.

Figure 14.- Continued.
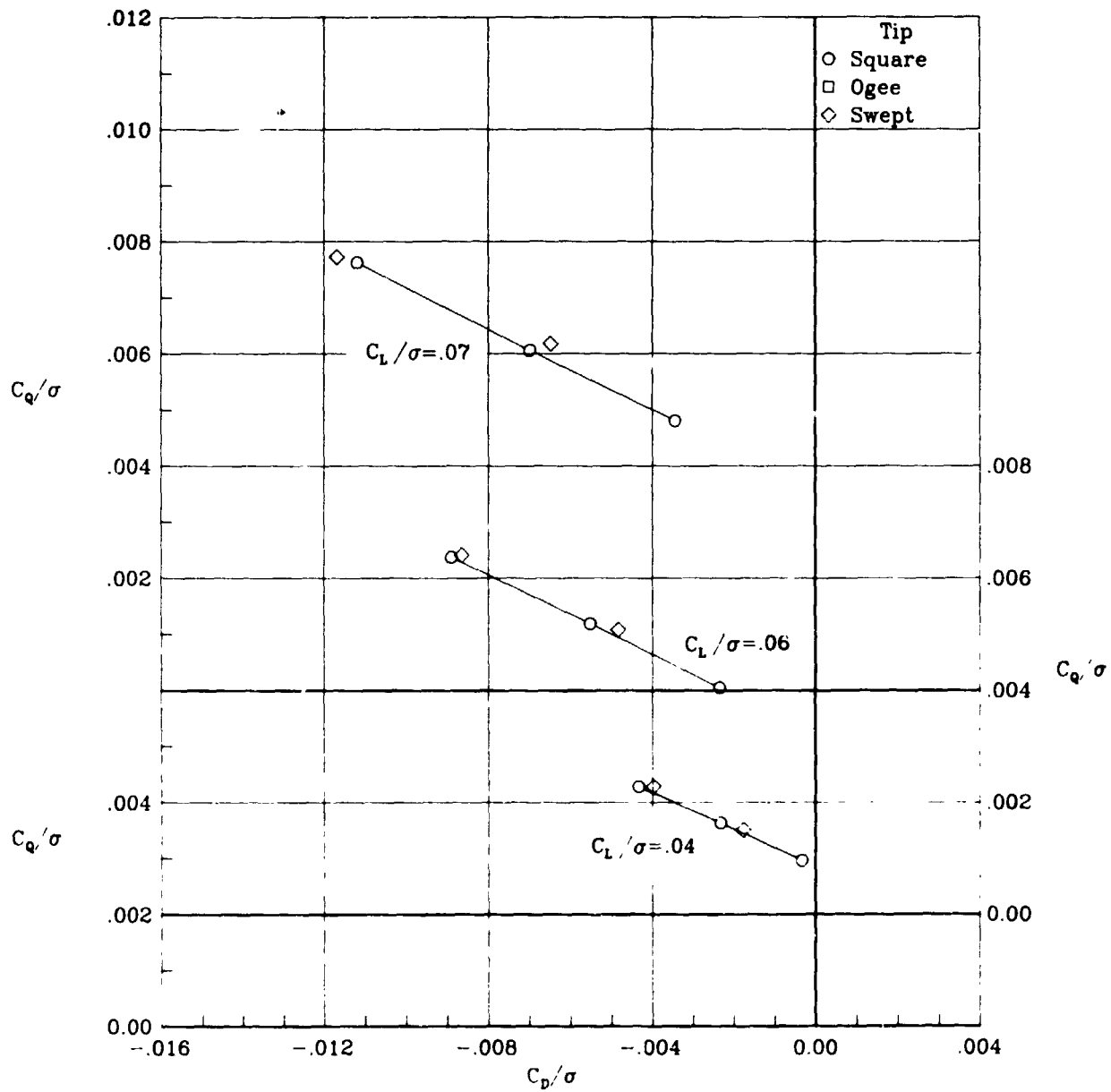
(d) μ = 0.40; N = 1200 rpm.

Figure 14.- Continued.

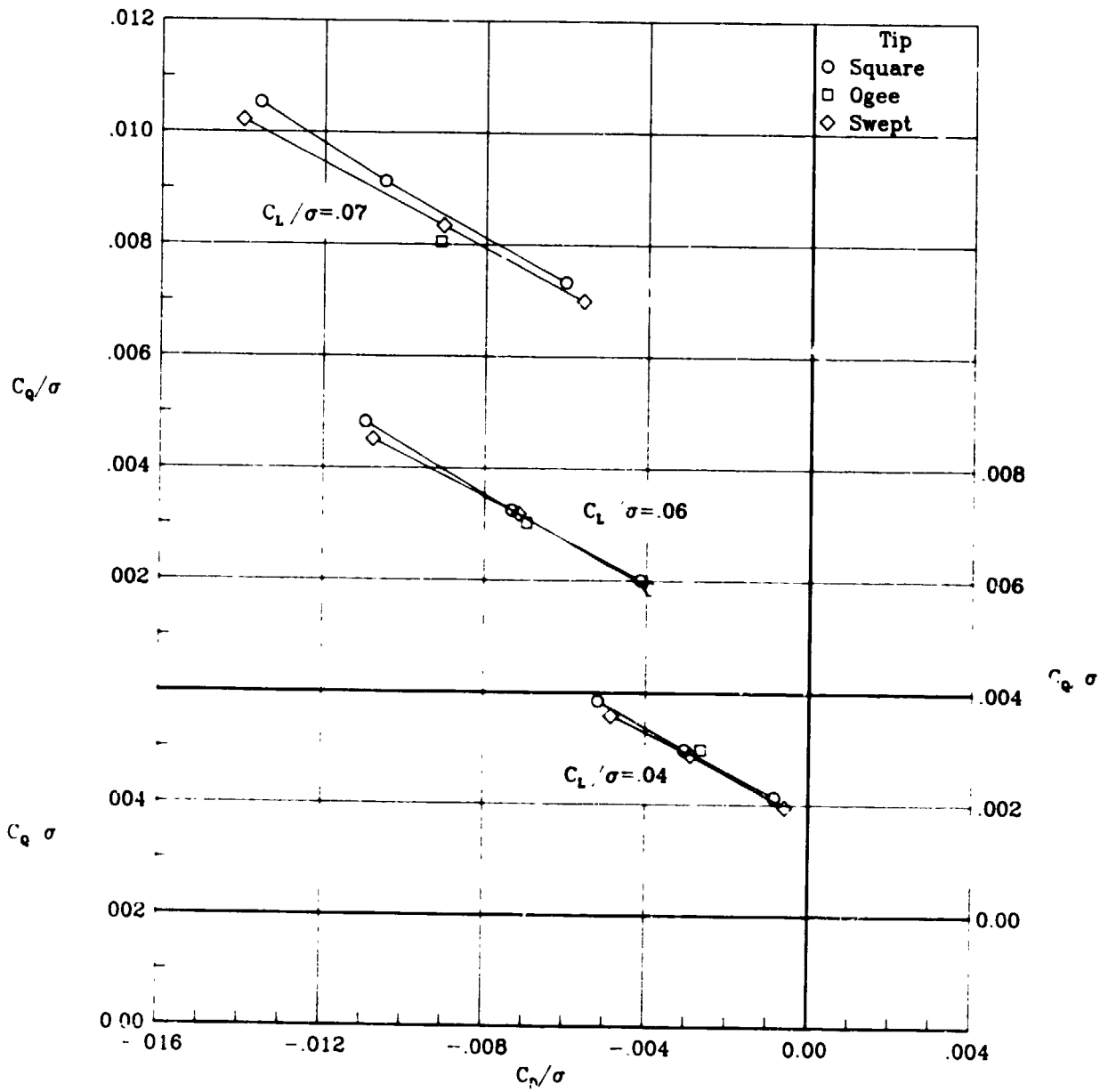(e) $\mu = 0.20$; N = 1340 rpm.

Figure 14.- Continued.

(f) $\mu = 0.30$; N = 1340 rpm.

Figure 14.- Continued.

(g) μ = 0.35; N = 1340 rpm.

Figure 14.- Concluded.